Aus dem Forschungsbereich für Translationale Entzündungsforschung
und Core Facility für Single Cell Multiomics
Leitung: Prof. Dr. Holger Garn
des Fachbereichs Medizin der Philipps-Universität Marburg

Influence of inflammatory mechanisms in obese adipose tissue on pathomechanisms of allergic airway inflammation in mice

Inaugural-Dissertation zur Erlangung
des Doktorgrades der Naturwissenschaften
dem Fachbereich Medizin der Philipps-Universität Marburg

vorgelegt von

Sarah Miethe
aus Coesfeld

Marburg, 2021

Angenommen vom Fachbereich Medizin der Philipps-Universität Marburg am:

15. Dezember 2021

Gedruckt mit Genehmigung des Fachbereichs Medizin

Dekanin: Prof. Dr. Denise Hilfiker-Kleiner

Referent: Prof. Dr. Holger Garn

1. Korreferent: Prof. Dr. Alexander Visekruna

Betreuer: PD Dr. Daniel P. Potaczek

„Jede wahre Geschichte ist eine unendliche Geschichte.“

- Michael Ende -

Table of Contents

I. Abbreviations

A

AAI	allergic airway inflammation
Ab	AbSeq labeling
ACK	ammonium-chloride-potassium
AHR	airway hyperresponsiveness
AMPK	adenosine monophosphate-activated protein kinase
AUC	area under curve
AW	airway

B

BAL	bronchoalveolar lavage
BCA	bicinchoninic acid assay
BMI	body mass index
BSA	bovine serum albumin
BV	blood vessel

C

CBA	cytometric bead assay
CCL	CC chemokine ligand
CCR	CC chemokine receptor
CD	cluster of differentiation
COPD	chronic obstructive pulmonary disease
CS	corticosteroid
CTLA-4	cytotoxic T-lymphocyte-associated protein 4, CD152
CXCL	C-X-C chemokine ligand
CXCR	C-X-C chemokine receptor

D

DC	dendritic cell
Der p	*Dermatophagoides pteronyssinus*
DMEM	Dulbecco's Modified Eagle Medium
DMSO	Dimethyl sulfoxide

E

EDTA	ethylenediaminetetraacetic acid
ELISA	Enzyme-linked immunosorbent assay
EOMES	Eomesodermin

F

FCS	fetal calf serum
FEV1	forced expiratory volume in one second
FGF	fibroblast growth factor
Foxp3	forkhead-box-protein P3

G

GATA3	GATA binding protein 3
GO-BP	Gene Ontology Biological Processes
GTT	glucose tolerance test

H

H&E	hematoxylin and eosin
HDL	high density lipoprotein
HDM	house dust mite
HFD	high fat diet

I

i.n.	intranasal
i.p.	intraperitoneal
ICS	inhaled corticosteroids
IgE	immunoglobulin E
IGFBP	insulin growth factor binding protein
IgG	immunoglobulin G
IL	interleukin
ILC	innate lymphoid cell
ITT	insulin tolerance test

L

LAG-3	lymphocyte-activation gene 3, CD223
LDL	low density lipoprotein
LEP	leptin
LEPR	leptin receptor

M

MCP-1	monocyte chemotactic protein 1
M-CSF	macrophage colony-stimulating factor
MHC	major histocompatibility complex
mRNA	messenger ribonucleic acid

N

NCD	non-communicable disease
ND	normal diet
NEAA	nonessential amino acids
NETs	neutrophil extracellular traps
NFAT	nuclear factor of activated T-cells
NHLBI	National Heart, Lung, and Blood Institute
NK	natural killer cells
NLRP3	NACHT, LRR and PYD domains-containing protein 3
NR4A	nuclear receptor subfamily 4A
NF-κB	nuclear factor 'kappa-light-chain-enhancer' of activated B-cells

O

OD	optical density
OVA	ovalbumin

P

PAS	periodic acid–Schiff
PBS	phosphate-buffered saline solution
PCA	Principal Component Analysis
PD-1	programmed cell death protein 1, CD279
PFA	paraformaldehyde

Ph	phenograph
POMC	proopiomelanocortin

R

rh	recombinant human
rm	recombinant mouse
RNA	ribonucleic acid
RPMI	medium, named after the *Roswell Park Memorial Institute*
RT	room temperature

T

T2D	type 2 diabetes
T-bet	T-box transcription factor (*Tbx21*)
TCF	T cell factor
Tcm	central memory T cells
TCR	T cell receptor
Tem	effector memory T cells
Temra	terminally differentiated effector memory T cells
Th	T helper
TIM-3	T-cell immunoglobulin and mucin-domain containing-3, CD366
TNF-α	tumor necrosis factor alpha
TOX	thymocyte selection-associated high mobility group box
Treg	regulatory T cell
Trm	resident memory T cells
Tscm	stem memory T cells

U-X

UMAP	Uniform Manifold Approximation and Projection
VE-H_2O	deionized water
XPB1	X-box binding protein 1

II. List of Figures

III. List of Tables

1. Introduction

1.1 Non-communicable diseases

The combination of genetic predisposition, environment (allergen exposure, nutrients), immunological mechanisms, and behavioral factors play a decisive role in the development of non-communicable diseases (NCDs), which are responsible for 70% of all deaths worldwide (WHO, 2021a). They are mostly chronic diseases including cardiovascular diseases, cancer, diabetes, and chronic respiratory diseases such as asthma and chronic obstructive pulmonary disease (COPD). Major risk factors for NCDs are smoking, physical inactivity, excessive alcohol consumption, unhealthy diets, and other life style- or environment-related factors (WHO, 2021a). Due to the high prevalences, which are further rising along with urbanization and globalization, the long-term consequences, and the complexity of such diseases, a better understanding for prevention is inevitable. In the following chapters the NCD asthma and its potential interaction with obesity will be described in more detail.

1.2 Heterogenic pathogenesis of asthma

1.2.1 Epidemiology and definition

Asthma is a chronic inflammatory disease, with an increasing prevalence in the last years. Currently over 300 million people are diagnosed with asthma worldwide and it represents the most prevalent chronic illness among children (WHO, 2020). The probability of developing bronchial asthma in the course of a lifetime is around 8% in Germany (Langen et al., 2013). This leads to asthma being a global burden on the health care system. While the mortality rate is comparatively low in relation to the prevalence with around 460,000 deaths per year, the quality of life is reduced tremendously according to the global burden of disease study (GBD, 2020).

The National Heart, Lung, and Blood Institute (NHLBI) specified asthma as a “common chronic disorder of the airways that is complex and characterized by variable and recurring symptoms, airflow obstruction, bronchial hyperresponsiveness, and an underlying inflammation”, with symptoms varying from coughing and wheezing to shortness of breath (National Asthma Education and Prevention Program, 2007). Limitations of the airflow are essentially caused by the bronchoconstriction mediated by vagus nerves, airway wall thickening provoked by edema and airway remodeling as well as the secretion of highly viscous mucus (Buhl et al., 2021). Exacerbations of asthma can be triggered by allergens, pollutants, viral infections, and drugs (Holgate et al., 2015). Asthma itself has a highly heterogeneous pathogenesis and several allergic comorbidities, such as allergic rhinitis, atopic dermatitis and food allergy are known, while also non-allergic comorbidities like obesity or gastroesophageal reflux might occur (Holgate et al., 2015).

1.2.2 Diagnostics and therapy of asthma

The diagnosis of asthma is based on four main aspects: examination of medical history, symptoms, and physical condition; variable and reversible airway obstruction; chronic airway inflammation; and hypersensitivity of the airways (airway hyperresponsiveness [AHR]). Furthermore, a prick test or the determination of specific IgE antibodies in serum may be useful in the context of allergy diagnostics. Various diagnostic options are available to examine lung function in more detail. Spirometry provides information about the forced expiratory volume in one second (FEV1) and the ratio of FEV1 to forced vital capacity (FVC) can be used to distinguish between restriction and obstruction, whereby a lower FEV1/FVC ratio is an indicator for obstruction. A bronchospasmolysis test is used to detect bronchial asthma; hereby it is measured, whether the obstruction is completely reversible with bronchodilators such as short-acting β-2-sympathomimetics. If the patient is currently asymptomatic and there is no bronchial obstruction despite a suspicion of asthma, a provocation test with inhalation of methacholine can be performed to detect a hyperreactive bronchial system (Buhl et al., 2021).

Currently, a detailed therapeutic approach scheme has been established for asthma, which is divided into 5 stages of therapy. Based on the intensity and severity of asthma symptoms, it differentiates between on demand/reliever acute therapy for intermittent asthma and long-term therapy for the disease that becomes persistent. The main aim is to adapt a poorly controlled/uncontrolled asthma into a well-controlled asthma to eliminate primary and avoid secondary symptoms. For on demand therapy either fixed combinations of inhaled corticosteroids (ICSs) with beta-2-adrenergic agonist formoterol or other short-acting beta agonists are recommended by the Global Initiative for Asthma (GINA). As soon as on demand therapy is no longer sufficient, therapeutic approaches should be extended to continuous long-term anti-inflammatory therapy. Depending on the severity of the asthma, long-term therapy with low doses of ICSs can additionally be combined with long-acting beta agonists. In case of even higher severity, the doses of ICSs might be increased still in combination with long-acting beta agonists. For patients with further exacerbations and/or uncontrolled symptoms a potential add-on treatment can be considered. However, this last therapeutic approach needs to be personalized based on the asthma phenotype, e.g. anti-IL-5 treatment in case of an eosinophilic asthma (GINA, 2021). Unfortunately, with exception of the last-mentioned option, these therapeutic approaches do not consider the underlying endotypes and an one-fits-all strategy does not optimally support all asthmatic patients, especially not those resistant to corticosteroid (CS) treatment. Therefore, the underlying mechanisms need to be understood in more depth, to offer further and more precise treatment strategies.

1.2.3 Phenotype versus endotype

Asthma exhibits a complex pathophysiology, therefore, the phenotype-endotype concept needs to be considered (Figure 1). The clinical picture of asthma includes characteristics of the clinics, physiology and hereditary, which are used to divide patients into groups, so-called “phenotypes”. However, in case of asthma, the definition of phenotypes as simple observable characteristics resulting from the combination of hereditary and environmental influences is obsolete (Kuruvilla et al., 2019). Considering not only the clinical picture but also further cellular and molecular mechanisms, such as specific (molecular) biomarkers or responsiveness to targeted drugs, the so-called

"inflammatory/molecular phenotype" arises. It includes the association of inflammatory processes at a cellular/molecular level with the clinical phenotype (Ray et al., 2015). So-called "endotypes" define further the specific biological pathomechanisms underlying the clinically observable phenotypes. As a highly heterogenic disease, asthma can therefore not be defined by a single specific mechanism, but rather several different endotypes underlie this disease (Oțelea, Rașcu, 2018). Difficulties arise in distinct classification of asthmatic patients, as various asthma phenotypes show overlapping characteristics and, in addition, the endotypes are commonly referred to as just type 2 or type 2-low/non-type 2 so far (Kuruvilla et al., 2019). The asthma phenotypes are underlain by at least partly varying mechanisms, also within the mechanistic/endotype group, and are characterized by different levels of severity, ranging from mild over moderate to severe, and different treatability (Lötvall et al., 2011).

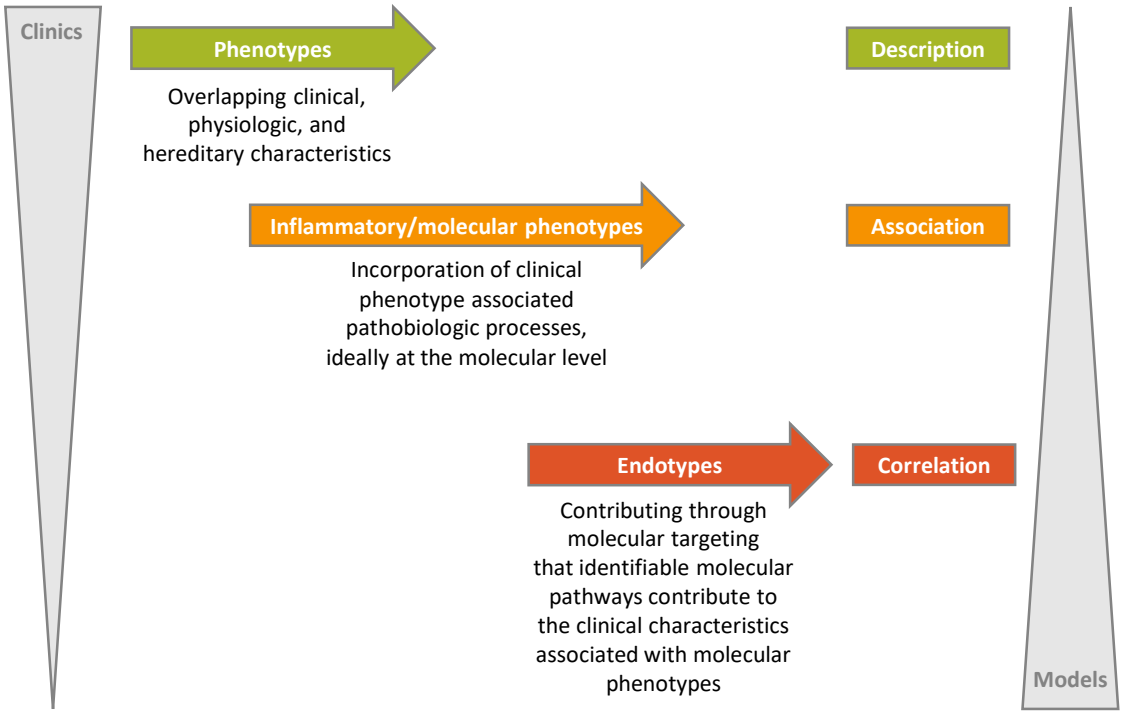

Figure 1: Phenotype-Endotype-Concept [adapted from (Ray et al., 2015)]

Characterizing the asthmatic phenotypes, the clinical picture of patients is taken into consideration. Further, the molecular phenotype might as well be investigated based on human samples obtained within human studies. However, when it comes to understanding of the underlying pathomechanisms, i.e. definition of specific endotypes, the accessibility to and the usefulness of patient samples is limited. Thus, other approaches

such as *in vitro* or *in vivo* models need to be applied. In turn, limitations of *in vivo* mouse models might include a lack of the full concordance between the "clinical" pictures of allergic airway inflammation (AAI) observed in mice or other model systems and the classical asthma phenotypes seen in human. Therefore, mouse models need to be well established, so that the induced inflammatory and pathomechanisic processes resemble the human situation very well. Nevertheless, the mouse-to-human translational aspects need to be taken into account when interpreting the results.

1.2.4 Phenotypes and endotypes associated with type 2-driven asthma

In the following, the main asthmatic phenotypes with their molecular phenotype/endotype will be described. Current research on asthma contributes to the identification of more drivers playing a role in the pathogenesis of asthma, thus definitions of phenotypes and their underlying endotypes are rather fluid and at least partly overlapping (Figure 2).

Early-onset allergic, adult-(late-)onset eosinophilic and exercise-induced asthma are the main phenotypes representing the type 2-driven asthma (Holgate et al., 2015, Koczulla et al., 2017, Lötvall et al., 2011, Wenzel, 2012). The most common triggers for type 2-driven asthma are allergens such as pollen, house dust mite (HDM) or animal dander (Holgate et al., 2015, Schatz, Rosenwasser, 2014). Typical features of early-onset allergic asthma include obviously an early onset, atopic sensitization, immediate hypersensitivity type of allergic reaction and responsiveness to CS (Wenzel, 2012). Although those characteristics arise, neither effective tests for atopic asthma in children nor a specific cut-off age has been defined, which makes it difficult to specifically determine early-onset allergic asthma (Koczulla et al., 2017). As the name suggests, adult-onset eosinophilic asthma first appears in the adulthood and is related to an increase in eosinophils in sputum, bronchoscopic samples or blood (Wenzel, 2012). In this phenotype, a severe disease onset can occur, which is often accompanied by chronic sinusitis and nasal polyps (Koczulla et al., 2017, Wenzel, 2012). Until now, the knowledge of immune mechanisms related to exercise-induced asthma remains very limited. Patients show typically mild asthma symptoms and suffer from a reactive bronchoconstriction after exercising (Wenzel, 2012).

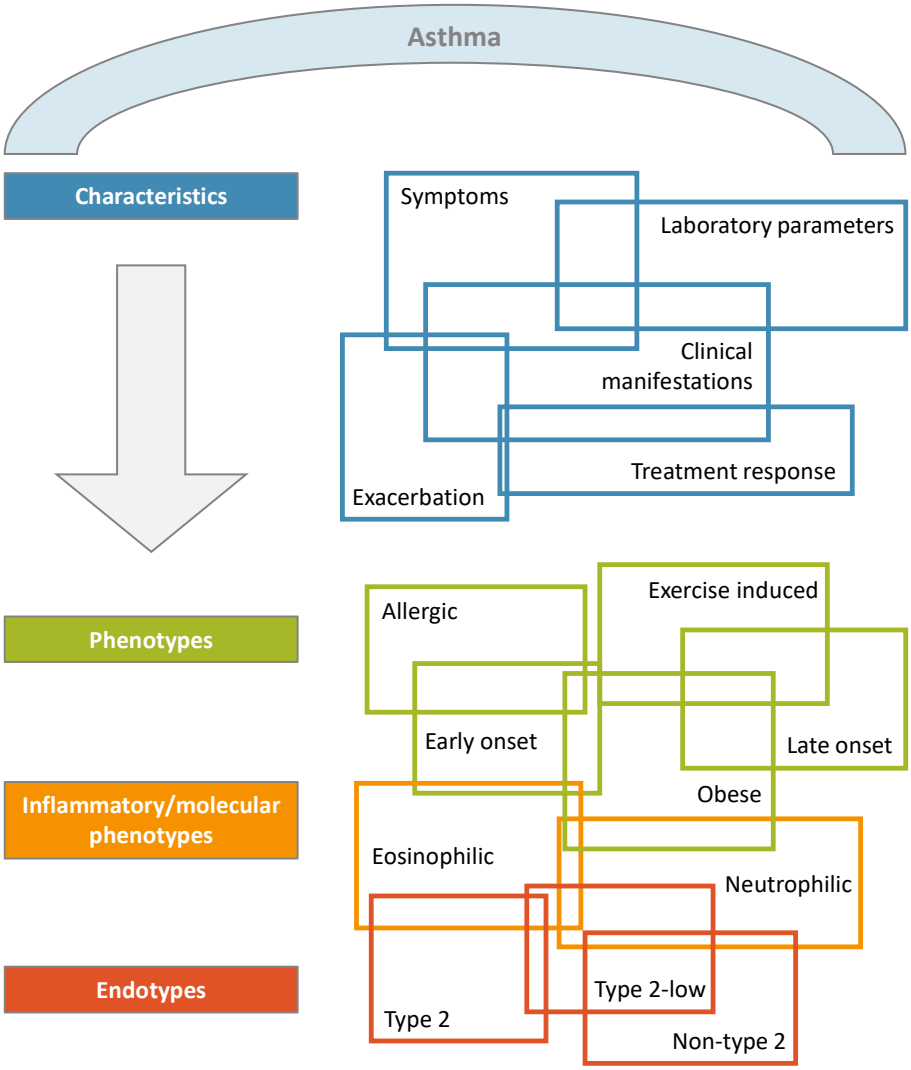

Figure 2: Schematic representation of the modified "asthma umbrella" indicating the heterogeneity of asthma with overlapping characteristics [adapted from (Kim, 2012, Wenzel, 2012)]

The type 2-driven asthma is observed in around half of the patients with asthma (Woodruff et al., 2009) and often correlates with severe symptoms and eosinophilic inflammation (Fahy, 2015). Type 2-driven mechanisms are initiated by dysregulation of the epithelial barrier associated with the release of alarmins such as thymic stromal lymphopoietin (TSLP), interleukin (IL)-25, and IL-33, playing an important role in the activation of type 2 mechanisms. TSLP specifically primes dendritic cells to induce the differentiation of naïve T into Th2 cells, whereas IL-25 and IL-33 activate innate lymphoid cells type (ILC) 2 (Kato, 2019, Potaczek et al., 2020). Thus, the release of type 2 cytokines is initiated, which play a crucial role in the development of atopy reactions and resulting eosinophilic inflammation. Most important type 2 cytokines are IL-4, IL-5, and IL-13, which are produced mostly by Th2 or ILC2s but also mast cells and eosinophils. The

cytokines further support the differentiation from naïve T into Th2 cells. In addition, IL-4 but also IL-13 stimulate B cells to produce immunoglobulin E (IgE). IL-13 additionally induces AHR and enhances mucus production, whereas IL-5 is able to recruit and activate eosinophils (Gandhi et al., 2016, Lambrecht, Hammad, 2015, Potaczek et al., 2017, Potaczek, Kabesch, 2012). Besides, also hyperproduction of mucus and higher smooth muscle contractibility are the results of the inflammation stimulated by type 2 cytokines (Gandhi et al., 2016, Potaczek et al., 2017).

1.2.5 Phenotypes and endotypes associated with type 2-low/non-type 2-driven asthma

Common causes of the non-type 2-driven asthma include airway infections, smoking, obesity or other irritants (Holgate et al., 2015, Schatz, Rosenwasser, 2014). In contrast to type 2, phenotypes of non-type 2-driven asthma are commonly associated with low response to CSs (Green et al., 2002). The obesity-associated and neutrophilic (smoke-related) asthma phenotypes belong to the non-type 2 forms of the disease (Holgate et al., 2015, Koczulla et al., 2017, Lötvall et al., 2011, Wenzel, 2012). The obesity-associated asthma shows several clinical pictures and might therefore be further subdivided. The features of the most common obesity-associated asthma phenotype comprise lack of atopy, a late onset and a higher prevalence in females (Koczulla et al., 2017). Another phenotype combining asthma with obesity is characterized by an early onset of asthma. In this form of obesity-associated asthma, obesity aggravates the already existing asthma (Dixon, Poynter, 2016). On top of asthma symptoms, common clinical presentations of different forms of obesity-related asthma includes breathlessness provoked by obesity, chest tightness and, frequently, gastroesophageal reflux (Wenzel, 2012). Compared to type 2 phenotypes, those associated with the non-type 2-driven asthma are most probably showing even more mutual mechanistic differences. Risk factors leading to the dysregulation of innate immune responses are for example smoking or obesity, with no background of type 2 inflammation during the childhood (Koczulla et al., 2017). Smoking or chronic use of steroids leads to the development of increased numbers of neutrophils in the sputum, lung or blood, which is the main characteristic of the neutrophilic asthma (Koczulla et al., 2017). Besides, this asthma is not typically

associated with AHR but rather with more air trapping and thicker airway walls resulting in reduced lung function (Wenzel, 2012).

The endotypes, which differ from the distinct type 2 cytokine pathways remain mainly uncharacterized and are so far only defined by the absence type 2 inflammatory processes. Therefore, they are only referred to as non-type 2 or more recently also as type 2-low endotypes (Fahy, 2015, Kuruvilla et al., 2019, Ray et al., 2015). Most probably, the non-type 2-driven asthma cannot be described as a single mechanistic entity. Rather several varying disease mechanisms underlie several endotypes of the disease, which are still quite under-investigated. Common functional features of the non-type 2-driven asthma include activation of Th1 and Th17 pathways and a contribution of metabolic factors. The neutrophilic inflammation is promoted by interferon-γ (IFN-γ), tumor necrosis factor α (TNF-α) and IL-17 (Agache, Akdis, 2016, Chung, 2015). The pro-inflammatory cytokine IL-1β is also known to be increased in the neutrophilic asthma correlating with elevated level of the NACHT, LRR and PYD domains-containing protein 3 (NLRP3) inflammasome (for further details see below, 1.3.2 Inflammatory mechanisms linking obesity and asthma) and IL-8, as common chemoattractant cytokine neutrophils (Simpson et al., 2014). In the chapters below, potential mechanisms of the interaction between obesity and asthma will be described. Only to mention, the spectrum of clinical coexistence of obesity and asthma is, however, much wider and not restricted to the most common obesity-associated asthma phenotype and early onset asthma aggravated by obesity shortly characterized above.

1.3 Obesity as risk factor for asthma

1.3.1 Chronic low-grade systemic inflammation in obesity

Overweight and obesity are growing health problems in many parts of the world, implying an increased risk of chronic diseases such as type 2 diabetes (T2D) and cardiovascular diseases. According to WHO, more than half of Germans are already overweight and even more than 20% are obese (WHO, 2017). Obesity is a disease with excessive increase of fatty tissue in the body and is defined by a body mass index (BMI) ≥ 30 kg/m^2

(WHO, 2021b). Further, obesity is associated with a chronic low-grade systemic inflammation due to the production of inflammatory mediators in the adipose tissue, and thus contributes to the pathology of several obesity-associated diseases (Sivapalan et al., 2015). In addition to its function as energy storage, adipose tissue is considered to be an endocrine organ and plays an important role in the regulation of whole-body fatty acid homeostasis (Galic et al., 2010). It is capable of producing a variety of cytokines, hormones, extracellular matrix proteins, and many other factors referred to as adipokines. Adipokines are peptide substances having the same characteristics as cytokines, chemokines, and hormones (Sood, Shore, 2013). If the endocrine functions are dysregulated by excessive increase of adipose tissue, it contributes to changes in immune and metabolic responses by excess production of adipokines and other mediators (Al-Sahrif, 2017).

The most common adipokine in the adipose tissue is adiponectin, which is relevant for the control of the energy balance and promotes insulin sensitivity and fatty acid oxidation (Gelsinger et al., 2010). Anti-inflammatory effects of adiponectin include triggering IL-10 and IL-1 receptor agonist production, suppression of nuclear factor κB (NF-κB) signaling, and inhibition of IL-6 and TNF-α (Jartti et al., 2009, Sood, Shore, 2013). The appetite regulating hormone leptin is another important adipokine. Leptin binds to its receptor in the hypothalamus, which leads to subsequent activation of the Janus kinase-signal transducer and activator of transcription protein (JAK-STAT3) signaling pathway and production of certain peptides resulting in reduction of food intake (Ahima, 2008). In obese patients, however, a leptin resistance may develop causing increased leptin levels, hunger, and further weight gain (Pan, Myers, 2018). In contrast to adiponectin, leptin has pro-inflammatory effects exerted through modulation of immune mechanisms, such as increased IFN-γ stimulation or activation of mast cells and NF-κB (Francisco et al., 2018). Another hormone triggering NF-κB activation and production of cytokines is resistin. It further modulates insulin sensitivity, and increased levels of resistin in obese patients provoke insulin resistance (Muc et al., 2014, Steppan et al., 2001). Ghrelin, as important appetite hormone, is responsible for food intake, decreased fat utilization, and also regulation of metabolism and energy balance homeostasis (Wiedmer et al., 2007, Yuksel et al., 2012). Similarly to the aforementioned

adiponectin, ghrelin can inhibit the expression of pro-inflammatory cytokines such as IL-1β, IL-6, and TNF-α (Dixit et al., 2004). On the contrary, levels of ghrelin are reduced in obese patients; therefore, its anti-inflammatory effects are lacking (Tschöp et al., 2001).

Next to adipokines, also inflammatory cells residing in the adipose tissue contribute to the low-grade systemic inflammation caused by an excessive adipose tissue. Especially macrophages accumulate in the obese adipose tissue and participate in inflammatory mechanisms. Macrophages can be divided into two main types, i.e. M1 and M2, whereby M1 macrophages promote inflammatory activities and insulin resistance, which is opposite to M2 macrophages that are rather able to block inflammatory processes. For instance, M1 macrophages contribute to inflammatory processes by the release of pro-inflammatory cytokines such as IL-6, TNF-α, and monocyte chemoattractant protein 1 (MCP-1) (Chylikova et al., 2018). It has been shown that an increased expression of MCP-1 in the adipose tissue is not only associated with further macrophage infiltration but is also associated with insulin resistance (Kanda et al., 2006).

Not only macrophages but also T cells are found in increased numbers in the obese adipose tissue. The differentiation and proliferation of $CD8^+$ and $CD4^+$ T cells can be induced by several adipokines (Song, Deng, 2020). Further, $CD8^+$ T cells are involved in the inflammatory cascade, as depletion of $CD8^+$ T cells lowered the mRNA expression of IL-6 as well as TNF-α in the adipose tissue (Nishimura et al., 2009). γδ T cells are a specific subgroup of T cells which execute opposing roles, being either pro- or anti-inflammatory depending on their localization (Carding, Egan, 2002). They can also be resident in the adipose tissue. Mehta et al. analyzed the function of γδ T cells in a mouse model of obesity (Mehta et al., 2015). In obese $TCR\delta^{-/-}$ mice, gene expression levels of CC chemokine receptor (CCR) 2, IL-6 and TNF-α were reduced in the adipose tissue, which was accompanied by an improved insulin sensitivity. These observations suggested that γδ T cells are crucially involved in the regulation of inflammatory processes as well as insulin resistance in the adipose tissue (Mehta et al., 2015). Besides, insulin-growth factor binding protein 3 (IGFBP-3) might also contribute to insulin resistance. It is the most important of six binding proteins of insulin growth factor 1 (IGF1) and can be

produced by adipocytes, with an increased synthesis during adipocyte differentiation (Wabitsch et al., 2000). It has been shown in mouse models and *in vitro* using human adipocytes that elevated levels of IGFBP-3 are responsible for insulin resistance and impaired glucose uptake (Alhasson et al., 2018, Chan et al., 2005, Silha et al., 2002).

1.3.2 Inflammatory mechanisms linking obesity and asthma

The epidemiologic correlation of asthma and obesity has been already seen in 1999 by Camargo et al., suggesting that the BMI positively associates with emerging late-onset asthma (Camargo et al., 1999). Some of the effects of obesity on asthma are rather mechanical, whereas others are more associated with the enhancement of asthma-associated inflammation (Figure 3). Besides, asthma and obesity share some of the inflammatory mechanisms. Those linking both diseases will be described below.

Figure 3: Schematic representation of implications of obesity on the development of asthma (Miethe et al., 2018)

Starting with the above-mentioned adipokines, they also play an important role in the pathophysiology of asthma. Several effects of adipokines on the lung have been reported. For instance, leptin upregulates the cytokine production by normal lung fibroblasts and is able to promote AAI (Watanabe et al., 2019, Zheng et al., 2018). In a recent study on the role of leptin in asthma, it was shown that it induces X-box binding protein 1 (XPB1), a molecule affecting the cytokine secretion of B and T cells and consequently leading to the subsequent increase in the release of Th2 cytokines (Zheng et al., 2018). Next to cytokines, leptin is also capable of upregulating several chemokines in the lung such as CC chemokine ligand (CCL) 11/Eotaxin, CCL2/MCP-1, C-X-C chemokine ligand (CXCL) 8/IL-8 and CXCL10/IP-10 (Watanabe et al., 2019). In contrast, anti-inflammatory effects of adiponectin could alleviate the AAI in a murine ovalbumin

(OVA)-based AAI model (Shore et al., 2006). In another mouse study, combining the OVA model with a high fat diet (HFD), protective effects of adiponectin were partially regulated by activation of adenosine monophosphate-activated protein kinase (AMPK) pathways, known to play a role in the cellular metabolism (Zhu et al., 2019). However, in obese patients, adiponectin levels are reduced and, therefore, anti-inflammatory effects are missing, potentially implicating inflammatory processes in obesity-associated asthma (de Lima Azambuja et al., 2015).

Depictured in Figure 4 among other mechanisms is the activation of the inflammasome NLRP3 in M1 macrophages, which promotes AHR in obese patients (Bantulà et al., 2021). Inflammasomes are cytosolic multiprotein complexes of the innate immune system that play a crucial role in activation of pro-inflammatory cytokines such as IL-1β. The inflammasome NLRP3 is a subset of the NLR family and is not only a strong inducer of IL-1β production, but also an important mediator for the development of AHR in obese mice. AHR was not developed in obese $Nlrp^{-/-}$ mice; the same applied also for obese $IL17^{-/-}$ mice, whereby IL-17 can likewise induce IL1-β production (Kim et al., 2014). Aforementioned, NLRP3 plays not only a role in asthma but is involved in metabolic mechanisms, too. Saturated fatty acids potentially promote the NLRP3 inflammasome activation and therefore may be associated with metabolic inflammation (Ralston et al., 2017). Furthermore, higher AHR has been associated with obesity and correlated with increased expression of CD38 in the lungs of HFD/OVA mice (Chong et al., 2018). CD38 is known to play a role in AHR by upregulation of TNF-α in smooth muscle cells (Guedes et al., 2008).

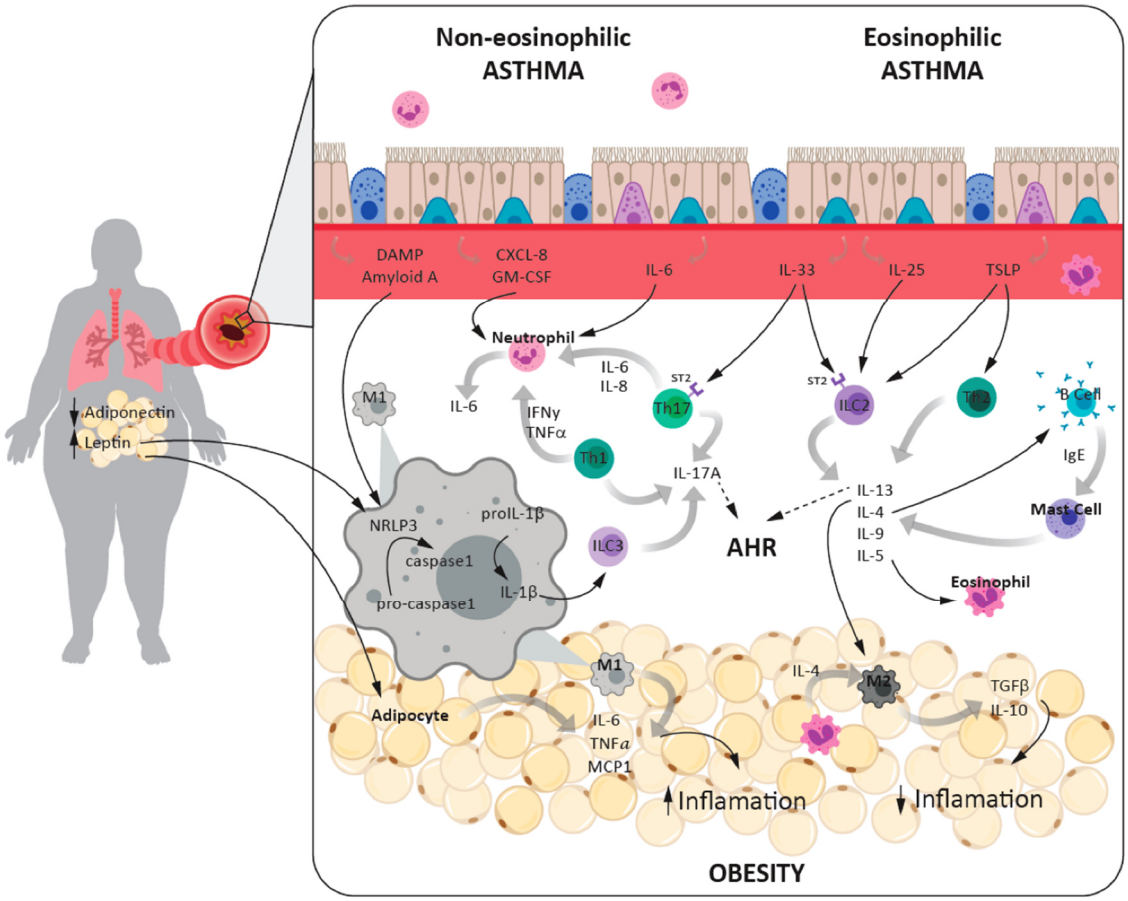

Figure 4: Inflammatory processes in the adipose tissue interacting with asthma-associated mechanisms (Bantulà et al., 2021)

Eosinophilic granulocytes are attracted by the type 2 cytokine IL-5. Activated eosinophils release toxic granules promoting tissue damage and inflammation (Carr et al., 2018). In a study, the model combining OVA exposure and HFD the obese mice showed initially reduced eosinophils in bronchoalveolar lavage (BAL), with later eosinophil trafficking from bone marrow to lung tissues and increased levels of IL-5, TNF-α, and IL-10 compared to lean OVA sensitized mice (Calixto et al., 2010). Another study demonstrated, in addition to increased eosinophil numbers in BAL following a combined HFD/HDM exposure, an involvement of ILCs in the development of AAI exacerbation in a HFD group (Everaere et al., 2016). IL-8, a cytokine that can be produced by the airway epithelium, is in turn the main contributor to neutrophil recruitment (Ordoñez et al., 2000). Neutrophils can provoke inflammation by releasing neutrophil extracellular traps (NETs), which are then able to activate mast cells and eosinophils (Pham et al., 2017, Wright et al., 2016). Neutrophilic inflammation commonly associated with non-type 2 mechanisms is controversially discussed with regard to the obesity-associated asthma

phenotype, as different studies either show a correlation between increased numbers of neutrophils in the sputum and obesity-associated asthma or do not demonstrate it (Desai et al., 2013, Moore et al., 2014, Telenga et al., 2012, Todd et al., 2007).

Airway remodeling is a major characteristic of the chronic asthma pathophysiology. In asthmatics, airway epithelial cells have a flattened structure instead of the a rather columnar one characteristic for healthy individuals without allergy and asthma (Shahana et al., 2005). Bioenergetic differences are seen in epithelial cells between lean and obese asthmatic patients, with increased glycolysis and lower production of nitric oxide observed in the latter (Komakula et al., 2007, Winnica et al., 2019). In mice, a HFD has been shown to affect the numbers of lung cells, with increased numbers of alveolar type 2 cells and pronounced proliferation of lung parenchymal epithelial stem cells (Hegab et al., 2018). Increased production of mucus is another pathophysiological feature of asthma. Interestingly, obese mice subjected to OVA-induced AAI demonstrate even higher mucus production than their lean counterparts, which is mediated by Munc18b-controlled higher expression of Muc5a (Hao et al., 2018). Mucus hyper-production of human airway epithelial cells can be aggravated by leptin and resistin, leptin by regulating the IL-13-induced MUC5AC pathway and resistin through various mechanisms involving phosphorylation of ERK1/2, p38 or NF-κB (Hao et al., 2017, Kwak et al., 2018). Another adipokine affecting human bronchiolar epithelial cells in the way opposite to pro-inflammatory leptin and resistin, is adiponectin, the anti-inflammatory adipokine that contributes to cell proliferation and wound repair (Zhu et al., 2013).

Recently, the role of vitamin D in obesity-associated asthma is gaining interest. It has been known for long time, that vitamin D levels are low in obese individuals (Parikh et al., 2004, Wortsman et al., 2000). Study of vitamin D in mouse models showed diminished vitamin D concentrations in obese mice as well and additionally even lower levels in the obese mice subjected to the OVA-based model of AAI, suggesting a link between vitamin D and development of airway inflammation (Zhang et al., 2017). Vitamin D deficiency arising along with a HFD led to an increased expression of pro-inflammatory cytokines and was correlating with AHR. Supplementation of vitamin D was in turn able to attenuate AHR in obese mice (Han et al., 2020).

1.4 Hypothesis and aim

As mentioned above, asthma is a highly heterogenic disease with different clinical faces (phenotypes) and mechanisms underlying those (endotypes). Coexistence of asthma and obesity may result in obesity-associated asthma. As not only asthma but also obesity is increasing in prevalence, research on the obesity-associated asthma phenotypes is of raising interest. Moreover, similarly to asthma in general, also the obesity-associated asthma phenotypes shows several clinical pictures that are most probably underlain by varying endotypes. However, these mechanisms are not fully understood yet. The current one-fits-all therapeutic approach for asthma was initially established for the treatment of allergic asthma and turned out to be not really useful for several other asthma phenotypes including obesity-associated asthma. Moreover, mouse models of AAI reflecting features of human asthma in combination with obesity have been developed to gain in-depth knowledge on the underlying mechanisms of obesity-associated asthma.

Previous research indicated that obesity influences the development and the clinical course of asthma. Therefore, the underlying hypothesis of this work is that inflammatory mechanisms associated with obesity modify the inflammatory phenotype of an induced AAI and that altered activation processes in $CD4^+$ T cells are crucially involved in these changes. Within this study, it is evaluated, whether metabolic processes leading to weight gain are linked to alterations of asthma-associated inflammatory processes in the lung. Hence, systemic inflammatory signals generated by the obese adipose tissue such as cytokines/adipokines are investigated with regard to their effects on the lung leading to subsequent changes of the cellular/molecular endotype of an induced mixed (eosinophilic and neutrophilic) inflammatory asthma phenotype.

The aim of this study was to investigate characteristics of an HDM-induced AAI in mice with a continuous HFD in order to gain further insights into the specific mechanisms underlying the obesity-associated asthma. Taken into account that type 2- as well as non-type 2-driven mechanisms were found in obese asthmatic patients, a mouse model with an HDM-induced mixed inflammatory phenotype was used as basis for these investigations.

Specifically, the activation of type 2- and non-type 2-driven immune mechanisms resulting in an equal increase in eosinophil and neutrophil counts in the BAL was induced for in-depth investigation of the underlying endotype. The following research questions will be specifically addressed:

- Are inflammatory mechanisms in the adipose tissue linked to metabolic processes and/or weight gain?
- Does obesity alter the inflammatory phenotype of an induced mixed, type 2/non-type 2-driven AAI?
- How do the inflammatory mechanisms in the adipose tissue contribute to the alterations of inflammatory processes in the lung?
- Which cellular and molecular changes in the BAL and lung are associated with obesity and the induced AAI?
- Do obesity-associated inflammatory processes have an impact on the function of HDM-induced T cells?

2. Materials and methods

2.1 Devices and chemicals

2.1.1 Devices

Name	Provider
37 °C shaker	LAUDA-GFL, Burgwedel, DE
AccuCheck Inform II	Roche, Mannheim, DE
Attune™ NxT flow cytometer	Life Technologies, Carlsbad, CA, US
CASY cell counter and analyzer TT	Omni Life Science, Bremen, DE
CellDrop FL fluorescence cell counter	Denovix, Wilmington, US
Centrifuge (Megafuge ST plus series)	Thermo Fisher, Osterode am Harz, DE
Cytocentrifuge (Resospin)	Sigma Laborzentrifugen, Osterode am Harz, DE
FACS Canto II	BD, San Jose, CA, US
Freezing container (MrFrosty)	Sigma-Aldrich, Steinheim, DE
gentleMACS™ dissociator	Miltenyi Biotec, Bergisch Gladbach, DE
Incubator (HERAcell VIOS 250i)	Thermo Scientific, Langenselbold, DE
Microplate reader (Infinite F200 Pro)	Tecan, Männedorf, CH
Microscope (AE31E)	Motic, Barcelona, ES
Microtome (HM 355S)	Thermo Scientific, Rockford, IL, US
Scale (Pioneer™)	Ohaus, Nänikon, CH
X-ray film processor (SRX-101-A)	Konica Minolta, Marunouchi, JP

2.1.2 Chemicals

Name	Provider
Advanced DMEM/F12	Gibco, Grand Island, NY, US
Ammonium chloride	Carl Roth, Karlsruhe, DE
Anti-mouse CD28 (Ultra-LEAF purified)	Biolegend, San Diego, CA, US
Anti-mouse CD3 (Ultra-LEAF purified)	Biolegend, San Diego, CA, US
Anti-mouse IFN-γ (Ultra-LEAF purified)	Biolegend, San Diego, CA, US
Anti-mouse IL-4 (Ultra-LEAF purified)	Biolegend, San Diego, CA, US
Bovine serum albumin (BSA)	Anprotec, Bruckberg, DE
CASYton (buffer solution)	Omni Life, Bremen, DE
Chloroform (trichloromethane)	Carl Roth, Karlsruhe, DE

Name	Provider
Collagenase D from *clostridium histolyticum*	Sigma-Aldrich, Steinheim, DE
cOmplete™ protease inhibitor cocktail	Roche, Mannheim, DE
Deoxyribonuclease I from bovine pancreas	Sigma-Aldrich, Steinheim, DE
Dermatophagoides pteronyssinus (*Der p*) (used for HDM-specific IgG ELISA)	Stellergenes Greer, Lenoir, NC, US
Dimethyl sulfoxide (DMSO)	Carl Roth, Karlsruhe, DE
DMEM high glucose medium	Anprotec, Bruckberg, DE
Entellan mounting medium	Merck, Darmstadt, DE
Eosin	Carl Roth, Karlsruhe, DE
Ethanol 100%	Carl Roth, Karlsruhe, DE
Ethylenediaminetetraacetic acid (EDTA)	Sigma-Aldrich, Steinheim, DE
Fetal calf serum (FCS)	Anprotec, Bruckberg, DE
Formaldehyde 37%	Sigma Aldrich, St. Louis, MO, USA
Glacial acetic acid	Acros Organics, Geel, BE
Hematoxylin	Carl Roth, Karlsruhe, DE
Isopropanol (2-propanol)	VWR, Fontenay-sous-Bois, FR
L-Glutamine	Anprotec, Bruckberg, DE
Liquid nitrogen	Linde, Gablingen, DE
MEM nonessential amino acids 100x (NEAA)	Capricorn, Ebsdorfergrund, DE
Mouse Fc-Block (CD16/CD32)	BD Pharming, Ashland, US
Penicillin/streptavidin	Anprotec, Bruckberg, DE
Periodic acid	Carl Roth, Karlsruhe, DE
Phosphate-buffered saline (PBS)	Sigma Aldrich, St. Louis, MO, USA
Potassium hydrogen carbonate	Acros Organics, Geel, BE
Recombinant human (rh) TGF-β1 protein (HEK293 derived)	Peprotec, Rocky Hill, NJ, US
Recombinant mouse (rm) IL-2 protein	Peprotec, Rocky Hill, NJ, US
rmIL-4 protein	Peprotec, Rocky Hill, NJ, US
Roti-clear (dewaxing)	Carl Roth, Karlsruhe, DE
RPMI cell culture medium	Anprotec, Bruckberg, DE
Schiff's reagent	Carl Roth, Karlsruhe, DE
TRIzol reagent	Ambion, Carslbad, CA, US
β-mercaptoethanol	Carl Roth, Karlsruhe, DE

2.1.3 Flow cytometric antibodies

Directed to	Conjugate, Final dilution, Reactivity, Clone	Provider
CCR4 (CD194)	PE, 1:500, armenian hamster anti-mouse, 2G12	Biolegend, San Diego, CA, US
CD103	BV421, 1:500, armenian hamster anti-mouse, 2E7	Biolegend, San Diego, CA, US
CD11b	PE/Cyanine 7, 1:500, rat anti-mouse, M1/70	Biolegend, San Diego, CA, US
CD11c	PE, 1:500, armenian hamster anti-mouse, N418	Biolegend, San Diego, CA, US
CD206	AF488, 1:500, rat anti-mouse, C068C2	Biolegend, San Diego, CA, US
CD25	APC, 1:500, rat anti-mouse, 3C7	Biolegend, San Diego, CA, US
CD3	FITC, 1:500, rat anti-mouse, 17A2	Biolegend, San Diego, CA, US
CD4	BV510, 1:500, rat anti-mouse, RM4-5	Biolegend, San Diego, CA, US
CD45	PE, 1:500, rat anti-mouse, ILB-5/25	Invitrogen, Rockford, IL, US
CD45	Alexa Fluor® 700, 1:500, rat anti-mouse, 30-F11	Biolegend, San Diego, CA, US
CD45	BV711, 1:500, rat anti-mouse, 30-F11	Biolegend, San Diego, CA, US
CD45R/B220	BV605, 1:500, rat anti-mouse, RA3-6B2	Biolegend, San Diego, CA, US
CD8α	AF488, 1:500, rat anti-mouse, 53-6.7	Biolegend, San Diego, CA, US
CD8α	BV421, 1:500, rat anti-mouse, 53-6.7	Biolegend, San Diego, CA, US
CTLA-4 (CD152)	PE/Cyanine7, 1:500, armenian hamster anti-mouse, UC10-4B9	Biolegend, San Diego, CA, US
F4/80	APC, 1:500, rat anti-mouse, BM8	Biolegend, San Diego, CA, US
Foxp3	PE, 1:250, rat anti-mouse, MF-14	Biolegend, San Diego, CA, US
GATA3	AF657, 1:250, mouse anti-human/mouse, L50-823	BD Pharming, Ashland, US
LAG-3 (CD223)	APC/Fire™ 750, 1:500, rat anti-mouse, C9B7W	Biolegend, San Diego, CA, US

Directed to	Conjugate, Final dilution, Reactivity, Clone	Provider
Ly-6G	PerCP/Cyanine5.5, 1:500, rat anti-mouse, 1A8	Biolegend, San Diego, CA, US
PD-1 (CD279)	FITC, 1:500, rat anti-mouse, 29F.1A12	Biolegend, San Diego, CA, US
SiglecF	PE, 1:500, rat anti-mouse, S17007L	Biolegend, San Diego, CA, US
TCRγδ	BV421, 1:500, armenian hamster anti-mouse, CL3	Biolegend, San Diego, CA, US

2.1.4 Animal experiments

Name	Provider
BALB/c strain	The Jackson Laboratory, Sulzfeld, DE
C57BL/6 strain	The Jackson Laboratory, Sulzfeld, DE
Control diet with w/10% energy from fat C 1090 - 10	Altromin, Lage, DE
Dermatophagoides pteronyssinus (used for i.n. HDM application)	ALK-Abelló, Hørsholm, DK
Glucose 20%	B. Braun, Melsungen, DE
Insuman Rapid 100 IE/ml	Sanofi-Aventis, Frankfurt, DE
Ketamine 10%	Medistar, Ascheberg, DE
Obesity-inducing diet with w/60% energy from fat (35%fat) C 1090 - 60	Altromin, Lage, DE
Xylazine (Rompun 2%)	Bayer, Leverkusen, DE

2.1.5 Buffers and solutions

Name	Composition
ACK-lysis buffer	H_2O, 0.15 M ammonium chloride, 10 mM potassium hydrogen carbonate, 0.5 mM EDTA
Digestion medium	RPMI with supplements, 40 U/ml DNase, 2 mg/ml collagenase
DMEM with FCS	DMEM, 10% FCS
Freezing medium	Advanced DMEM/F12, 10% DMSO, 10% FCS
Lavage buffer	50 ml PBS with 1 tablet cOmplete

Name	Composition
RPMI with supplements for cell isolation	RPMI, 1% penicillin/streptavidin, 1% L-Glutamine, 10% BSA
RPMI with supplements for T cell differentiation	RPMI, 1% penicillin/streptavidin, 50 µM β-mercaptoethanol, 1% L-Glutamine, 1% NEAA
Sample buffer (BAL cells)	PBS, 1% BSA
Sorting buffer	PBS, 0.5% BSA, 2 mM EDTA
Staining buffer	PBS, 0.5% BSA

2.1.6 Kits

Name	Provider
Agilent RNA 6000 pico kit	Agilent Technologies, Waldbronn, DE
BCA assay	Thermo Scientific, Rockford, IL, US
$CD4^+$ $CD62L^+$ Tcell isolation kit	Miltenyi Biotec, Bergisch Gladbach, DE
DNase kit	Qiagen, Hilden, DE
Fixation/permeabilization kit	Invitrogen, Carlsbad, CA, US
Proteome Profiler™ Mouse Adipokine Array	R&D Systems, Minneapolis, MN, US
Proteome Profiler™ Mouse XL Cytokine Array	R&D Systems, Minneapolis, MN, US
Qubit™ RNA HS assay kit	Invitrogen, Rockford, IL, US
RNeasy mini kit	Qiagen, Hilden, DE
RAL Diff-Quik™	RAL Diagnositics, Martillac, FR

2.1.7 Consumables

Name	Provider
30 µm & 100 µm strainer	Miltenyi Bergisch-Gladbach, DE
Cryotubes 1.5 ml	Sarstedt, Nümbrecht, DE
Flow cytometry tubes 5 ml, 75x12 mm	Sarstedt, Nümbrecht, DE
Fuji medical x-ray film 100NIF	Fujifilm, Tokyo, JP
Heparin tubes 1.3 ml	Sarstedt, Nümbrecht, DE
LS/MS columns	Miltenyi Bergisch-Gladbach, DE
M/C tubes (gentleMACS)	Miltenyi Bergisch-Gladbach, DE
Microscope sildes	Marienfeld, Lauda-Königshofen, DE
RNase free tubes 1.5 ml	Thermo Scientific, Langenselbold, DE
QIAshredder column	Qiagen, Hilden, DE

2.1.8 Software

Name	Provider
ClustVis	BIIT, Tartu, EE
FlowJo/SeqGeq	BD, Ashland, US
GraphPad Prism 9	GraphPad, San Diego, CA, US
ImageJ/Fiji	Open Source, developed by Wayne Rasband, https://imagej.net/software/fiji/

2.2 *In vivo* experimental setup

The care of the animals was carried out by trained animal care personnel according to the respectively valid instructions. Mice were housed in the intended groups (Table 1) in individually ventilated cages. Mice had access to food and water *ad libitum* and the rooms had an electronically controlled 12h/12h day/night rhythm. Nestlets made of dust-free cotton fibers and wooden boards with holes served as enrichment. All animal experiments were performed under federal guidelines for the use and care of laboratory animals and were authorized by the local responsible authorities (Nr. G65/2018, Ex-8-2021, *Regierungspräsidium Gießen*, Germany) and included an ethical evaluation. After weaning, i.e. at the age of three to four weeks, animals assigned to the HFD groups were given a diet with 60% calories from fat (see Table 1 and Figure 5). Animals in the normal diet (ND) groups were given an associated control diet instead. Blood samples for measurement of immunoglobulin G (IgG) antibody response and metabolic analyses were taken via the *vena facialis* at ages of 4, 12, 14, 15, and 18 weeks and finally, at the age of 20 weeks. At 17 weeks of age, a glucose tolerance test (GTT) was performed in all animals, and at 19 weeks of age, an insulin tolerance test (ITT) was conducted to test the metabolic status of the animals. In a subgroup of the animals additional GTT and ITT were performed at 13 and 15 weeks of age. At the age of 15 weeks, the intranasal (i.n.) HDM extract application was initiated under anesthesia (200 µl intra peritoneal [i.p.] injection of 50 mg/kg body weight ketamine + 15 mg/kg body weight xylazine) to induce the asthma phenotype. The mixed type 2/non-type 2 phenotype was induced by five i.n. applications at intervals of one week with 50 µl of allergen (HDM) at a low concentration (1.3 mg/ml *Der p* in PBS).

Finally, mice were euthanized by a lethal dose of narcosis (200 µl i.p. injection of 400 mg/kg body weight ketamine + 40 mg/kg body weight xylazine), blood was drawn via the *arteria axillaris* and subsequent organ removal followed.

Table 1: Classification of the experimental and control groups.

Group	Genetic background	Diet	Induction of a mixed asthma phenotype
1	BALB/c or C57BL/6	Normal diet	No, PBS control
2	BALB/c or C57BL/6	Normal diet	Yes, HDM
3	BALB/c or C57BL/6	High fat diet	No, PBS control
4	BALB/c or C57BL/6	High fat diet	Yes, HDM

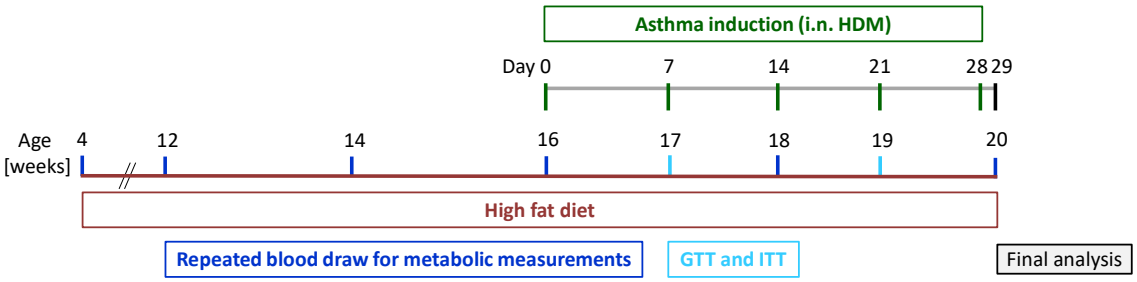

Figure 5: Schematic representation of the experimental outline
i.n.: intranasal, HDM: house dust mite, GTT: glucose tolerance test, ITT: insulin tolerance test

2.3 Glucose/Insulin Tolerance Test

For the GTT, food was withdrawn from animals for 6 hours (fasting). Afterwards, basal glucose levels were measured and glucose (50 mg/animal) was i.p. injected. This was followed by blood glucose measurements after 15, 30, 60, 90, and 120 minutes. At each time point, a drop of blood was taken from the tail vein and the blood glucose level was determined with an Accu Check. The ITT was performed two weeks later according to the same scheme, but instead of glucose, insulin (0.75 IU/kg body weight) was injected.

2.4 Plasma extraction

Mice were sacrificed as described in chapter 2.2 *In vivo* experimental setup. Final blood was drawn directly from the *arteria axillaris* into heparin tubes to isolate the plasma. Therefore, samples were kept at room temperature (RT) for at least 2 h and then

centrifuged at 4,000 rpm for 20 min at 4 °C. The clear plasma supernatants were removed and subsequently frozen at -20 °C for further analysis. A volume of 80 µl of each plasma sample were given to the central laboratory of the University Hospital of Gießen and Marburg for measurement of the metabolic parameters glucose, cholesterol, HDL-, LDL-, non-HDL cholesterol, and triglycerides. Remaining plasma was used to determine HDM-specific IgGs (see 2.5 Enzyme-linked immunosorbent assay).

2.5 Enzyme-linked immunosorbent assay

Enzyme-linked immunosorbent assay (ELISA) was used to determine HDM-specific IgGs in plasma. The protocols were optimized and carried out by Ms. Andrea Berlin (medical doctoral student in our group) within her thesis work.

2.6 Bronchoalveolar lavage cell isolation and staining

For BAL cell isolation, airways were rinsed with lavage-buffer. The obtained BALs were centrifuged at 1,300 rpm for 10 min at 4 °C and the supernatants were frozen at -20 °C for further analysis (see 2.10 Proteome Profiler Antibody Arrays). The cell pellets were resuspended in 1 ml sample buffer and subsequently counted. Therefore, 50 µl were transferred to 10 ml CASYton and measured with the CASY cell counter. For the cytospin, 100 µl of the cell suspensions were diluted by adding 300 µl sample buffer. 200 µl of the diluted BAL cells were centrifuged onto a glass slide with the cytocentrifuge at 700 rpm for 5 min. Prior to the Diff-Quik staining, the slides were dried for at least 1 h. The staining was conducted using the RAL Diff-Quik kit as follows:

- 1 min fixation solution
- 1 min Diff-Quik I
- 30 s Diff-Quik II
- rinsing with demineralized water

Eosinophils, neutrophils, macrophages, and lymphocytes were differentiated by characteristic morphologic criteria.

2.7 Cell isolation from lung and adipose tissue

2.7.1 Lung cell isolation

The lungs were perfused via the heart with PBS. The left lobe of the lungs were tied up and flushed with 6% paraformaldehyde (PFA) for tissue fixation. These lobes were stored in 6% PFA for later histological preparation (see 2.9 Histological preparation and staining). Right lobes were removed and transferred with 5 ml digestion medium to gentleMACS C tubes and subsequently to the gentleMACS dissociator for 16 s. After shaking incubation with 170 rpm for 30 min at 37 °C, the lung cell suspensions were again dissociated with the gentleMACS dissociator for 16 s. Suspensions were filtered through a 100 µm strainer, the strainer was washed with 5 ml RPMI with supplements and cells were centrifuged at 1,300 rpm for 5 min at 4 °C. Supernatants were discarded, pellets resuspended in 2 ml ACK lysis buffer and incubated for 2 min at RT. Red blood cell lyses were stopped by addition of 8 ml RMPI with supplements, cells were filtered through a 30 µm strainer and centrifuged at 1,300 rpm for 5 min at 4 °C. Supernatants were discarded and pellets resuspended in 5 ml RPMI with supplements. For cell counting, 5 µl were transferred to 10 ml CASYton and measured with the CASY cell counter. $2.5x10^6$ cells were transferred to flow cytometry tubes for $CD45^+$-PE staining and subsequent flow cytometric cell sorting (see 2.12 BD Rhapsody single cell analysis). The remaining cells were centrifuged at 1,300 rpm for 5 min at 4 °C, the supernatants discarded and pellets resuspended in staining buffer for the subsequent flow cytometric protocol (see 2.8 Flow cytometric analysis).

2.7.2 Visceral adipose tissue cell isolation

Visceral adipose tissues were taken and the ovaries and blood vessels were carefully removed. A small part of the visceral adipose tissues was directly snap frozen in liquid nitrogen and stored at -80 °C for later RNA-isolation (see 2.11 RNA-isolation from visceral adipose tissue). Another small part was transferred to 6% PFA for later histological preparation (see 2.9 Histological preparation and staining). Remaining visceral adipose tissues were dissected into small pieces and shaken for 30 min at 37 °C with 2 ml digestion medium. Following this incubation, cells were smashed through a 100 µm strainer, the digestions were stopped by addition of 8 ml RPMI and centrifugation at

1,300 rpm for 5 min at 4 °C. Thereafter, the cell pellets at the bottom and the adipocytes floating on top were processed separately. First, adipocytes in the floating layer were transferred to a 12-well plate and 1 ml DMEM with 10% FCS were added and cells were incubated for 48 h at 37 °C. After the 48 h incubation of the adipocytes, the supernatants were removed and frozen at -20 °C for further analysis (see 2.10 Proteome Profiler Antibody Arrays and 2.13.3 Stimulation and analysis of differentiated T cells). Then, 500 µl of DMEM without supplements were added to the adipocytes and incubated for another 48 h. Hereafter, also these supernatants were removed and frozen at -20 °C. The adipocytes were scraped off and transferred to new tubes. To remove all remaining adipocytes from the wells, 1 ml PBS was used to wash each well and then transferred to the corresponding tube. The samples were frozen at -20 °C for later protein determination. The cell pellets resulting from the above-mentioned centrifugation were resuspended, filtered through a 30 µm strainer and centrifuged at 1,300 rpm for 5 min at 4 °C. The supernatants were discarded and pellets resuspended in staining buffer for subsequent flow cytometry (see 2.8 Flow cytometric analysis).

2.8 Flow cytometric analysis

Cells isolated from lung and visceral adipose tissue (see 2.7 Cell isolation from lung and adipose tissue) or differentiated T cells (see 2.13 *In vitro* differentiation and stimulation) were transferred to a V-bottom plate and centrifuged at 1,500 rpm for 3 min at 4 °C. The supernatants were discarded and 20 µl Fc-Block added. Subsequently, 50 µl of respectively diluted and appropriately combined antibodies directed to surface markers were added to the respective samples, mixed and incubated for 30 min at 4 °C in the dark. Diluted single antibodies as single staining controls or staining buffer without antibodies as unstained control were processed equally to the combined antibodies. Afterwards, 100 µl of staining buffer were added and plates centrifuged at 1,500 rpm for 3 min at 4 °C. For the fixation of the cells of an extracellular staining (see below for intracellular staining), the supernatants were discarded and 100 µl of 2% PFA were added, cells resuspended and incubated for 20 min at 4 °C in the dark. The fixation was stopped with 100 µl staining buffer and the plates centrifuged at 1,500 rpm for 3 min at 4 °C. Cells were washed again with 200 µl staining buffer and resuspended afterwards in 200 µl staining buffer. For analysis, cells were transferred to flow cytometric tubes.

If staining of intracellular antigens was applied, this was performed subsequent to a preceding extracellular staining. Therefore, cells were centrifuged, supernatant was discarded and 200 µl of fixation/permeabilization solution were added, resuspended and incubated for 30 min at 4 °C in the dark. The fixation was stopped by centrifugation at 1,500 rpm for 3 min at 4 °C. The cells were washed with 200 µl permeabilization buffer, the supernatants were discarded and 20 µl Fc-Block added. Then, 50 µl of respectively diluted and appropriately combined antibodies directed to intracellular markers were added to the respective samples, mixed and incubated for 30 min at 4 °C in the dark. Diluted single antibodies as single staining controls or staining buffer without antibodies as unstained control were processed equally to the combined antibodies. Afterwards, 100 µl permeabilization buffer were added, cells were centrifuged at 1,500 rpm for 3 min at 4 °C and supernatants discarded. The cells were washed again with 200 µl staining buffer and then resuspended in 200 µl staining buffer. For analysis, the cells were transferred to flow cytometric tubes. All samples were measured using an Attune NxT Flow or FACS Canto II Cytometer. Compensation and gating were done with the FlowJo software. Initially, all cells were gated to exclude debris based on the forward and sideward scatter, duplicate cells were excluded, and leukocytes were defined by $CD45^+$. The further gates were set on the associated surface markers for each cell type, i.e. $CD4^+$ cells; $CD8^+$ cells; B cells: $B220^+$; eosinophils: $SiglecF^{+high}$, $CD3^-$; neutrophils: $Ly6G^+$, $CD3^-$; TCRγδ cells: $TCR\gamma\delta^+$, $CD4^-$, $CD8^-$; M1 macrophages: $CD11c^+$, $F4/80^+$, $CD11b^-$, $CD206^-$, $CD103^-$; M2 macrophages: $CD11b^+$, $CD206^+$, $F4/80^+$, $CD11c^-$, $CD103^-$; Th2 cells: $CD4^+$, $CCR4^+$, $GATA3^+$; Treg cells: $CD4^+$, $CD25^+$, $Foxp3^+$; and co-inhibitory receptors: $PD\text{-}1^+$, $CTLA\text{-}4^+$, $LAG\text{-}3^+$.

2.9 Histological preparation and staining

The previously fixed in 6% PFA lungs and adipose tissues were embedded in warm 2% agar. Hereafter, 2 mm thin cuts of the solidified agar with the tissue specimens were prepared and embedded again in 2% agar. After cooling, the blocks were transferred to embedding cassettes and paraffin embedding was done in the Pathology Department of the University Hospital of Gießen and Marburg. Afterwards, 3 µm sections were made from the paraffin blocks using a microtome. Lung sections were stained with hematoxylin and eosin (H&E) and periodic acid-Schiff (PAS) to visualize tissue inflammation

and mucus producing cells. Adipose tissue sections were stained with H&E for subsequent quantification of adipocyte size of up to 50 adjacent adipocytes per animal, performed using ImageJ as described by Parlee et al. (Parlee et al., 2014). In Table 2 the steps of both staining procedures are listed.

Table 2: PAS and H&E staining procedure.

PAS	H&E
• 5 min PBS • rinse VE-H_2O • 10 min periodic acid 0.5% • 3 min running tap water • rinse VE-H_2O • 15 min Schiff's reagent • 15 min running tap water • rinse VE-H_2O • 1 min 70% ethanol • 1 min 80% ethanol • 1 min 96% ethanol • 1 min 100% ethanol • 15 min Roti-Clear • mount coverslip using Entellan	• 5 min PBS • rinse VE-H_2O • 3 min hematoxylin • 5 min running tap water • rinse VE-H_2O • 2 min eosin with glacial acetic acid • rinse VE-H_2O • 1 min 70% ethanol • 1 min 80% ethanol • 1 min 96% ethanol • 2x 1 min 100% ethanol • 2x 10 min Roti-Clear • mount coverslip using Entellan

2.10 Proteome Profiler Antibody Arrays

BALs were analyzed with a Proteome Profile Mouse XL Cytokine Array, which was carried out by Ms. Andrea Berlin (medical doctoral student in our group) within her thesis work. Adipocyte supernatants were analyzed with the Proteome Profiler Mouse Adipokine Array. The analyses with both arrays were performed as described in the manufacturer's protocol. For the cytokine array, BAL samples of 5-6 animals were pooled per ND/HDM and HFD/HDM groups of either BALB/c or C57BL/6 mice, respectively. For the adipokine array, the adipocyte supernatants were pooled from each experimental group from the C57BL/6 mice (n=5-6). A bicinchoninic acid (BCA) assay was conducted as described in the manufacturer's protocol in advance to calculate the protein amounts of the adipocyte supernatants, and subsequently, the volume of each sample was adjusted to the group with least protein amount. For the cytokine/adipokine arrays, the pooled samples were incubated with an antibody coupled membrane and visualized using

chemiluminescent detection reagents. The membranes were analyzed with Fiji to determine the optical density of each dot.

2.11 RNA-isolation from visceral adipose tissue

The previously prepared visceral adipose tissue samples (see 2.7.2 Visceral adipose tissue cell isolation) were used to isolate RNA for transcriptomic analysis via sequencing. gentleMACS M tubes with 1 ml TRIzol were prepared and stored on ice. The tissue samples were weighed and added into the M tubes with TRIzol. For tissue dissociation, the M tubes were put onto the gentleMACS dissociator using the program RNA 2.01 for 84 s. Afterwards, the tubes were incubated for 5 min at RT and then centrifuged at 2,000 rpm for 10 min at 4 °C. The following steps are described exemplarily for one sample but were processed in parallel. While leaving the oily upper phase in the tube, the solution (max. 750 µl) was given onto a QIAshredder column and centrifuged at 13,000 rpm for 2 min at 4 °C. In case of higher volumes, a new collection tube was used to collect the samples. The flow-throughs were pooled and 200 µl chloroform added, mixed by inversion for 15 s and incubated for 2 min at RT. After centrifugation at 12,000 g for 15 min at 4 °C, the clear upper phase was transferred into a new RNase-free tube. 500 µl isopropanol were added, incubated for 30 min at -80 °C and centrifuged afterwards at 12,000 g for 10 min at 4 °C. The supernatant was discarded and the RNA pellet washed with 1 ml 70% ethanol. After centrifugation at 12,000 g for 5 min at 4 °C, the supernatant was discarded again and the pellet resuspended in 40 µl RNase free water. The following cleanup of the RNA was done according to the manufacturer's protocol of the RNeasy Mini kit. As such, 310 µl of RLT buffer were added to the sample and subsequently mixed with 350 µl 70% ethanol. The solution was transferred to the RNeasy columns and centrifuged at 10,000 rpm for 15 s at RT, the flow-through was discarded. 350 µl of the RW1 buffer were added and centrifuged at 10,000 rpm for 15 s at RT, the flow-through was discarded again. For the DNase treatment, 10 µl of DNase I were mixed with 70 µl RDD buffer and transferred onto the membrane. The RNeasy column was incubated for 15 min at RT. 350 µl of RW1 buffer were added and centrifuged at 10,000 rpm for 15 s at RT, the flow-through was discarded. Subsequently, the RNeasy column was washed twice with 500 µl RPE buffer and centrifuged 10,000 rpm for 15 s at RT and for 2 min in the second round. The RNeasy column was

placed onto a new 2 ml collection tube and centrifuged at full-speed for 1 min at RT. The RNeasy column was then placed onto a new 1.5 ml RNase-free tube, 40 µl RNase free water were added onto the membrane and incubated for 1 min at RT. After centrifugation at 10,000 rpm for 1 min at RT the eluate was again pipetted on the membrane and centrifuged at 10,000 rpm for 1 min at RT into the same 1.5 ml RNase-free collection tube. The RNA concentration was determined using the Qubit RNA HS assay kit and the RNA quality was examined using the Agilent RNA 6000 Pico Kit. Library preparation using the TruSeq Stranded mRNA kit and NextSeq high output sequencing of the RNA was done at the Core Facility for Next Generation Sequencing by Dr. Andrea Nist. Sequencing raw data were processed by Mr. Fahd Alhamdan.

2.12 BD Rhapsody single cell analysis

For BD Rhapsody single cell analysis, $CD45^+$ cells were sorted from whole lung cell preparations (see 2.7.1 Lung cell isolation). An unstained control sample was prepared from pooled cells from the experimental groups 2 and 4. Lung cell samples were centrifuged at 1,500 rpm for 3 min at 4 °C, supernatants were discarded and cells washed with 200 µl sorting buffer. 20 µl of Fc-Block were added with subsequent addition of 0.5 µl of CD45-PE-antibody in 200 µl sorting buffer; to the unstained control 200 µl sorting buffer were added without the CD45-PE-antibody. After adequate mixing, samples were incubated for 30 min at 4 °C in the dark. Thereafter, 400 µl of sorting buffer were added and tubes centrifuged at 1,500 rpm for 3 min at 4 °C with two repeating washing steps. After the final washing the step, the samples were resuspended in 300 µl sorting buffer and directly given to Dr. Hartmann Raifer at the Flow Cytometry Core Facility, Marburg for flow cytometric cell sorting of PE positive $CD45^+$ cells. Resulting $CD45^+$ cells were centrifuged at 1,500 rpm for 5 min at 4 °C. The supernatants were discarded and the cells resuspended in 1 ml freezing medium. Cells were transferred to cryotubes and frozen for 24 h at -80 °C in a freezing container, before being stored at liquid nitrogen. The subsequent BD Rhapsody single cell analysis was performed by Ms. Kim Pauck in our Core Facility for Single Cell Multiomics, Marburg. For this purpose, cell samples from 3 animals of each experimental group of the C57BL/6 mice were tagged for later identification of individual animals during data analysis. Using a targeted immune panel, 400 genes were sequenced and application of 49 AbSeqs

enabled the complex analysis of surface marker expression for each cell. Raw data were processed using the BD pipeline on SevenBridges and then further analyzed and visualized with SeqGeq.

2.13 *In vitro* differentiation and stimulation

2.13.1 Isolation of $CD4^+$ $CD62L^+$ splenocytes

For the isolation of murine naïve T cells, spleens were taken from C57BL/6 mice after cervical dislocation. Spleens were meshed with the plunger of a 1 ml syringe through a 100 µm strainer and the resulting cell suspensions were washed with 5 ml RPMI. After centrifugation at 1,300 rpm for 5 min at 4 °C the supernatants were discarded, pellets resuspended in 2 ml ACK lysis buffer and incubated for 2 min at RT. Red blood cell lyses were stopped by addition of 8 ml RMPI with supplements. Cells were filtered through a 30 µm strainer into a new 15 ml tube and centrifuged at 1,300 rpm for 5 min at 4 °C. The supernatants were discarded, pellets resuspended in 10 ml buffer (see $CD4^+CD62L^+$ T cell isolation kit from Miltenyi Biotec) and cells were counted with the CellDrop. Further isolation of naïve T cells was done with the $CD4^+CD62L^+$ T cell isolation kit from Miltenyi Biotec, with slightly adapted incubation times. Briefly, not more than 10^8 cells were resuspended in 400 µl buffer and incubated with 100 µl $CD4^+$ T cell biotin-antibody cocktail for 10 min at 4 °C. Afterwards, 300 µl buffer and 200 µl anti-biotin MicroBeads were added and incubated for 15 min. Magnetic separations were done by applying the cell suspensions onto LS columns, washing with 3 ml buffer and collecting the cells in the flow through. The collected $CD4^+$ T cell suspensions were centrifuged and re-suspended in 800 µl buffer. 200 µl CD62L MicroBeads were added and incubated for 15 min at 4 °C. The cells were washed with 10 ml buffer, centrifuged and resuspended in 500 µl buffer. The second magnetic separations for positive selections of $CD62L^+$ cells were done by applying the cell suspensions onto the MS columns and subsequent washing two times with 500 µl buffer. By removing the columns from the magnet, adding 1 ml buffer onto the columns and immediately flushing out the cells with the plunger, the $CD4^+CD62L^+$ T cells were collected.

2.13.2 Differentiation of naïve T cells to Th2 and Treg cells

Naïve $CD4^+CD62L^+$ T cells isolated as described above were counted with the CellDrop and seeded in 600 µl of Treg, Th2 or Th0 differentiation media (see Table 3), respectively, with approximately 300,000 cells/well in a 48-well plate coated with 5 µg/ml anti-CD3 and cultured for 72 h. Afterwards, successful differentiation was confirmed via flow cytometric analysis with staining of CD4, GATA3, and CCR4 for Th2 cells and CD4, CD25, and Foxp3 for Treg cells (see 2.8 Flow cytometric analysis).

Table 3: Media composition for the differentiation of Th2 and Treg cells, and Th0 cells as control.

Component	Th2	Treg	Th0
anti-CD28	1 µg/ml	1 µg/ml	1 µg/ml
anti-IFNγ	5 µg/ml	5 µg/ml	-
anti-IL-4	-	5 µg/ml	-
rhTGFβ	-	10 ng/ml	-
rmIL-4	20 ng/ml	-	-
rmIL-2	50 U/ml	100 U/ml	50 U/ml

2.13.3 Stimulation and analysis of differentiated T cells

In vitro activation of differentiated Th2 and Treg cells was achieved by another 48 h cultivation on a 5 µg/ml anti-CD3 coated 96-well plate (Figure 6). For this purpose, previously differentiated $CD4^+$ T cells (see 2.13.2 Differentiation of naïve T cells to Th2 and Treg cells) were seeded in 100 µl media with 100,000 cells per well. The successful activation was confirmed by flow cytometric analysis with staining of PD-1, CTLA-4, and LAG-3 cells within the Th2 or Treg cell population. To investigate whether adipocyte-derived components can inhibit the activation of T cells, the differentiated T cells were incubated, in presence of anti-CD3 and rmIL-2, with a pool of supernatants from *in vitro* cultured adipocytes obtained from HFD-fed mice or DMEM with 10% FCS as negative control. After incubation for 48 h the cells were diluted 1:2 by removing the old media and resuspending the cells in 200 µl of fresh media. Cells of one well were then transferred into two new wells and incubated for another 48 h without the adipocyte supernatant. Flow cytometric analysis was used to measure the changes.

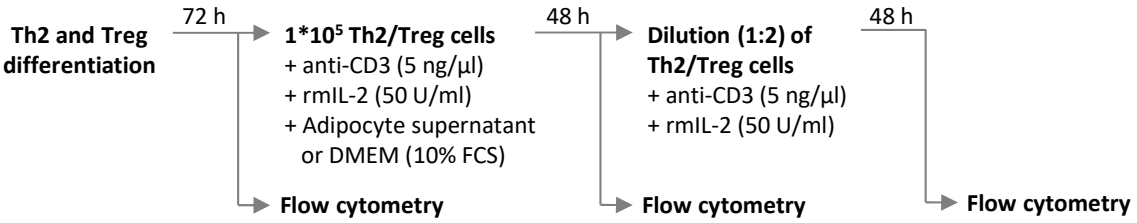

Figure 6: Schematic representation of the *in vitro* stimulation experiment
Differentiated Th2 and Treg cells with induced activation were incubated with adipocyte supernatant.

2.14 Statistics and bioinformatics

GraphPad Prism 9 software was used to analyze the results. If not indicated otherwise, data are presented as box and whiskers plot with min to max and median. Two tailed student's t-tests were performed for comparison of two groups from the animal experiments. To maintain conciseness within the figures, only group comparisons with biological relevance are depicted. One tailed student's t-tests were performed for the *in vitro* data. Outliers were defined and excluded via ROUT with Q=1%. The heatmap representing results of the adipokine array was created with ClustVis. Principal Component Analysis (PCA) plot was performed by Dr. Clemens Thölken from the Institute for Medical Bioinformatics and Biostatistics.

3. Results

3.1 Strain-dependent differences in lung inflammation are linked to weight gain in a mouse model of obesity-associated asthma

3.1.1 Metabolic changes and weight gain in a HFD mouse model

An HDM mouse model in combination with a continuous HFD for a total of 16 weeks was used to investigate obesity-associated alterations of the inflammatory phenotype of an induced AAI. Mice with two different genetic backgrounds, specifically BALB/c and C57BL/6, were used to cover known differences in weight gain in response to HFD and exhibition of immune responses (Fukushima et al., 2006, Jovicic et al., 2015). Plasma levels of metabolic parameters, GTT, and ITT as well as weight gain were analyzed to evaluate systemic outcomes of the HFD in BALB/c and C57BL/6 mice. Both strains receiving a HFD (60% calories from fat) showed after eight weeks significantly increased plasma levels of metabolic parameters such as cholesterol, LDL cholesterol, and glucose in comparison to the ND-fed mice (Figure 7). Metabolic parameters in the HFD groups remained at increased levels over time and did not accelerate further (data not shown). Plasma levels of triglycerides, HDL and non-HDL cholesterol were also increased in both strains receiving a HFD (data not shown). This indicates that continuous consumption of HFD causes similar alterations of metabolic parameters in plasma of BALB/c and C57BL/6 mice.

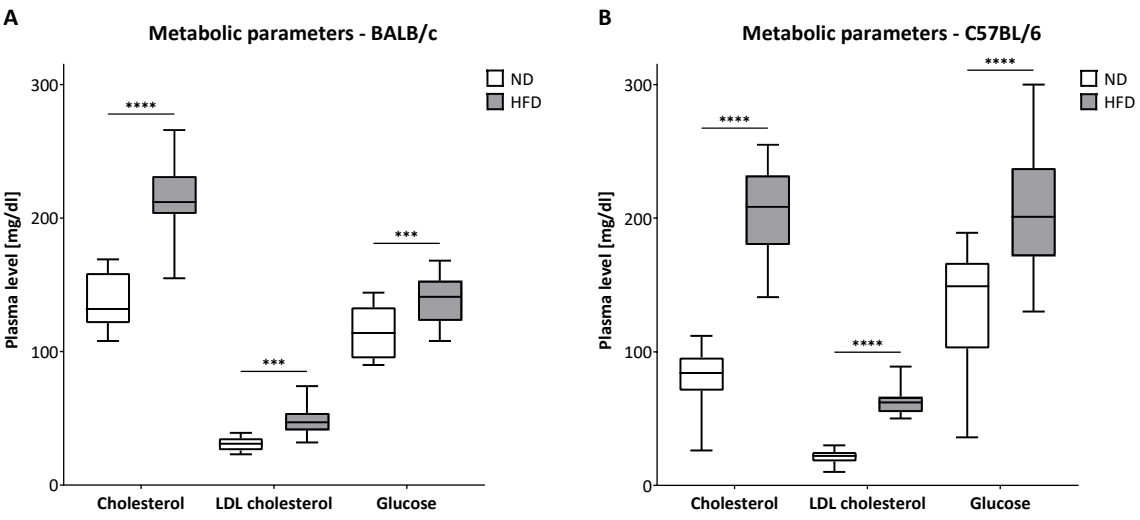

Figure 7: Increased plasma levels of metabolic parameters in HFD-fed BALB/c and C57BL/6 mice.
Plasma levels of cholesterol, low-density lipoprotein (LDL) cholesterol, and glucose measured after eight weeks on high fat diet (HFD) or normal diet (ND) in BALB/c mice (A) and C57BL/6 mice (B), n=9-22, *** $p \leq 0.001$, **** $p \leq 0.0001$.

A frequent co-morbidity of obesity is T2D, which is characterized by a resistance to insulin and high blood sugar. As diagnostic tools for diabetes, oral GTT and/or ITT are commonly used in patients and can be conducted to measure insulin resistance or sensitivity, respectively (American Diabetes Association, 2020, Okita et al., 2014). Therefore, in addition to the metabolic plasma parameters, fasting glucose levels were measured in the blood after i.p. injection of glucose or insulin to examine further metabolic alterations in response to HFD. No strain dependent differences were seen in the GTT or ITT when comparing HFD groups to the respective ND groups. In both cases, significant increases in the area under curve (AUC) could be observed in the HFD groups, indicating that HFD-fed mice of both strains developed an impaired glucose tolerance, as well as an attenuated hypoglycemic response to insulin injection (Figure 8). However, in BALB/c mice, the ND group with HDM application showed a slightly higher glucose intolerance compared to the PBS group. This effect was not seen in the C57BL/6 strain. Furthermore, HFD/HDM BALB/c mice demonstrated an increase in the ITT values compared to HFD/PBS group, whereas in turn a significant reduction was seen between the two HFD groups of C57BL/6 mice. Nevertheless, both strains showed metabolic features of T2D in response to the HFD.

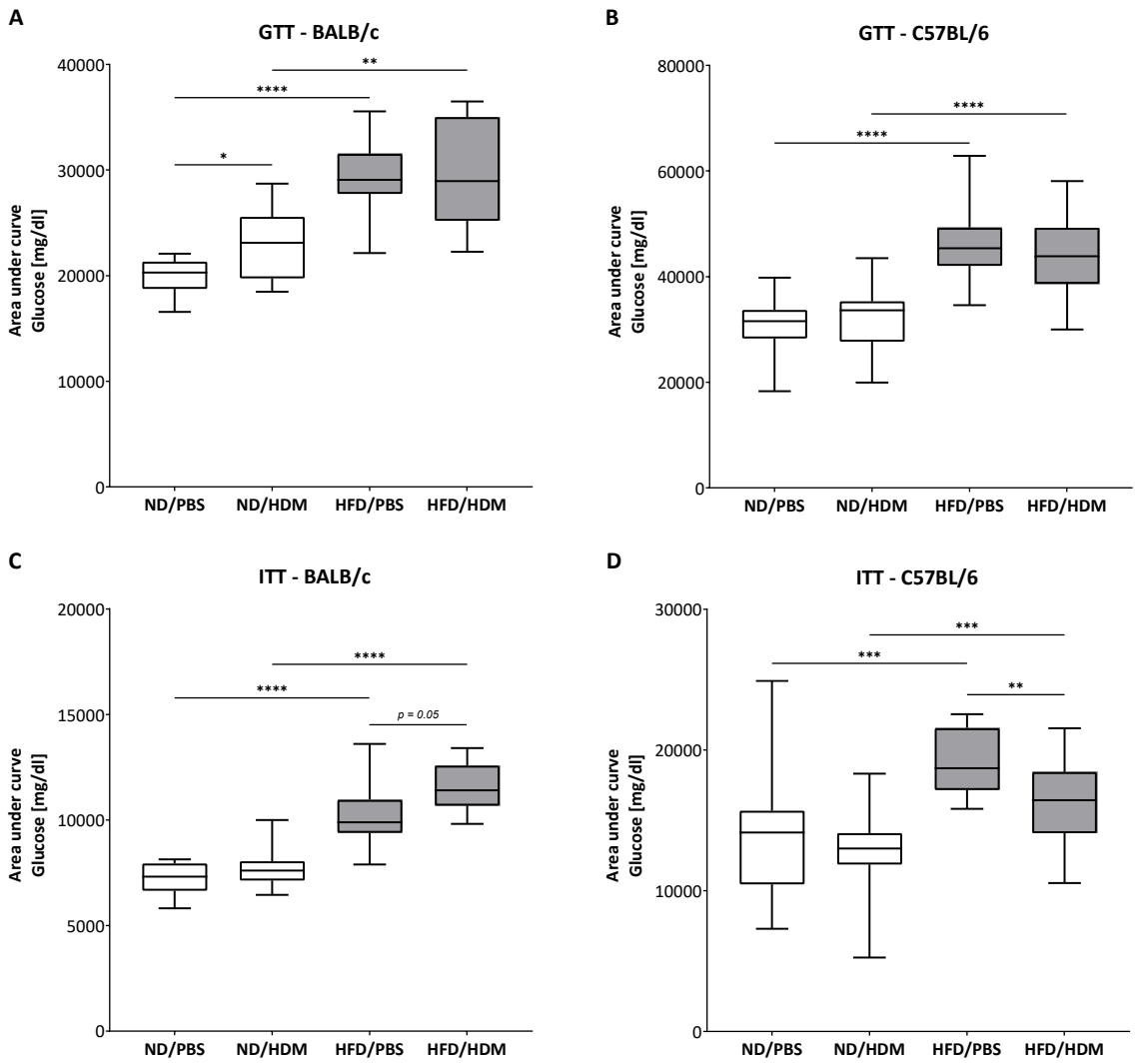

Figure 8: Impaired glucose tolerance and attenuated hypoglycemic response to insulin injection in HFD-fed BALB/c and C57BL/6 mice.
Area under curve (AUC) depicts the glucose tolerance test (GTT) and insulin tolerance test (ITT) of BALB/c mice (A/C) and C57BL/6 mice (B/D). After 6 h of fasting, blood glucose was measured before and 15, 30, 60, 90, and 120 min after glucose injection (50 mg/animal) or insulin injection (0.75 IU/kg body weight), n=12-20, * $p \leq 0.05$, ** $p \leq 0.01$, *** $p \leq 0.001$, **** $p \leq 0.0001$, ND: normal diet, PBS: phosphate-buffered saline, HDM: house dust mite, HFD: high fat diet.

Although BALB/c mice showed metabolic changes in GTT, ITT, and in metabolic parameters after receiving a HFD, they did not gain weight when fed with a HFD in comparison to the ND-fed mice as shown in Figure 9A. At several times significant but still low differences in body weight were seen between HFD and ND-fed BALB/c mice (e.g. at the age of 17 weeks 22.4 ± 1.4 g vs. 21.3 ± 0.9 g). On the contrary and consistent with the literature (Jovicic et al., 2015), C57BL/6 mice on a HFD significantly gained weight starting at 2 weeks of HFD resulting in ~20% higher body weight after 16 weeks of HFD in comparison to the ND groups (28.9 ± 4.2 g vs. 23.2 ± 1.7 g, Figure 9B). HDM

application had no influence on weight gain in neither of the two mouse strains. In mice, there is so far no specific distinction between being overweight or obese, in contrast to the commonly used BMI evaluation in humans. HFD-fed C57BL/6 mice will be considered obese in the following descriptions.

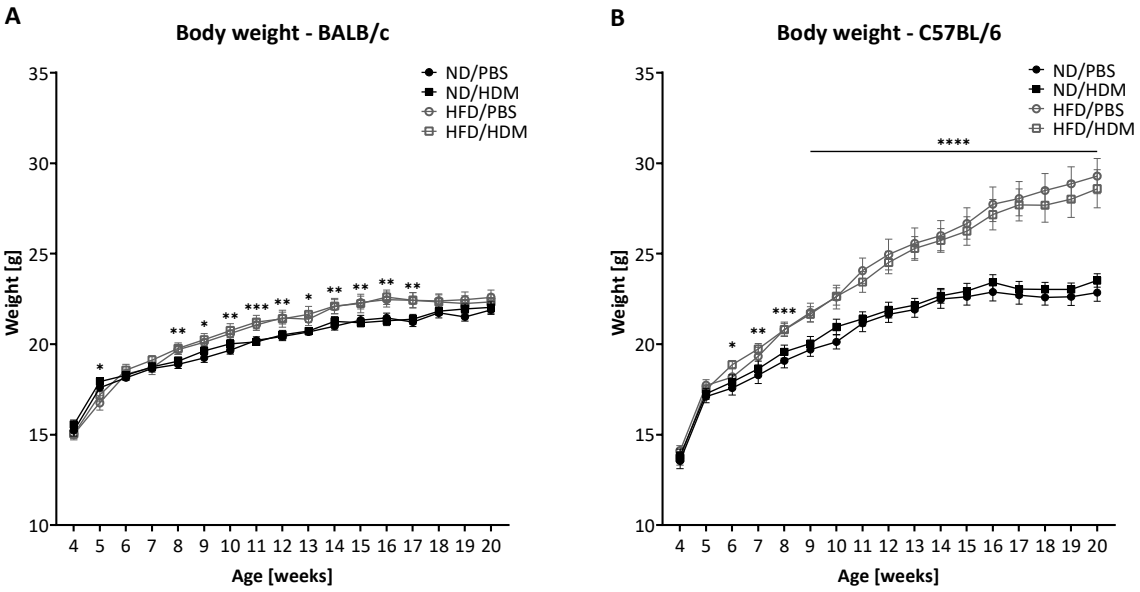

Figure 9: Weight gain in response to a HFD only in C57BL/6 mice, but not in BALB/c mice.
Body weight of BALB/c mice (A) and C57BL/6 mice (B) shown as mean ± standard error of the mean (SEM), significances were calculated between the mean of ND groups and the mean of HFD groups as HDM-application had no influence on weight gain, n=12-19, * $p \leq 0.05$, ** $p \leq 0.01$, *** $p \leq 0.001$, **** $p \leq 0.0001$, ND: normal diet, PBS: phosphate-buffered saline, HDM: house dust mite, HFD: high fat diet.

3.1.2 Investigation of cellular changes in the adipose tissue of HDM-exposed mice

Apart from investigating metabolic changes in response to HFD, alterations in adipose tissue such as adipocyte hypertrophy and presence of inflammatory cells were assessed. Hypertrophic adipocytes are not only associated with obesity but also by increased production of inflammatory cytokines (Makki et al., 2013). The adipocyte size was used to investigate whether the adipocytes were altered by HFD and whether this correlated with weight gain. H&E stained sections from visceral adipose tissue were used to measure and quantify the adipocyte areas (Figure 10A). Interestingly, adipocytes of HFD-fed BALB/c mice, which did not gain weight compared to ND-fed mice, increased significantly in size (Figure 10B). An increase was seen in the adipocytes of C57BL/6 mice

receiving a HFD as well (Figure 10C), however, the hypertrophy was more pronounced compared to BALB/c mice (mean adipocyte area for HFD-fed BALB/c mice: 1889 µm^2 vs. HFD-fed C57BL/6 mice: 3127 µm^2). Thus, both strains developed an adipocyte hypertrophy in response to HFD, even though BALB/c and C57BL/6 mice gained differentially in weight.

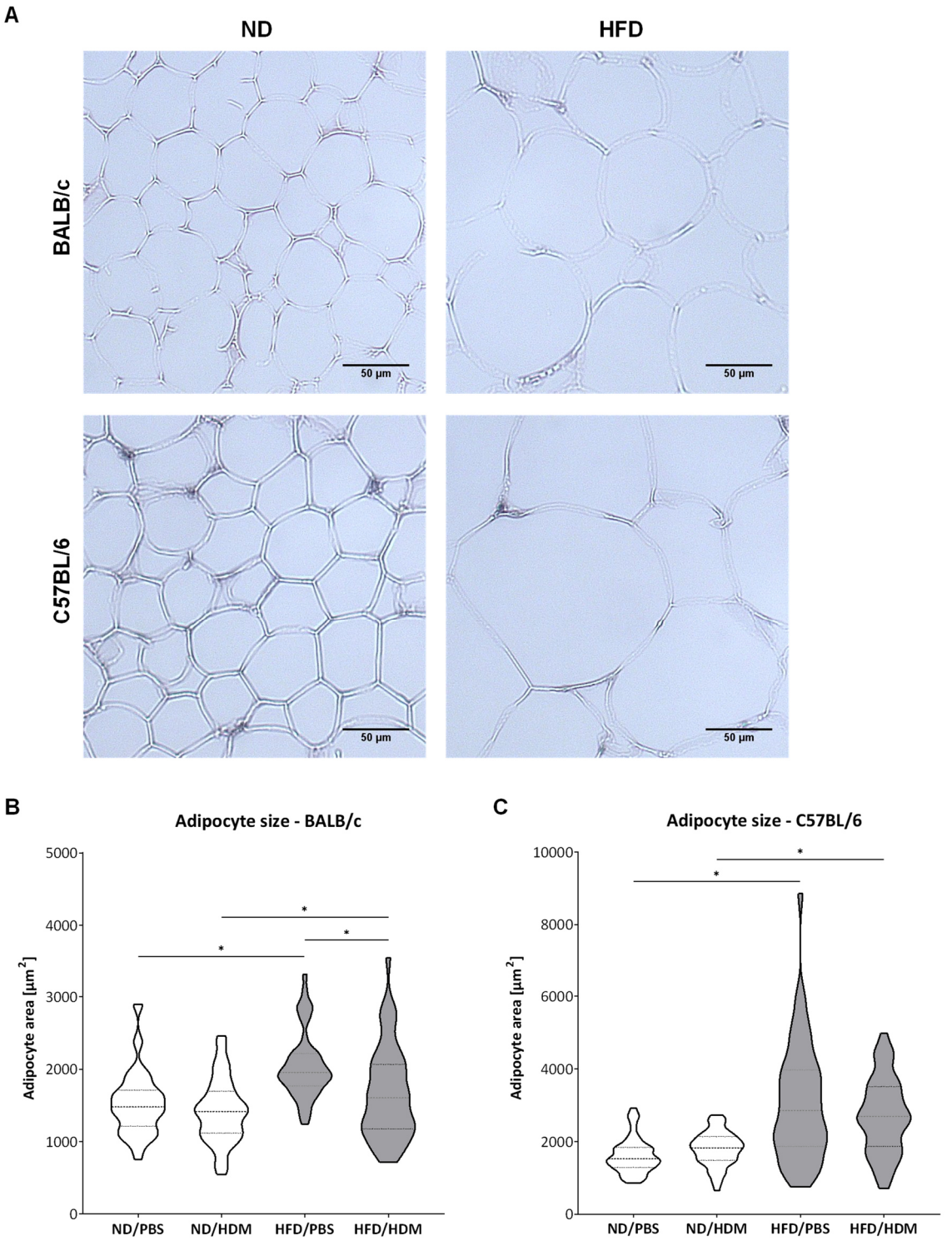

Figure 10 (previous page): HFD-fed BALB/c and C57BL/6 mice developed adipocyte hypertrophy.
H&E stained visceral adipose tissue sections of ND and HFD groups from BALB/c and C57BL/6 mice (A) used for measuring the adipocyte areas with ImageJ, which are depicted as violin plots of BALB/c mice (B) and C57BL/6 mice (C), n=5-6, * $p \leq 0.05$, ND: normal diet, PBS: phosphate-buffered saline, HDM: house dust mite, HFD: high fat diet.

To check whether the increased adipocyte hypertrophy is also associated with markers of inflammation in the adipose tissue, local inflammatory cells were investigated. For this purpose, flow cytometric analysis was used to analyze several immune cell populations within the adipose tissue. In BALB/c mice, the frequency of B cells and neutrophils were not altered in the adipose tissue of HFD-fed mice in comparison to ND-fed mice (Figure 11A/B, left). On the contrary, in obese C57BL/6 mice numbers of B cells as well as neutrophils were increased in the HFD/HDM group compared to the ND/HDM group (Figure 11A/B, right). The number of T cells in the adipose tissue was not affected by HFD in neither BALB/c nor C57BL/6 mice (data not shown). In both strains however, numbers of anti-inflammatory M2 macrophages were reduced with HFD, also reflected in the increased ratio of M1 to M2 macrophages in BALB/c and C57BL/6 mice (Figure 11C/D). Yet it needs to be noticed that the presence of anti-inflammatory M2 macrophages was much higher in BALB/c mice than in C57BL/6 mice. Taken together, numbers of inflammatory cells were enhanced in the adipose tissue of HFD-fed C57BL/6 mice. In contrast, increased numbers of inflammatory cells were not seen in HFD-fed BALB/c mice.

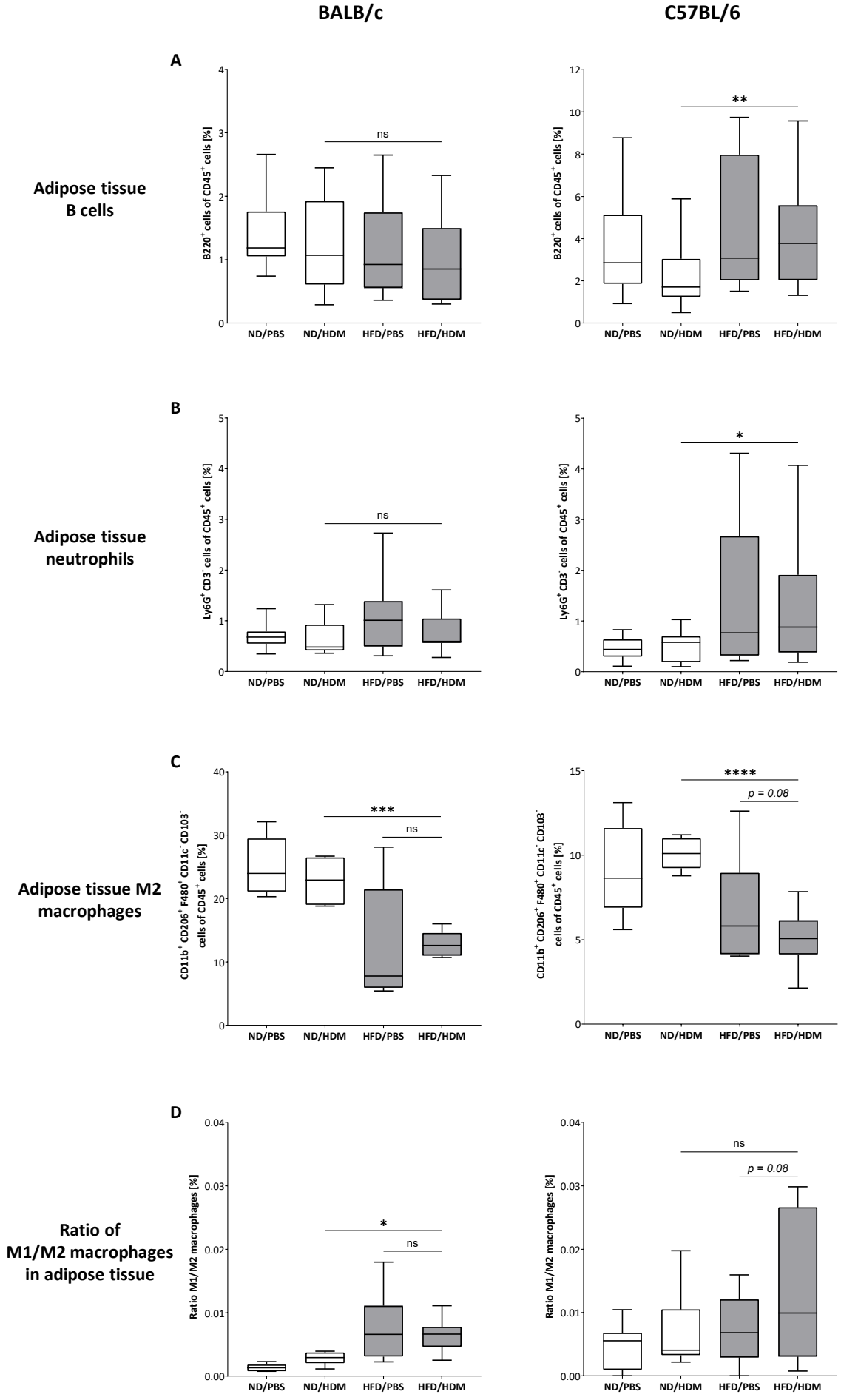
BALB/c
C57BL/6
A
Adipose tissue B cells
B220+ cells of CD45+ cells [%]
ns
**
ND/PBS
ND/HDM
HFD/PBS
HFD/HDM
B
Adipose tissue neutrophils
Ly6G+ CD3- cells of CD45+ cells [%]
ns
*
C
Adipose tissue M2 macrophages
CD11b+ CD206+ F480+ CD11c- CD103- cells of CD45+ cells [%]
***
ns
****
p = 0.08
D
Ratio of M1/M2 macrophages in adipose tissue
Ratio M1/M2 macrophages [%]
*
ns
ns
p = 0.08

Figure 11 (previous page): Frequency of immune cell populations in the adipose tissue of BALB/c and C57BL/6 mice.
Flow cytometric analysis of B cells (A), neutrophils (B), M2 macrophages (C), and ratio of M1 to M2 macrophages in the visceral adipose tissue of BALB/c (left) and C57BL/6 (right) mice, n=6-17, * $p \leq 0.05$, ** $p \leq 0.01$, *** $p \leq 0.001$, **** $p \leq 0.0001$, ns: not significant, ND: normal diet, PBS: phosphate-buffered saline, HDM: house dust mite, HFD: high fat diet.

3.1.3 Altered transcription profile in the obese adipose tissue of HDM-exposed C57BL/6 mice

Considering that weight gain seemed to be essentially associated with the development of inflammatory mechanisms in the adipose tissue, which was particularly seen in obese C57BL/6 mice, the following investigations were exclusively conducted in this strain. To investigate enhanced inflammatory processes in the adipose tissue, mRNA expression profiles were assessed. The RNA from visceral adipose tissue of the four experimental groups was isolated and sequenced to examine transcriptome profiles. The PCA plot of the 500 most differentially expressed genes revealed clear differences between the ND and HFD-fed groups (Figure 12). Interestingly, comparing the two ND groups, PBS and HDM-exposed mice depict a slightly distinct separation. However, this effect of HDM exposure on the adipose tissue is not seen in the HFD groups. Hence, HFD-induced alterations have a larger impact on the adipose tissue gene expression, than HDM exposure, whereby one outlier appeared in the HFD/HDM group.

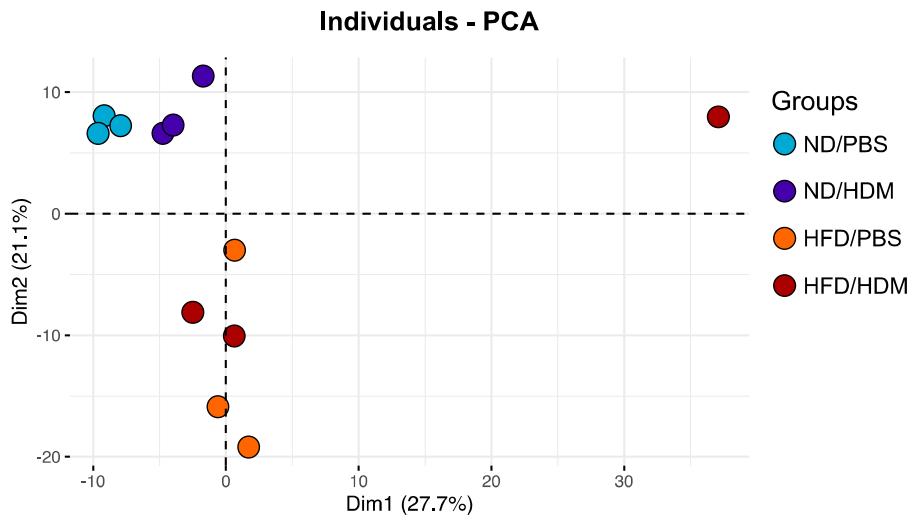

Figure 12: HFD changes the transcriptome profile in adipose tissue of C57BL/6 mice.
Principal component analysis (PCA) based on the top 500 variable expressed genes in the adipose tissue of C57BL/6 mice, n=3, ND: normal diet, PBS: phosphate-buffered saline, HDM: house dust mite, HFD: high fat diet.

In addition to the PCA plot, the transcription profile of the adipose tissue was visualized as a heatmap with four clusters emerging (Figure 13A). For the interpretation of the clusters, a pathway analysis was done. The results of which are depicted as network analysis of the top 10 pathways of each cluster (Figure 13B). As seen in the heatmap, the first cluster is represented by genes highly upregulated in the two HFD groups in comparison to the ND groups. The network analysis of cluster I revealed several pathways related to the immune system, including not only immune response in general but also complement activation as part of innate immune mechanisms as well as B cell receptor signaling as part of the adaptive immune response. Interestingly, some of these pathways were also present in cluster II, where mainly genes are represented that were upregulated in ND/HDM mice in comparison to the ND/PBS control group. This confirms not only a higher activation of the immune-related mechanisms in the adipose tissue by HFD itself but also suggests a systemic distribution of inflammatory signals affecting the transcriptome profile in the adipose tissue resulting from the HDM-exposure in the lung. In cluster III, network analysis resulted in several pathways related to lipid metabolic processes and bisphosphate metabolic processes. This cluster presented genes highly upregulated in the ND/PBS group, which was the only group without any kind of induced inflammatory processes. Hence, pathways involved in the regular metabolism could be seen in adipose tissue of lean PBS control mice, suggesting in turn a dysregulation of the metabolic processes in the other three experimental groups. These effects were even more pronounced in the two HFD groups compared to the ND/HDM group. Cluster IV is not depicted in Figure 13, as it was mainly defined by one outlier in the HFD/HDM group, also seen before in the PCA plot (Figure 12). Altogether, the AAI exerts systemic impacts on the adipose tissue, which are however overlaid by the local inflammatory processes in the obese adipose tissue induced by the HFD. Furthermore, the results suggest, that adaptive and innate immune response are activated by HFD in the adipose tissue of obese C57BL/6 mice.

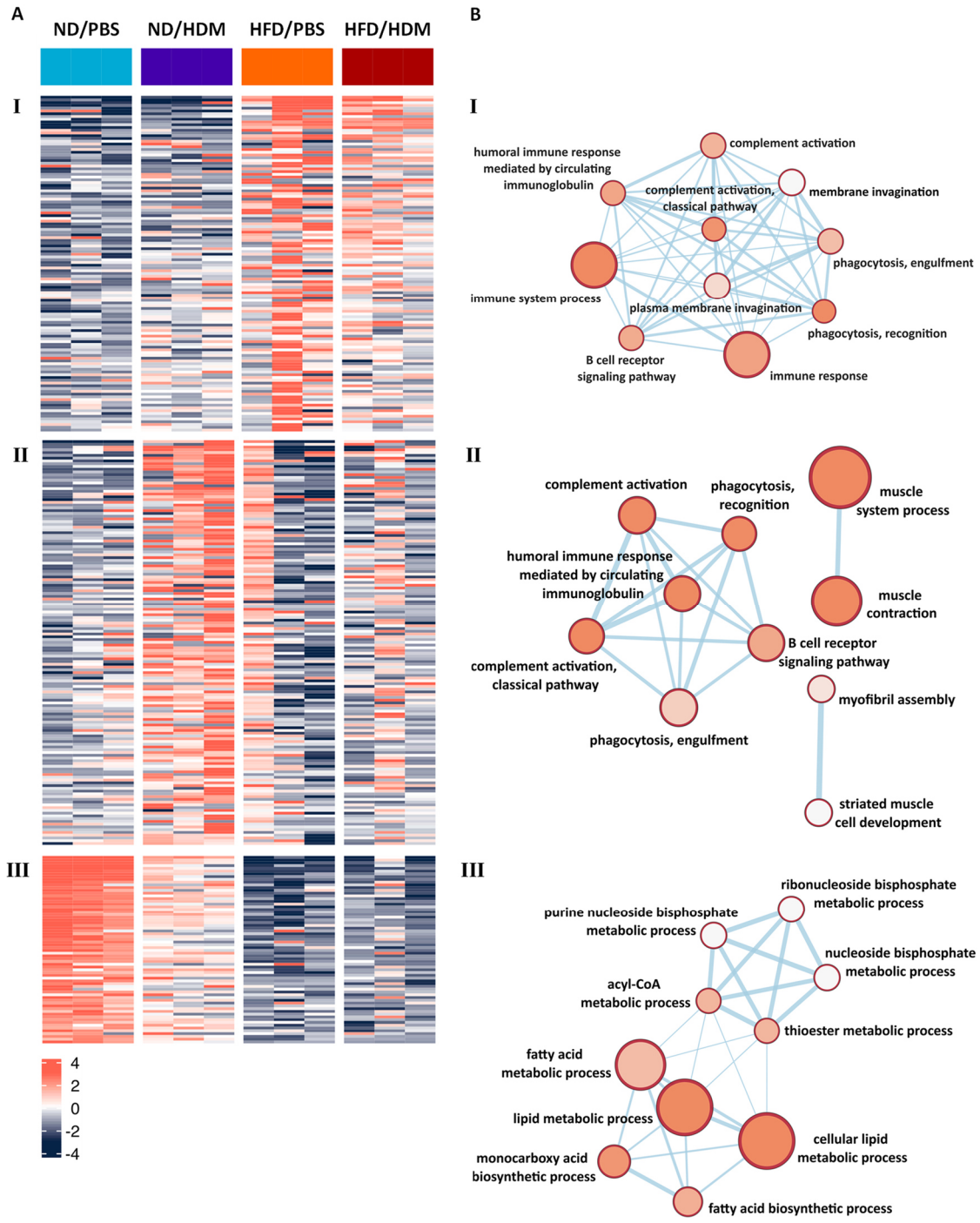

Figure 13: Gene expression heatmap and pathway analyses reveal HFD and HDM-expose induced differences in adipose tissue of C57BL/6 mice.

Heatmap based on the top 500 differentially expressed genes in the visceral adipose tissue of C57BL/6 mice (A), n=3. Gene Ontology Biological Processes (GO-BP) analysis of three major clusters defined by the heatmap depicted as network analysis of the top 10 pathways (B). Circle size corresponds to gene count, circle color indicates -$\log_{10}$(*P*-adj), ND: normal diet, PBS: phosphate-buffered saline, HDM: house dust mite, HFD: high fat diet.

To examine specific differences in the adipose tissue gene expressions between the two HDM-exposed groups with or without HFD, a pathway analysis was conducted of significantly differentially expressed genes between the ND/HDM and HFD/HDM groups. Gene Ontology Biological Processes (GO-BP slim) analysis of the 500 most differentially expressed genes demonstrated stronger involvements of cellular and metabolic processes as wells as immune system processes in the HFD/HDM group in comparison to the ND/HDM group (Figure 14). This is in line with the above-shown heatmap and network analysis depicting that local inflammatory processes in the adipose tissue of C57BL/6 mice were increased by HFD, which overlaid the effects of the induced AAI on the adipose tissue.

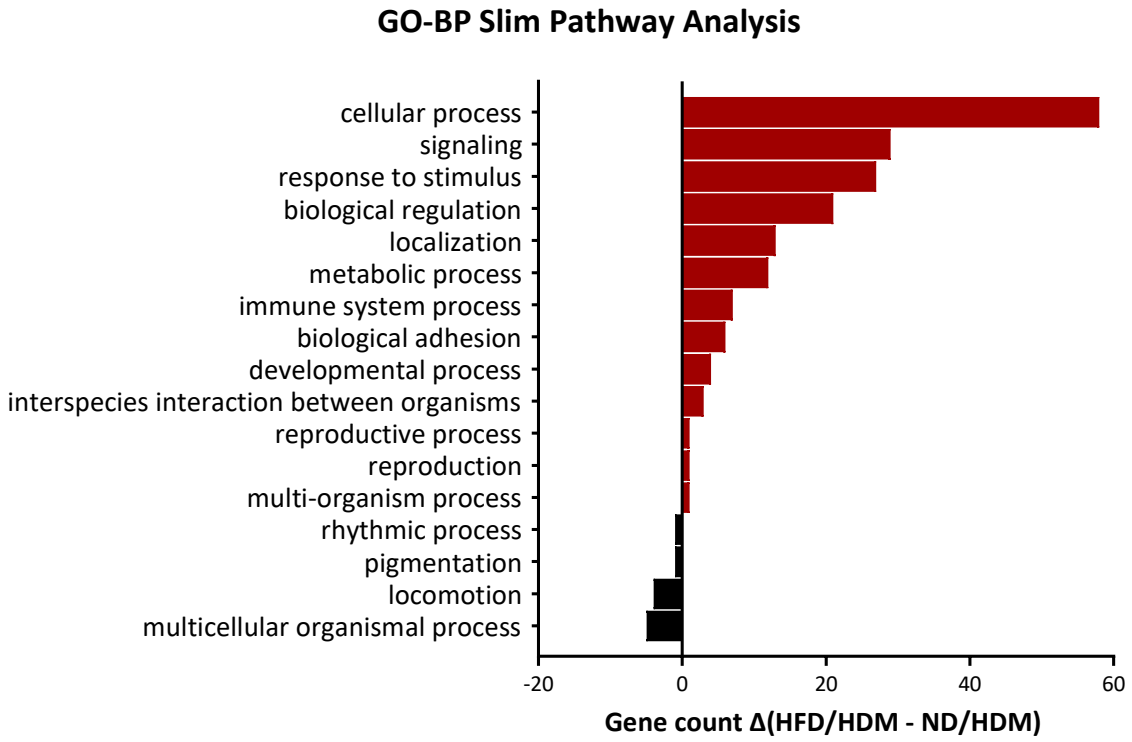

Figure 14: Differentially involved biological processes in adipose tissue of lean (ND) and obese (HFD) HDM-exposed C57BL/6 mice.
Gene Ontology Biological Processes (GO-BP slim) analysis of the 500 most differentially expressed genes shared between ND/HDM and HFD/HDM groups in the adipose tissue of C57BL/6 mice. Gene counts of significantly differentially expressed genes between the HDM-exposed groups, which are involved in different pathways are depicted as delta of the respective values of the HFD/HDM group to the ND/HDM group, n=3, ND: normal diet, HDM: house dust mite, HFD: high fat diet.

3.1.4 Adipocytes of obese HDM-exposed C57BL/6 mice release a variety of inflammatory signals

To further characterize functional differences in adipocytes of HFD/HDM C57BL/6 mice, the release of adipokines was also analyzed. Adipocytes of C57BL/6 mice from the four experimental groups were cultured for 48 h *in vitro* and the supernatants were analyzed with a Proteome Profiler Adipokine Array to examine mediators released by the adipocytes (Figure 15). The effects of HDM-exposure on the adipose tissue were not only seen as altered transcriptome profiles but also at the level of inflammatory factors released by adipocytes from ND/HDM mice. Not only inflammatory mediators such as leptin and IL-6 but also anti-inflammatory factors such as IL-10 and adiponectin were released at higher levels in comparison to the ND/PBS group. Obese HDM-exposed C57BL/6 mice showed the most pronounced release of inflammatory cytokines from adipocytes such as TNF-α, resistin, and IGFBP. Furthermore, the production of MCP-1 and macrophage colony-stimulating factor (M-CSF) was highly increased. Thus, adipocytes from HFD/HDM C57BL/6 mice release a variety of inflammatory signals to their environment further proving a high activation of inflammatory processes in the adipose tissue not only by the HFD but also through the HDM-induced AAI.

Taken together, HFD led to various alterations associated with obesity such as changes of metabolic mediators in the plasma, altered insulin resistance and glucose tolerance, as well as adipocyte hypertrophy in BALB/c and C57BL/6 mice, respectively. However, increased inflammatory signals typical for obese adipose tissue were only seen in C57BL/6 mice. Such inflammatory processes can be linked to the weight gain in response to HFD, which was missing in BALB/c mice. Thus, in C57BL/6 mice the HFD provides a good basis as model for further investigations of specific mechanism of the obesity-associated asthma phenotype as described in the following chapters.

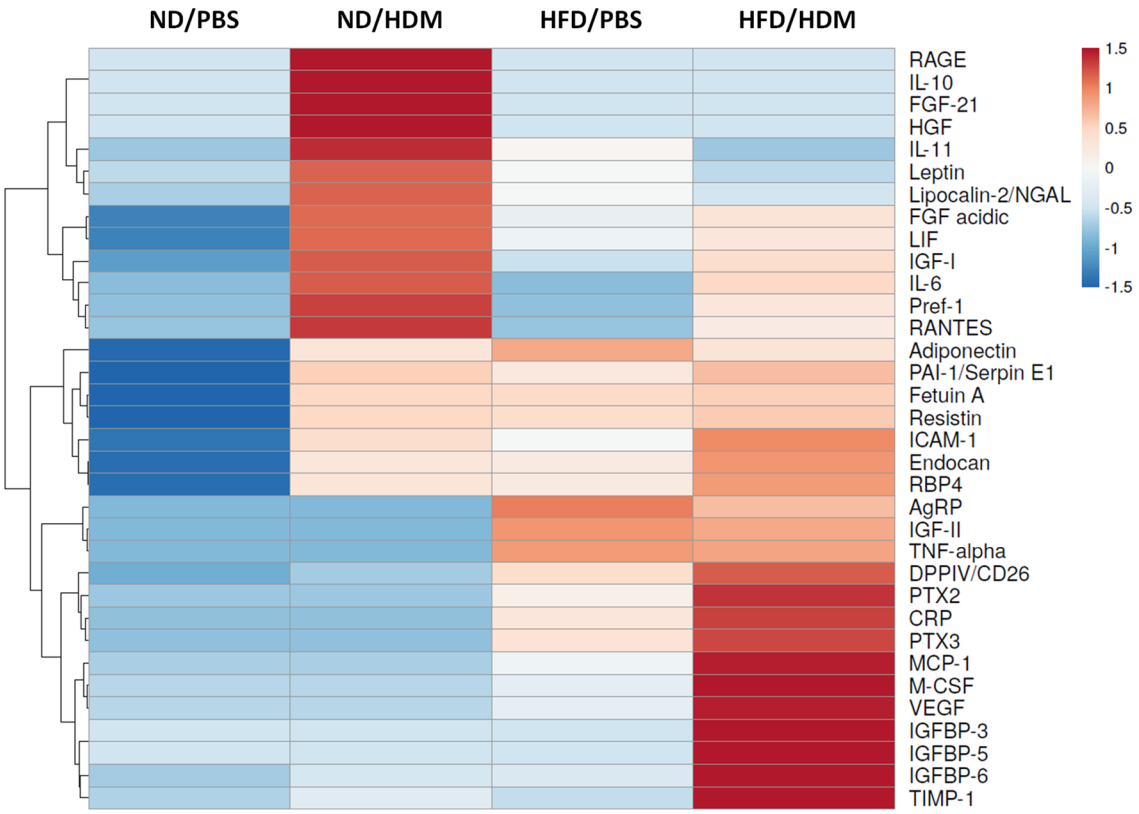

Figure 15: Inflammatory signals are released by adipocytes of obese (HFD) and HDM-exposed C57BL/6 mice.
Heatmap depicts optical densities of the Proteome Profiler Adipokine Array. Analyzed were pooled samples of supernatants from *in vitro* cultured adipocytes from 5-6 animals per experimental group of C57BL/6 mice, ND: normal diet, PBS: phosphate-buffered saline, HDM: house dust mite, HFD: high fat diet.

3.2 HDM-induced AAI phenotype is altered in obese C57BL/6 mice, but not in BALB/c mice

3.2.1 Inflammatory cell infiltration around the airways and mucus hypersecretion in HDM-exposed mice

The HDM model was used to induce a mixed type 2/non-type 2 phenotype of AAI in combination with a continuing HFD in the mice. The induction of a mixed asthma-like phenotype enabled the investigation of a possible shift towards a more type 2 or non-type 2 phenotype by the inflammatory mechanisms associated with obesity. The HDM model was previously established in BALB/c mice (Hagner et al., 2020) and has so far not been applied to mice with a C57BL/6 background. The AAI induction turned out to be as

successful in C57BL/6 animals as in BALB/c mice as the lung histology revealed comparable inflammation around the airways of both strains (Figure 16A). The HDM groups exhibited numerous inflammatory cells around the airways in comparison to the PBS control groups. Moreover, numbers of PAS stained mucus-producing goblet cells were increased in the HDM groups of both strains (Figure 16B). The HFD alone without HDM application did not lead to increased inflammatory cells or mucus hypersecretion in the lungs. Furthermore, no obvious differences could be recognized between the ND/HDM and HFD/HDM groups. Thus, both BALB/c and C57BL/6 mice developed representative and comparable lung tissue inflammation as well as mucus hypersecretion after HDM application, independently of the diet.

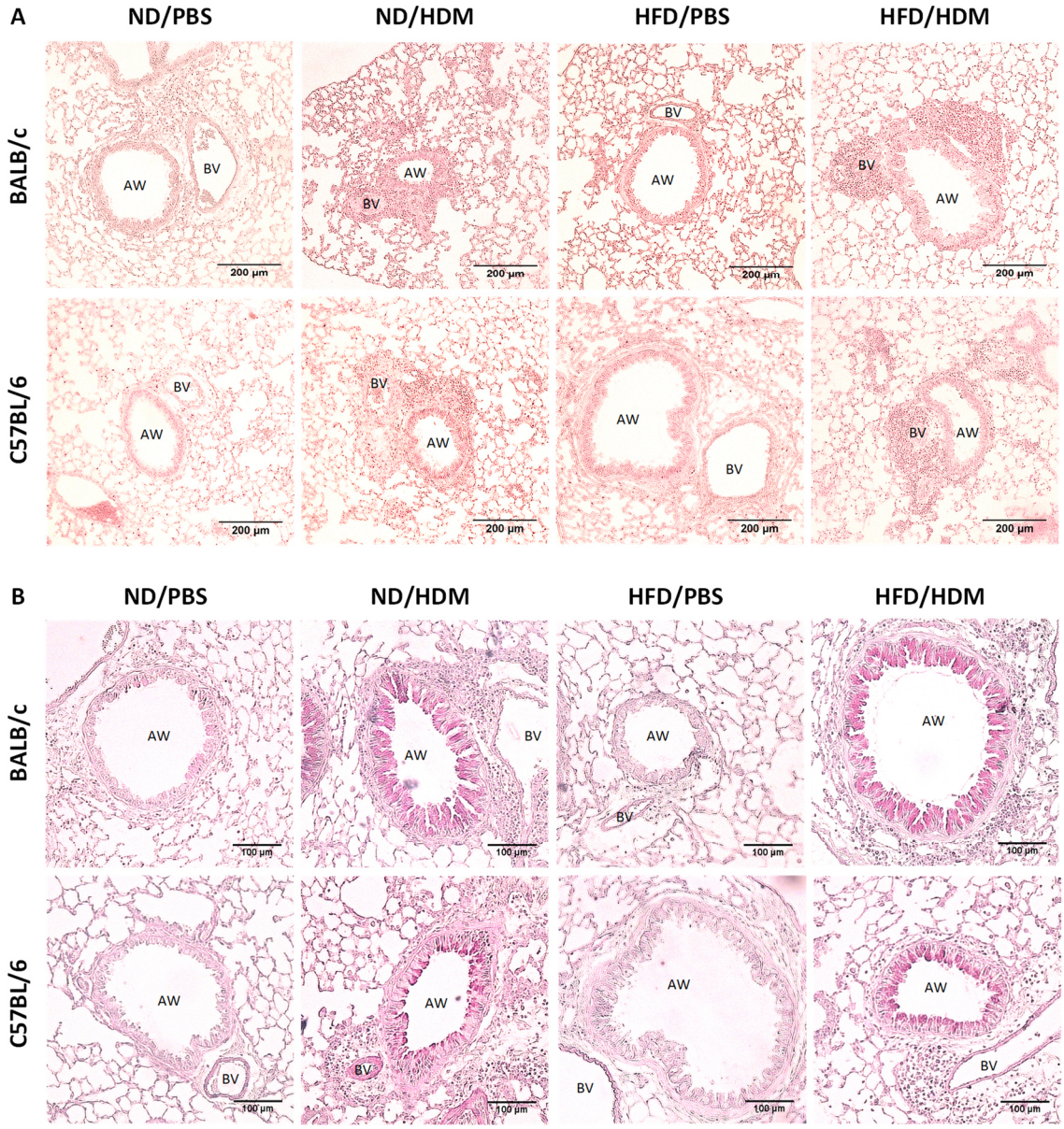

Figure 16 (previous page): Lung tissue inflammation and mucus-producing goblet cells around the airways of HDM-exposed BALB/c and C57BL/6 mice.
Hematoxylin & eosin (H&E) stained lung sections of BALB/c (top) and C57BL/6 (bottom) mice of HDM-exposed and/or HFD-fed groups showing increased inflammatory cell infiltration around the airways (A). Periodic acid-Schiff (PAS) stained lung sections of BALB/c (top) and C57BL/6 (bottom) mice of HDM-exposed and/or HFD-fed groups showing mucus-producing goblet cells in dark pink in the HDM-exposed groups (B). ND: normal diet, PBS: phosphate-buffered saline, HDM: house dust mite, HFD: high fat diet, AW: airway, BV: blood vessel.

3.2.2 Impact of HFD on HDM-specific humoral immune response in mice

To investigate systemic humoral immune responses to HDM exposure, levels of HDM-specific IgG were examined. Figure 17 depicts the results of the ELISA measuring optical densities of the plasma HDM-specific IgG as delta of the HDM to the PBS control group. BALB/c and C57BL/6 mice developed a specific humoral immune response to HDM application. In BALB/c mice, no difference was seen between the ND/HDM and HFD/HDM groups (Figure 17A). In contrast, even though at generally lower levels, amounts of HDM-specific IgG were significantly increased in the HFD/HDM group of the C57BL/6 mice as compared to the ND/HDM group (Figure 17B). This suggests an impact on systemic sensitization processes to HDM by continuous HFD in C57BL/6 mice.

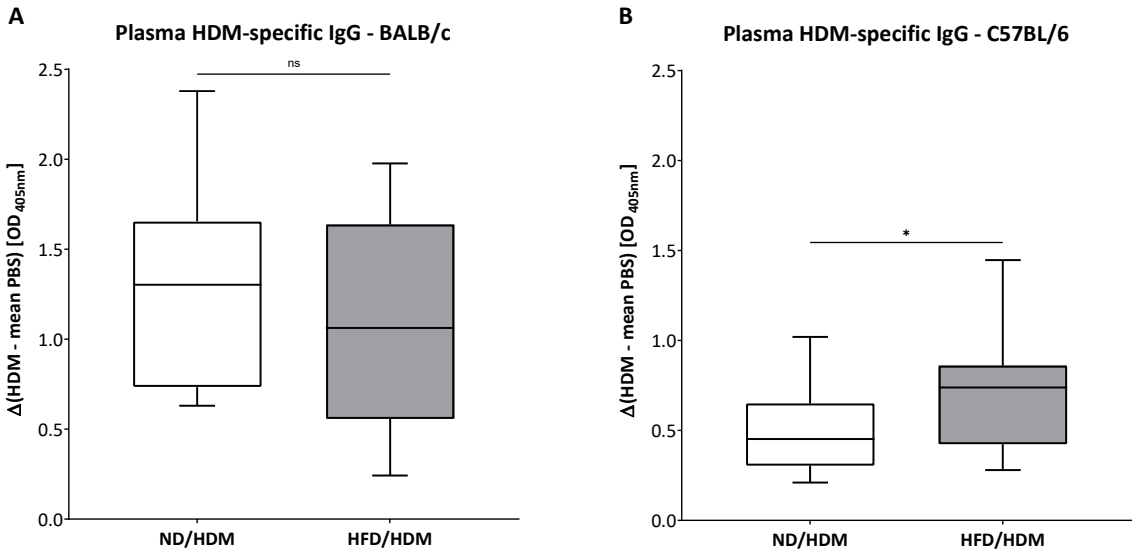

Figure 17: HDM-specific IgG plasma level reflect systemic sensitization to HDM in BALB/c and C57BL/6 mice.
Plasma level of HDM-specific IgG in BALB/c mice (A) and C57BL/6 mice (B). Optical densities of HDM-specific IgG ELISA are shown as delta of the HDM group to the respective PBS control group, n=12-18, * $p \leq 0.05$, ns: not significant, ND: normal diet, PBS: phosphate-buffered saline, HDM: house dust mite, HFD: high fat diet, IgG: immunoglobulin G, OD: optical density. (Data adapted from Ms. Andrea Berlin)

3.2.3 Immune cells and cytokines in the BAL of HFD-fed HDM-exposed mice

Next, the BAL cell distribution was determined to further examine the outcome of the mixed AAI, which was previously shown in BALB/c mice to result in an equal increase of eosinophils and neutrophils in the BAL (Hagner et al., 2020, Tan et al., 2019). As expected within the BALB/c strain, the HDM groups showed a comparable infiltration of eosinophils and neutrophils into the BAL. Comparing BAL cell composition in BALB/c mice between the ND/HDM and the HFD/HDM groups, no significant differences occurred between the eosinophil, neutrophil, macrophage, and lymphocyte numbers (Figure 18A-D, left). Additionally, the ratio of eosinophils to neutrophils in these mice was similar in the ND/HDM and HFD/HDM groups (Figure 19A). The C57BL/6 mice also developed an increase of eosinophils and neutrophils in the BAL of the ND/HDM group (Figure 18A/B, right). The applied HDM in the C57BL/6 mice developed a slightly higher increase of eosinophils than neutrophils in the ND/HDM groups. Analysis of BAL cell compositions between the ND- and HFD-fed HDM-exposed groups in C57BL/6 mice revealed similar numbers of eosinophils in these groups. On the other hand, absolute numbers of neutrophils and macrophages showed a tendency towards a decrease and lymphocyte numbers increased in the HFD/HDM group (Figure 18B-D, right). Hence, the ratio of eosinophils and neutrophils demonstrated a significant increase in the HFD/HDM group compared to the ND/HDM group in C57BL/6 mice (Figure 19B).

Summarizing, BALB/c mice did not show any changes in the BAL cell composition following induction of a mixed AAI in combination with a continuing HFD compared to the ND/HDM group. In contrast, results obtained in obese C57BL/6 mice demonstrated a more eosinophilic airway inflammation by reduction of neutrophil numbers in the HFD/HDM group. Next to alterations in the granulocyte compartment, increased lymphocyte numbers indicate an effect of the HFD on AAI at the level of adaptive immune cells. HFD alone did not affect the BAL cell composition in neither of the two mouse strains.

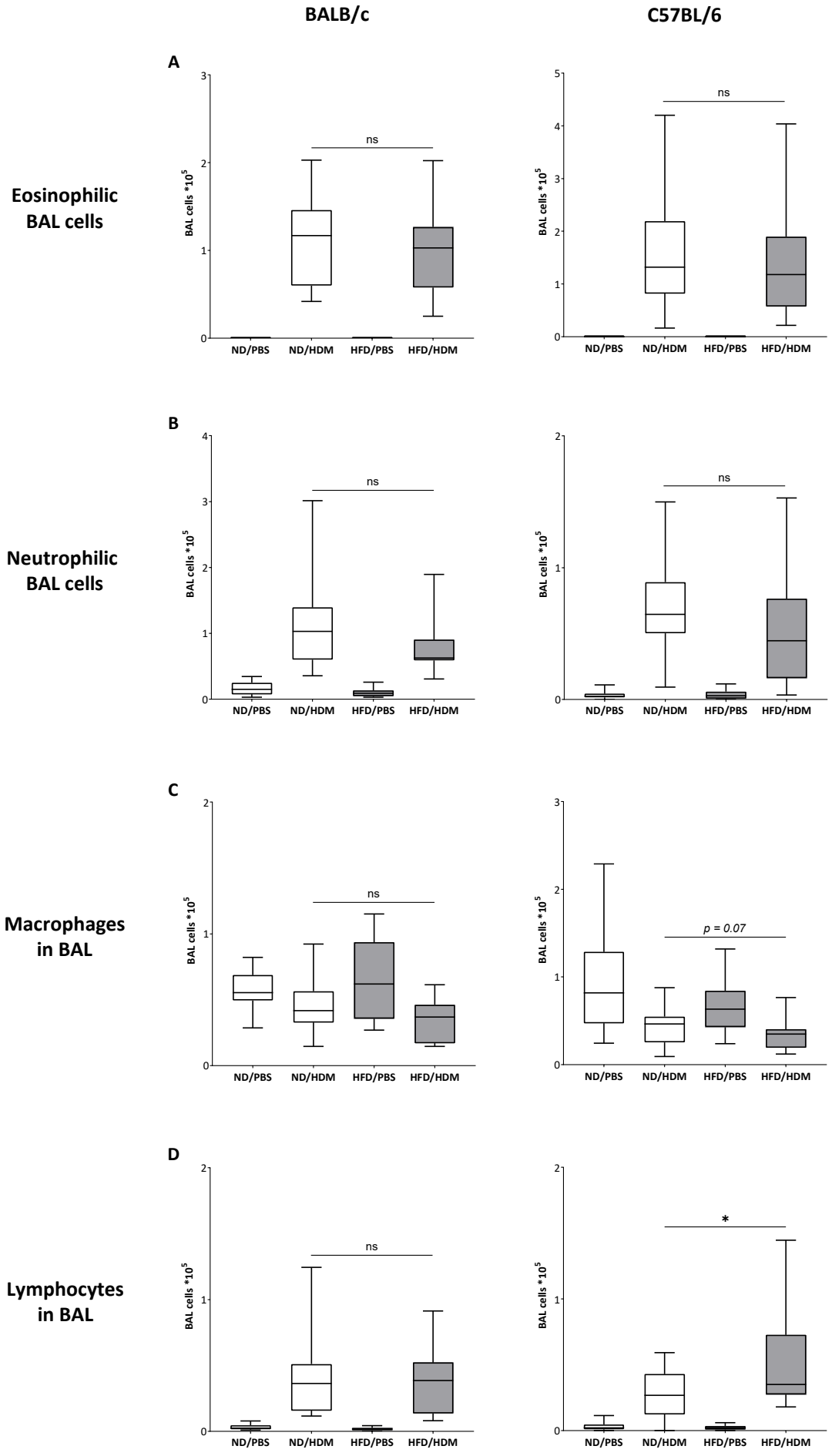
BALB/c
C57BL/6
A
Eosinophilic BAL cells
B
Neutrophilic BAL cells
C
Macrophages in BAL
D
Lymphocytes in BAL
BAL cells *10^5
ns
p = 0.07
*
ND/PBS
ND/HDM
HFD/PBS
HFD/HDM

Figure 18 (previous page): Altered bronchoalveolar lavage (BAL) cell composition in HFD-fed C57BL/6 mice, but not in BALB/c mice.
Absolute numbers of BAL eosinophils (A), neutrophils (B), macrophages (C), and lymphocytes (D) in BALB/c mice (left) and C57BL/6 mice (right), n=11-18, * $p \leq 0.05$, ns: not significant, ND: normal diet, PBS: phosphate-buffered saline, HDM: house dust mite, HFD: high fat diet.

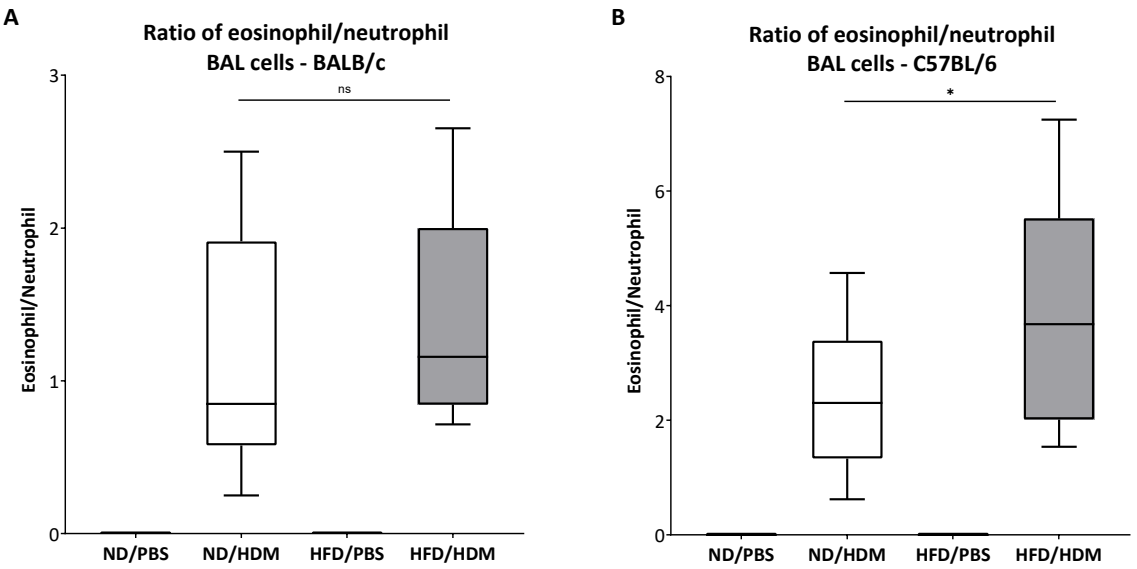

Figure 19: Altered ratio of eosinophils to neutrophils in the BAL of C57BL/6 mice.
Ratio of BAL eosinophils to neutrophils in BALB/c mice (A) and C57BL/6 mice (B), n=12-18, * $p \leq 0.05$, ns: not significant, ND: normal diet, PBS: phosphate-buffered saline, HDM: house dust mite, HFD: high fat diet.

The BAL of HDM-exposed BALB/c and C57BL/6 mice was further analyzed with a Proteome Profiler Cytokine Array (Figure 20). Distinct differences were seen between the two strains regarding presence of a variety of cytokines and chemokines demonstrated in Figure 20 as delta of the respective optical density values of the HFD/HDM to the ND/HDM group. BALB/c mice exhibited only minor or no changes between the ND/HDM and HFD/HDM groups in the cytokine/chemokine BAL profile. In contrast, cytokines playing a role in the regulation of immune responses such as the anti-inflammatory IL-10 and inflammatory TNF-α, as well as the inflammatory adipokines leptin and resistin, were shown to be upregulated in HDM-exposed C57BL/6 mice which had additionally received a HFD. In line with the above shown alteration in BAL cell composition, with relative higher eosinophil numbers in C57BL/6 mice, the proteome profiler revealed an increase of CCL11 and CCL12, which represent chemotactic factors for eosinophils. Moreover, concentrations of the proliferation stimulating fibroblast growth factor (FGF) acidic (also known as FGF1) as well as the IGFBP-3 and -5 were

increased in the HFD/HDM group. Next to TNF-α and resistin, the latter observations are consistent with the results of above shown adipokine cytokine array (Figure 15). Altogether, the results of these analyses point to an impact of the inflammatory fatty tissue mechanisms on the induced AAI in obese C57BL/6 mice.

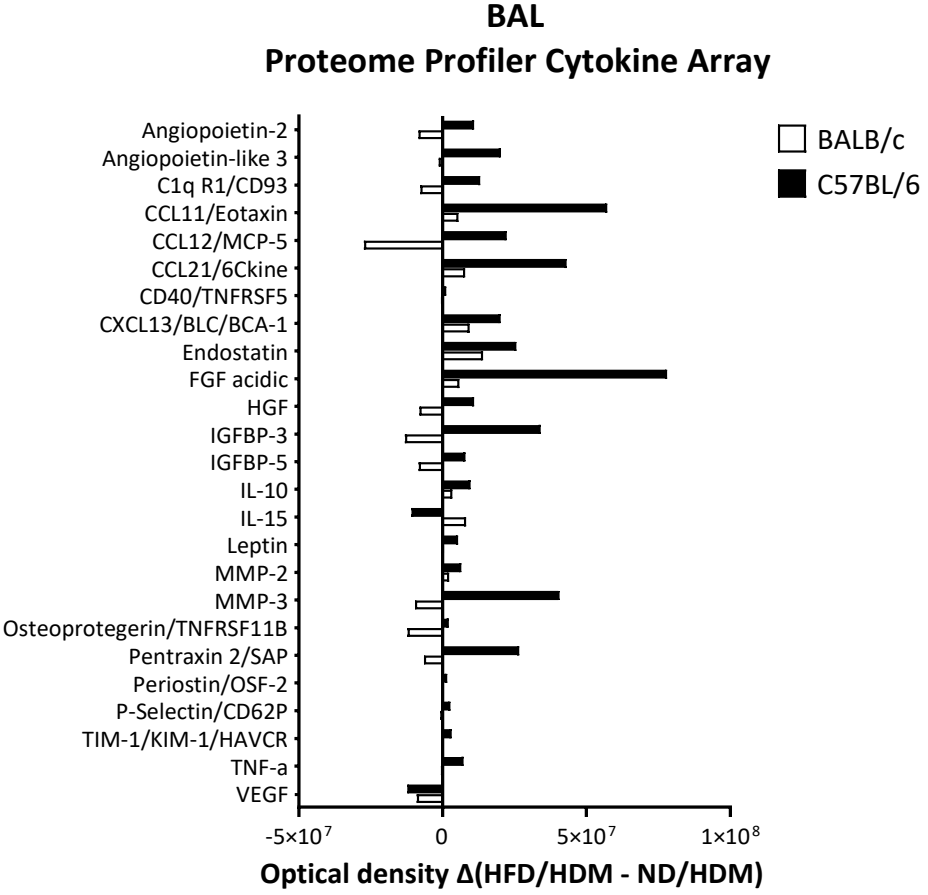

Figure 20: Cytokines and chemokines in the bronchoalveolar lavage (BAL) are especially increased in obese (HFD) HDM-exposed C57BL/6 mice compared to BALB/c mice.
Cytokines and chemokines in the BAL were measured with a Proteome Profiler Cytokine Array and optical densities are depicted as delta of the respective values of the HFD/HDM group to the ND/HDM group of BALB/c mice (white bars) and C57BL/6 mice (black bars). Shown cytokines and chemokines were selected based on at least 40% change in optical densities between ND/HDM and HFD/HDM groups of C57BL/6 mice, ND: normal diet, HDM: house dust mite, HFD: high fat diet. (Data adapted from Ms. Andrea Berlin)

3.2.4 Immune cells in the lung tissue of HFD-fed HDM-exposed mice

Flow cytometric analysis was used to analyze differences in the composition of relevant immune cells in the lungs. Consistent with the above shown ratio of eosinophils to neutrophils in the BAL the same ratio was examined in the lung tissue. Also here, in BALB/c mice, no difference was observed between the ND/HDM and HFD/HDM groups

while C57BL/6 mice developed, like in the BAL, an increased ratio of eosinophils to neutrophils in the lungs in the HFD/HDM group compared to the ND/HDM group (Figure 21A). Further, BALB/c revealed lower numbers of B cells in the HDM groups in comparison to the respective PBS control groups (Figure 21B, left). An increased ratio of $CD4^+$ to $CD8^+$ positive T cells could be observed in the HFD/HDM group compared to the HFD/PBS group (Figure 21C, left). However, no impact of HFD was seen on these two parameters when comparing the HDM-exposed with or without HFD-fed BALB/c mice. Yet, the frequency of TCRγδ cells was lower in the HDM groups but increased with HFD in BALB/c mice (Figure 21D, left). On the contrary, proportions of lymphocyte sub-populations in the C57BL/6 mice were significantly altered in obese HDM mice. Hence, increased relative cell numbers of B cells and a significantly higher ratio of $CD4^+$ to $CD8^+$ T cells were observed in the lungs of the HFD/HDM C57BL/6 mice (Figure 21B/C, right). Similar to BALB/c mice, TCRγδ cells were reduced following HDM exposure but in the C57BL/6 mice this effect was inverted in the HFD/HDM group, showing a significant increase in the relative number of these cells compared to the ND/HDM group while no difference between the HFD/PBS and the ND/PBS groups was observed (Figure 21D, left). Thus, next to changes in the granulocytic populations, also alterations of the lymphocyte populations were seen in the obese C57BL/6 mice with an induced AAI, which were completely missing in BALB/c mice. This points to enhanced inflammatory processes in the lungs associated with the weight gain of HFD-fed and HDM-exposed C57BL/6 mice.

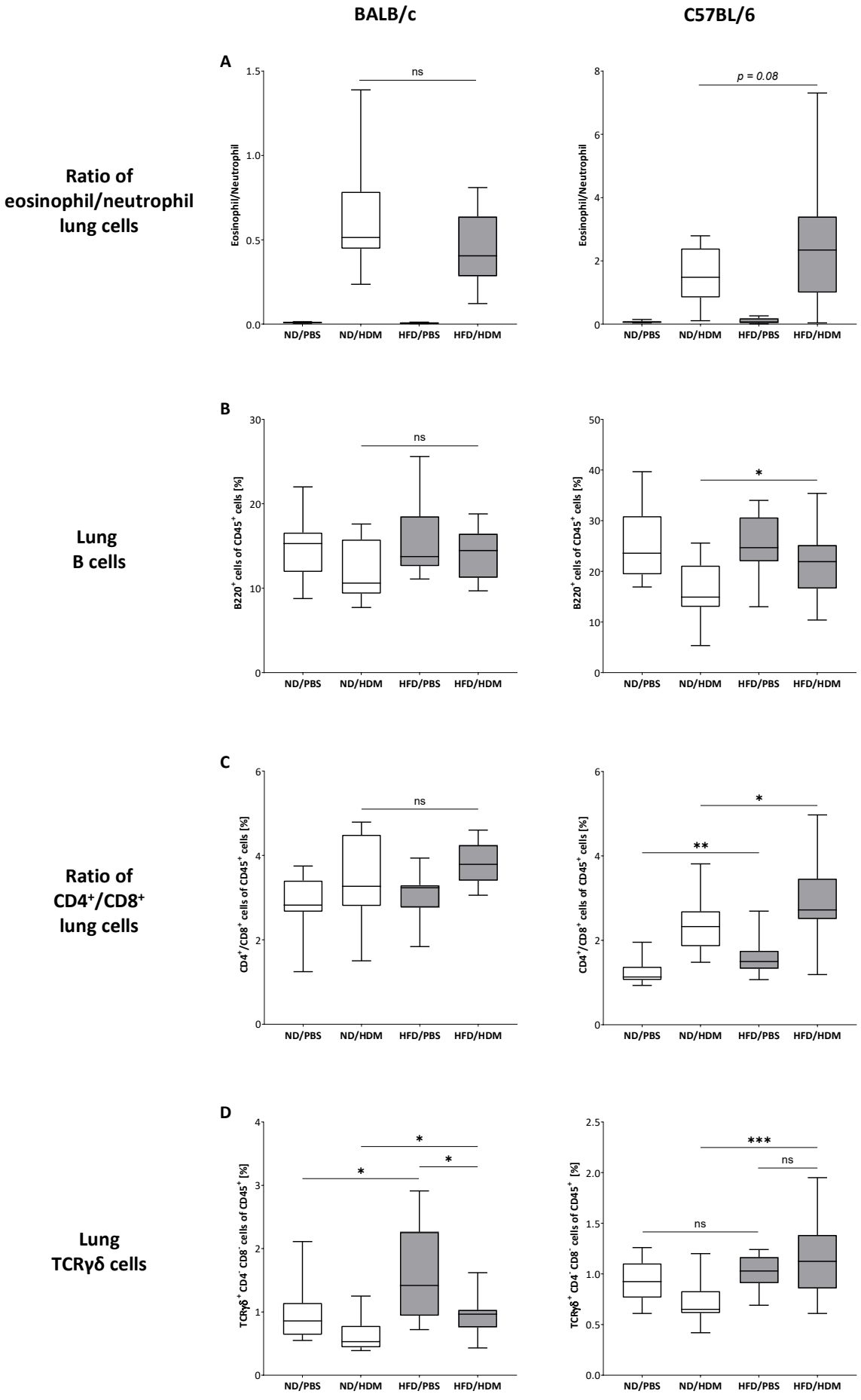
BALB/c
C57BL/6
A
Ratio of eosinophil/neutrophil lung cells
Eosinophil/Neutrophil
ns
p = 0.08
B
Lung B cells
B220+ cells of CD45+ cells [%]
ns
*
C
Ratio of CD4+/CD8+ lung cells
CD4+/CD8+ cells of CD45+ cells [%]
ns
*
**
D
Lung TCRγδ cells
TCRγδ+ CD4- CD8- cells of CD45+ [%]
*
*
*
***
ns
ns
ND/PBS
ND/HDM
HFD/PBS
HFD/HDM

Figure 21 (previous page): Specific changes in lung immune cell composition in obese (HFD) HDM-exposed C57BL/6 mice, but not in BALB/c mice.
Flow cytometric analysis of pulmonary eosinophils to neutrophils ratio (A), relative numbers of B cells (B), $CD4^+/CD8^+$ T cell ratios (C), and relative numbers of TCRγδ cells (D) in BALB/c mice (left) and C57BL/6 mice (right), n=12-18, * $p \leq 0.05$, ** $p \leq 0.01$, *** $p \leq 0.001$, ns: not significant, ND: normal diet, PBS: phosphate-buffered saline, HDM: house dust mite, HFD: high fat diet.

3.2.5 Overall evaluation of immune and inflammatory mechanisms in BALB/c and C57BL/6 mice

All prior presented results in combination with further data not shown in detail here, were applied to a complex PCA analysis to identify overall differences and similarities between mouse strains and experimental conditions (Table 4). Strain dependent differences are visualized by a clear separation of BALB/c groups on the left and C57BL/6 groups on the right in the resulting PCA plot shown in Figure 22. Besides, a distinct shift of the HDM groups of both strains in comparison to the PBS groups became obvious. In line with the results shown above, the differences between the ND/HDM and HFD/HDM groups are less pronounced in BALB/c mice than in C57BL/6 mice.

Table 4: Measured parameters included in the Principal Component Analysis.

Metabolic analysis	BAL cell composition	Flow cytometric analysis of cells from lung and adipose tissue	
• Weight • GTT • ITT	• Eosinophils • Neutrophils • Total BAL cells	• $SiglecF^{+high}$ $CD3^-$ Eosinophils • $Ly6G^+$ $CD3^-$ Neutrophils • $CD45^+$ Leukocytes • $CD3^+$ T cells	• $CD4^+$ T cells • $CD8^+$ T cells • $B220^+$ B cells • $CD8^+$ $TCR\gamma\delta^+$ cells • $CD4^-$ $CD8^-$ $TCR\gamma\delta^+$ cells

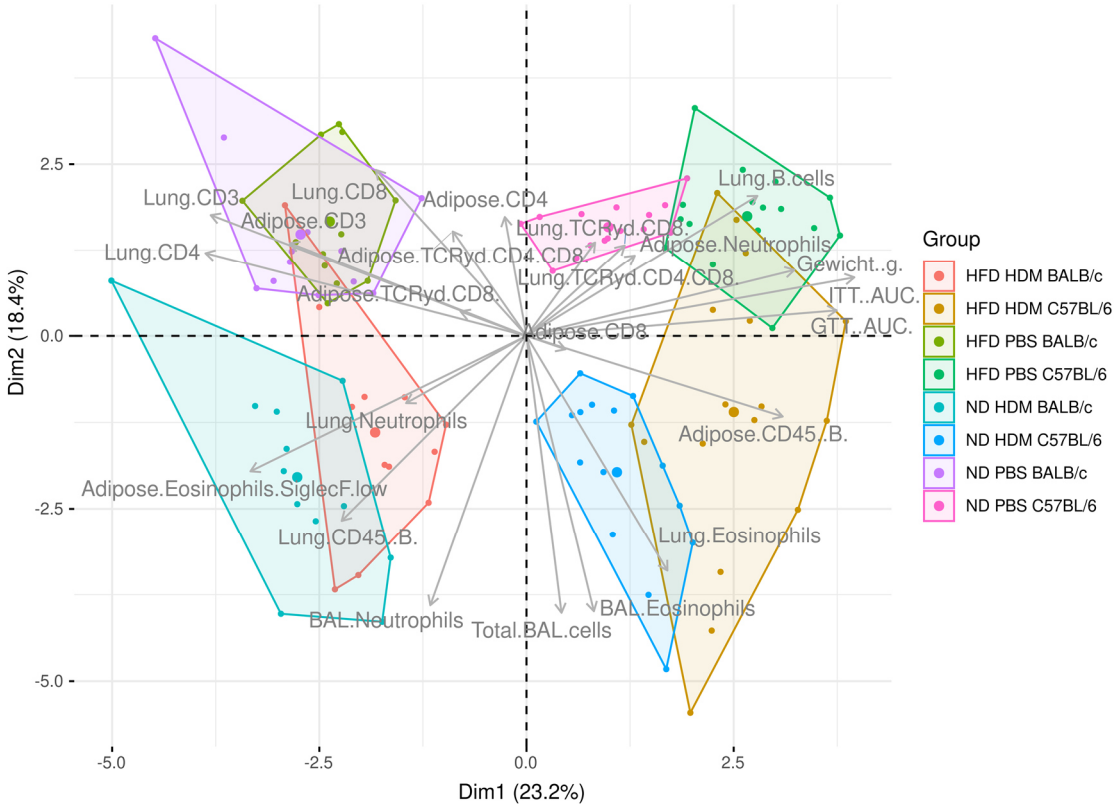

Figure 22: Principal component analysis (PCA) reveals distinct differences between HDM-exposed and/or HFD-fed BALB/c and C57BL/6 mice.
PCA plot summarizes overall differences and similarities of HFD-fed and HDM-exposed BALB/c and C57BL/6 mice, ND: normal diet, PBS: phosphate-buffered saline, HDM: house dust mite, HFD: high fat diet.

In summary, a continuous HFD resulted in obvious signs of obesity associated with changes in the inflammatory phenotype of an HDM-induced AAI only in C57BL/6 mice. These effects were completely missing in BALB/c mice, which did not gain weight in response to a HFD. Therefore, weight gain seems to be crucially associated with inflammatory changes modifying the phenotype of an induced AAI. Thus, in this model, an unhealthy diet alone does not have an influence on the induced AAI, but obesity is required for such alterations.

3.3 Single cell analysis reveals a distinct HDM-activated lung CD4$^+$ T cell population in lean mice, which is completely missing in obese mice

3.3.1 Altered expression profile in lung CD45$^+$ cells of HDM-induced airway inflammation in obese C57BL/6 mice

As shown before, obese C57BL/6 mice revealed an altered obesity-associated asthma inflammatory phenotype, whereby also changes in the lung leukocyte populations were demonstrated. For better understanding of the underlying mechanisms, CD45$^+$ lung cells were isolated from C57BL/6 mice. These cells were analyzed with the BD Rhapsody single cell analysis system, including parallel sequencing of cell specific mRNA and expression analysis of a variety of cell surface molecules. Subsequent dimension reduction and visualization of the data was done using Uniform Manifold Approximation and Projection (UMAP) overlayed with a phenograph clustering based on similarity approximation of the cells (Figure 23A). Thus, several cell clusters could be identified based on specific surface markers such as the B cells (CD19$^+$ and CD21/35$^+$), CD4$^+$ T cells, and CD8$^+$ T cells (Figure 23B). Other cell clusters such as macrophages/dendritic cells (DCs), granulocytes, and natural killer (NK) cells could be determined by combining surface markers and mRNA expression profiles (Figure 23C). Similar expression profiles and the presence of surface molecules of DCs and macrophages impeded the distinct definition of each subcluster. The grey colored phenograph cluster was found to be an artefact of AbSeq signals. Further, it needs to be mentioned, that in the dark green phenograph cluster, which included CD8$^+$ T cells (positive for the CD8b AbSeq, thus referred to as CD8$^+$), also other cells were present with less/no expression of CD8b. In-depth investigation of this cluster-part revealed the presence of immature NK cells (Abel et al., 2018), as expression of NK-1.1 but less CD49b, CD11b, and *Klrg1* was present compared to the neighboring yellow phenograph cluster identified as NK cells (data not shown).

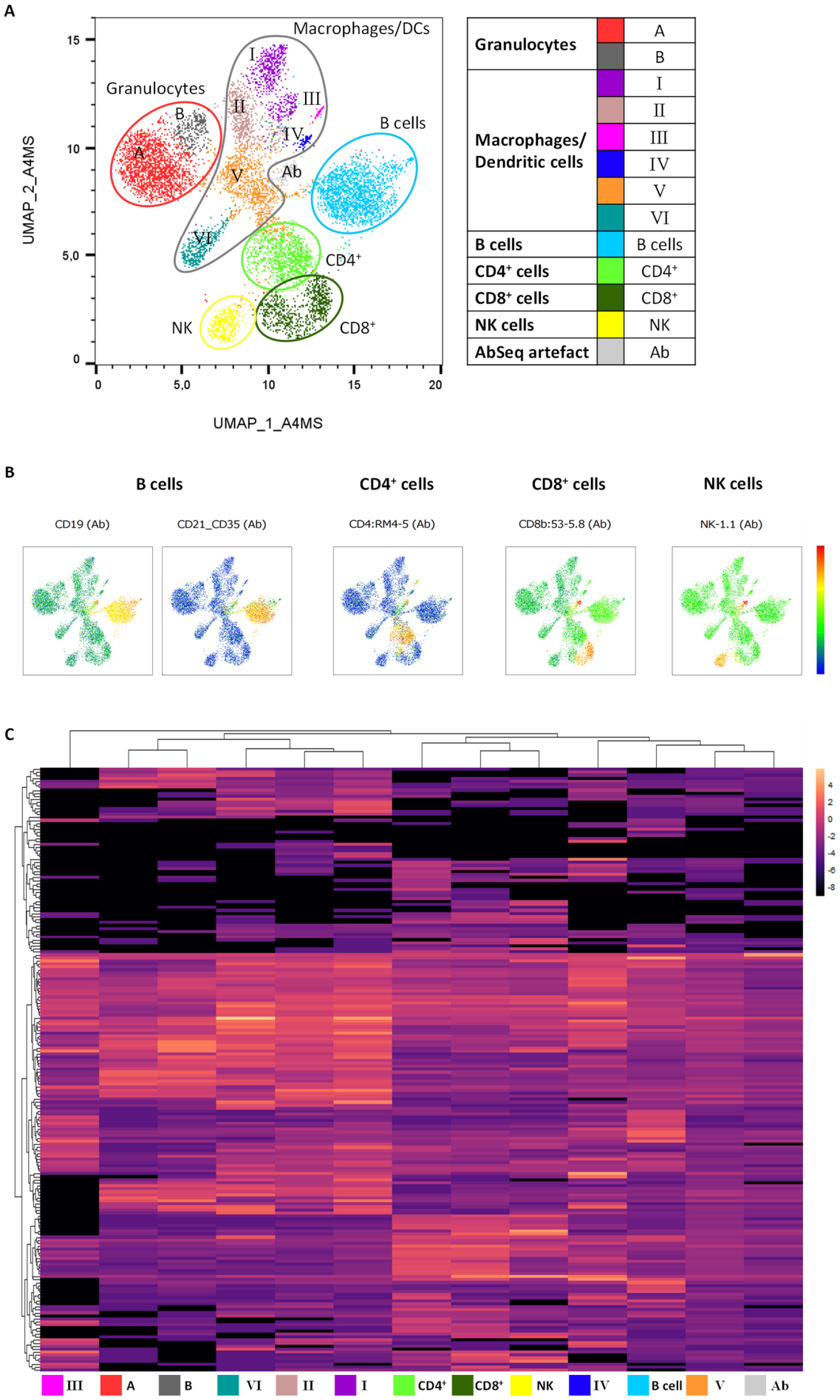
A
Macrophages/DCs
Granulocytes
B cells
CD4⁺
CD8⁺
NK
Ab
I
II
III
IV
V
VI
A
B
UMAP_2_A4MS
UMAP_1_A4MS
Granulocytes
Macrophages/ Dendritic cells
B cells
CD4⁺ cells
CD8⁺ cells
NK cells
AbSeq artefact
B
B cells
CD4⁺ cells
CD8⁺ cells
NK cells
CD19 (Ab)
CD21_CD35 (Ab)
CD4:RM4-5 (Ab)
CD8b:53-5.8 (Ab)
NK-1.1 (Ab)
C
III
A
B
VI
II
I
CD4⁺
CD8⁺
NK
IV
B cell
V
Ab

Figure 23 (previous page): Identification of lung leukocyte populations in C57BL/6 mice.
Single cell analysis of $CD45^+$ lung cells of C57BL/6 mice from all experimental groups (ND/PBS, ND/HDM, HFD/PBS, HFD/HDM) depicted as Uniform Manifold Approximation and Projection (UMAP) overlayed with cluster identification by phenograph analysis (A), colors indicate different phenograph clusters, which are defined in the table. Visualization of selected cell surface molecule expression by Abseq labeling (Ab) (B). Heatmap of gene/surface marker expression of leukocyte subpopulation clusters based on the similarities between cells by phenograph analysis (C), n=12, ND: normal diet, PBS: phosphate-buffered saline, HDM: house dust mite, HFD: high fat diet, DCs: dendritic cells, NK cells: natural killer cells.

To identify differences in lung leukocytes populations of the different experimental groups, cells from individual animals were depicted on the same UMAP as above but in separate graphs for each group (Figure 24). For better comparison, cell counts of each group were adjusted to the cell number of the group with the least cells, resulting in unified cell numbers for every group. As demonstrated in Figure 24, clear differences in several leukocyte clusters emerged between the groups. More precisely, in the granulocytic cell population, in parts of the macrophage/DC population and in the $CD4^+$ T cells, the HFD/HDM differed obviously from the other groups (highlighted by orange circles). The mapping of cells from each individual animal (depicted in red, green, and blue) on the UMAP demonstrates further a comparable distribution within the clusters. Table 5 displays the relative distribution of cells from each experimental group among the phenograph clusters, which supports the visual examination of cluster differences between the groups. Despite having only three animals per group, the results of the single cell data were nevertheless consistent with the above shown flow cytometric analyses of increased B cell numbers and alterations in $CD4^+$ to $CD8^+$ T cell ratio in lung tissue of HFD-fed HDM-exposed C57BL/6 mice (Figure 21). Obviously, specific leukocyte cell populations are altered in obese C57BL/6 mice with an induced AAI compared to HDM-exposed ND mice and to the respective control groups.

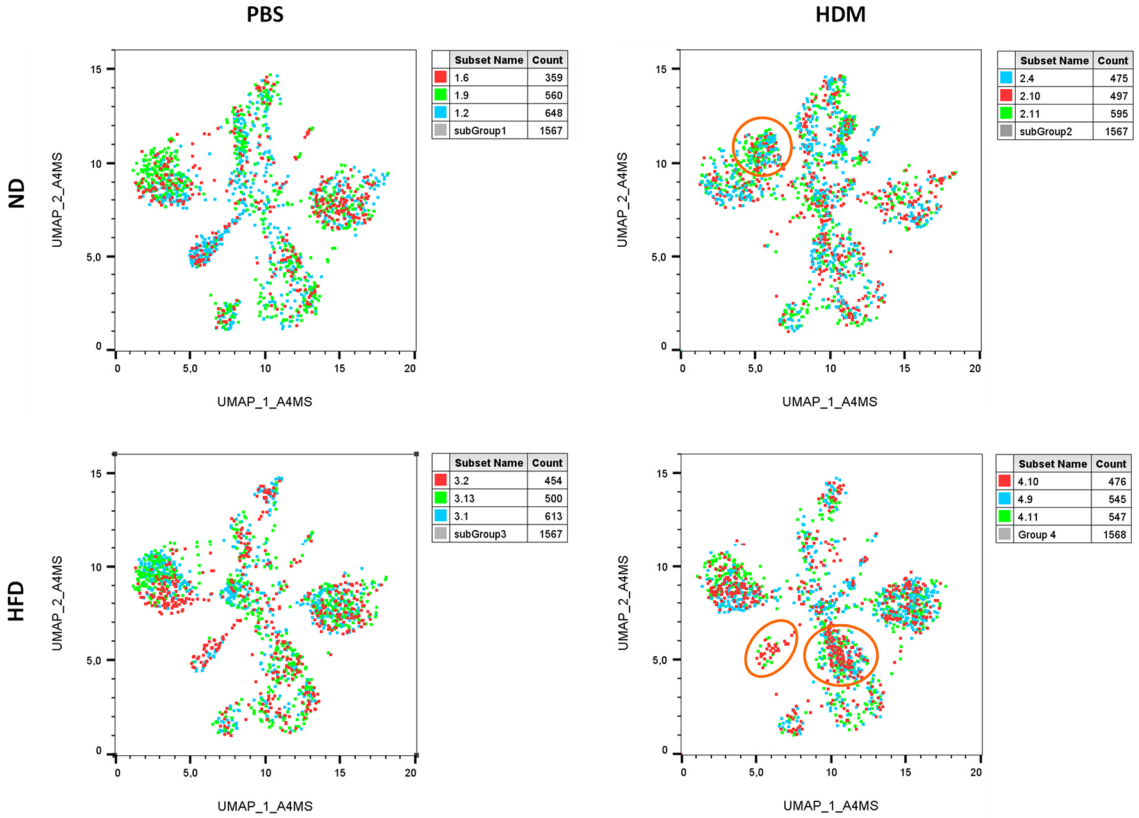

Figure 24: Composition of leukocyte cell populations is altered in lungs of HDM-exposed obese C57BL/6 mice.

Experimental groups separated for visualization of CD45$^+$ lung cells of C57BL/6 mice with Uniform Manifold Approximation and Projection (UMAP), colors indicate three individual animals of each group, orange circles highlight the most striking differences between experimental groups, ND: normal diet, PBS: phosphate-buffered saline, HDM: house dust mite, HFD: high fat diet.

Table 5: Relative distribution of cells among the individual phenograph clusters within each experimental group.

Colors illustrate relative distribution within one phenograph cluster (row) from least (white) to highest (dark green).

Phenograph cluster			ND/PBS [%]	ND/HDM [%]	HFD/PBS [%]	HFD/HDM [%]
Granulocytes		A	19,8	15,1	22,9	21,9
		B	0,5	11,0	0,3	0,1
Macrophages/ Dendritic cells		I	4,9	11,0	3,7	4,5
		II	8,5	8,8	5,3	4,0
		III	0,5	0,5	0,6	0,3
		IV	0,3	2,0	0,3	0,7
		V	9,9	13,9	14,5	13,0
		VI	9,7	0,8	3,0	2,6
B cells		B cells	21,9	11,9	24,2	26,0
CD4$^+$ cells		CD4	8,1	12,3	10,3	14,9
CD8$^+$ cells		CD8	10,3	6,5	10,3	6,7
NK cells		NK	4,7	3,9	3,6	3,1
AbSeq artefact		Ab	1,1	2,3	0,9	2,2

ND: normal diet, PBS: phosphate-buffered saline, HDM: house dust mite, HFD: high fat diet, NK cells: natural killer cells, Ab: AbSeq labeling

3.3.2 Distinct HDM-activated lung CD4$^+$ T cell population in lean mice is missing in obese HDM-exposed C57BL/6 mice

Based on the results shown above, demonstrating that T cells are involved in obesity-associated alterations of the phenotype of an induced AAI in C57BL/6 mice, further examination of the single cell analysis data was specifically focused on the CD4$^+$ population. Therefore, CD4$^+$ T cells were subclustered, based on the most common (surface) markers used to identify various CD4$^+$ T cell subpopulations (Table 6). As previously done, the individual cell information was visualized using UMAP and phenograph analysis (Figure 25A). A heatmap was plotted depicting specific genes and surface markers for the different CD4$^+$ T cell subclusters as mentioned in Table 6 and additional activation markers such as CD44, CD69, and CD28 (Figure 25B). Certain subclusters exhibited typical gene expression and surface markers associated with CD4 subpopulations such as Th1, Th17, and naïve T cells. However, one subcluster (i.e. phenograph cluster 7) characterized by high expression levels for several common receptors, such as programmed cell death protein 1 (PD-1), T-cell immunoglobulin and mucin-domain containing-3 (TIM-3), cytotoxic T-lymphocyte-associated protein 4 (CTLA-4), and lymphocyte-activation gene 3 (LAG-3) was found. Interestingly, markers specifically identifying diverse T cell subpopulations (*Tbx21* for Th1, *Gata3* for Th2, *Foxp3* for Treg) were also present in this cluster. This suggests that the unifying component in this cluster is not the affiliation of cells to a specific CD4$^+$ T cell subpopulation but rather the high expression of the above-mentioned receptors (see also below). The remaining clusters revealed overlapping gene expression characteristic for memory and effector T cells, whereby a clear identification of those cell clusters according to current T cell subpopulation definitions was not possible.

Table 6: Markers used for subclustering of $CD4^+$ T cells enabling identification of $CD4^+$ T cell subpopulations.
List of selected markers was developed with support of Dr. Christian Möbs, lab leader of the Department of Dermatology and Allergology at the University Hospital of Gießen and Marburg

Memory cells	**Tscm**	**Tcm**	**Tem**	**Temra**	**Trm**
	• $CD62L^+$ • $CD95^+$ • $CD197^+$ • $CD27^+$ • $CD122^+$	• $CD62L^+$ • $CD95^+$ • $CD197^+$ • $CD27^+$	• $CD62L^-$ • $CD95^+$ • $CD197^-$ • $CD27^-$	• $CD62L^-$ • $CD95^+$ • $CD197^-$	• $CD62L^-$ • $CD197^-$ • $CD69^+$ • $CD49a^{+/-}$ • $CD103^{+/-}$ • $CXCR6^{+/-}$ • $Eomes^{low}$ • $T\text{-}bet^{int}$
Helper subsets + regulatory cells	**Th1**	**Th2**	**Th17**	**Th17.1**	**Treg**
	• $CXCR5^-$ • $CXCR3^+$ • $CCR6^-$	• $CXCR5^-$ • $CXCR3^-$ • $CCR6^-$	• $CXCR5^-$ • $CXCR3^-$ • $CCR6^+$	• $CXCR5^-$ • $CXCR3^+$ • $CCR6^+$	• $CXCR5^-$ • $CD127^{low}$ • $CD25^{+(+)}$ • $Foxp3^+$
Naïve + exhausted T cells	**naïve**	**exhausted**	**terminally exhausted**	**memory like progenitor**	**other**
	• $CD62L^+$ • $CD95^-$ • $CD197^+$ • $CD27^+$	• $PD\text{-}1^+$ • $TIM\text{-}3^+$ • $CTLA\text{-}4^+$ • $LAG\text{-}3^+$	• $PD\text{-}1^{high}$ • TCF^- • $CD127^-$ • $EOMES^{high}$	• $PD\text{-}1^+$ • TCF^+ • $CD127^+$ • $EOMES^{low}$	• CCR2

For abbreviations, please refer to chapter I. Abbreviations.

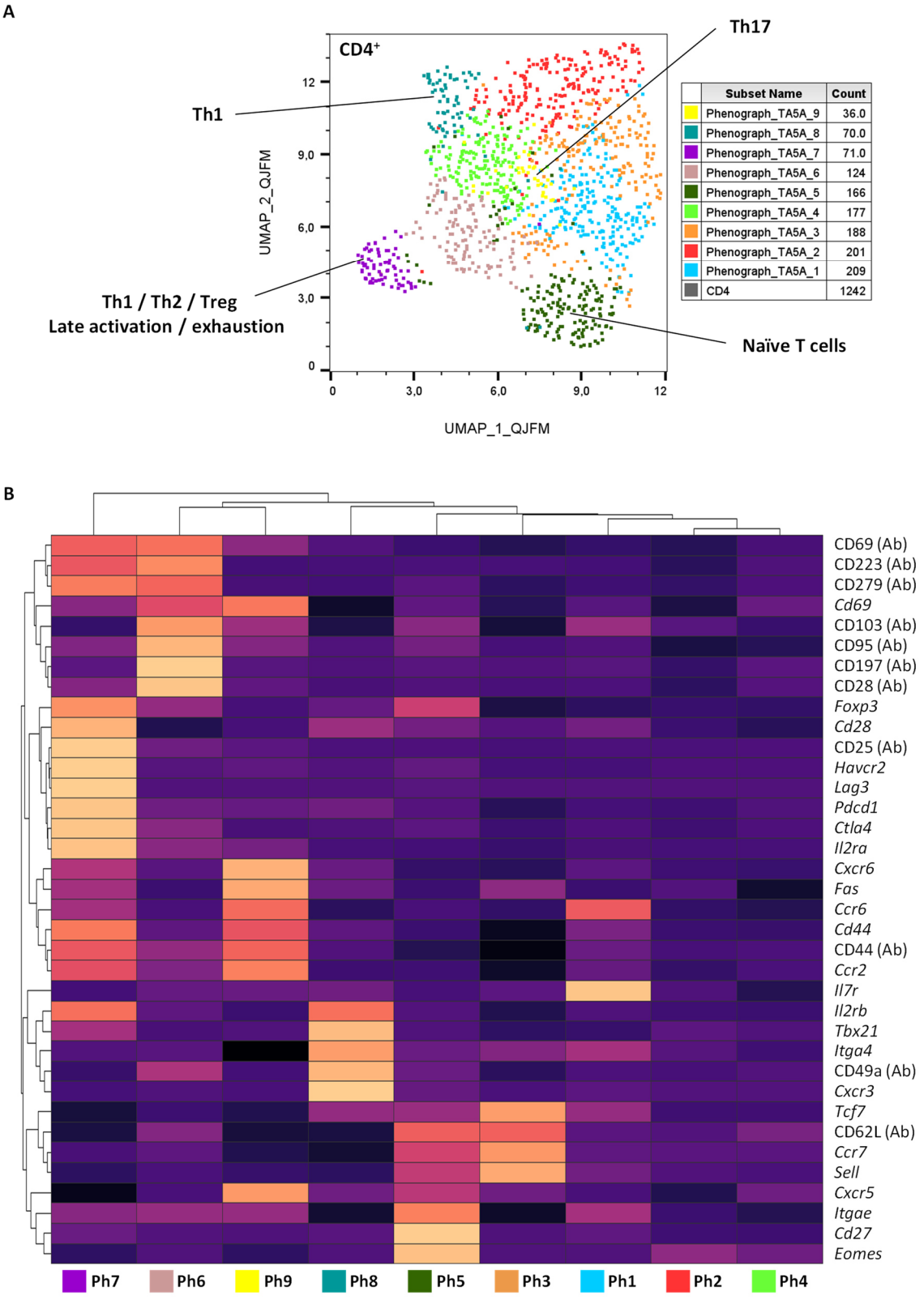

Figure 25: Phenograph identification and gene/surface marker expression profiles of lung CD4⁺ T cell subpopulations of C57BL/6 mice.

Subclustering of lung CD4⁺ T cells of C57BL/6 mice depicted as Uniform Manifold Approximation and Projection (UMAP) overlayed with cluster identification by phenograph analysis (A), colors indicate different phenograph clusters. Heatmap depicting expression profiles of selected genes and surface markers within CD4⁺ T cells of the phenograph subclusters (B), n=12, Th: T helper cell, Treg: regulatory T cell, Ab: AbSeq labeling, Ph: phenograph, ND: normal diet, PBS: phosphate-buffered saline, HDM: house dust mite, HFD: high fat diet.

As shown above for the entire lung leukocyte population, the UMAP for $CD4^+$ T cells was visualized with cells from individual animals in each experimental group indicated by the color code (Figure 26). $CD4^+$ T cell numbers were equally distributed between all groups. Thus, cell number adjustment was not necessary for comparable visualization of the plots. Most obvious, ND-fed C57BL/6 mice with an induced AAI exhibited the presence of one distinct cell cluster (identified as phenograph subcluster 7, see Figure 25) compared to the control ND/PBS mice. Interestingly, this cell cluster was completely missing in all other groups as well including HFD-fed C57BL/6 mice with an induced AAI. Notably, a highly equal distribution of cells from all three animals of the ND/HDM group was observed within this specific cell cluster, suggesting that these cells represent a typical feature of the respective experimental condition. Cells within this cluster were identified by expression of several $CD4^+$ T cell subpopulations markers, e.g. Th1 (*Tbx21*), Th2 (*Gata3*), and Treg (*Foxp3*), general T cell activations markers, e.g. CD69, CD25 but also several other T cell receptors (*Pdcd1/*PD-1, *Ctla4*, *Lag3/*CD223, *Havcr2)*. This indicates that an induced AAI leads to the expression of such receptors on different subtypes of activated T cells in lean mice, whereas HFD seem to markedly inhibit the expression of these receptors on Th1, Th2, and Treg cells. Expression of these receptors on Treg cells are associated with their activation, whereas such receptors expressed on effector T cells are rather related to the generation of inhibitory signals to other T cells. Together, expression of these markers in different $CD4^+$ T cell populations is considered to be involved in the dampening of ongoing immune reactions (Corthay, 2009, Wherry, Kurachi, 2015). Based on this, these receptors will further be referred to as co-inhibitory receptors, as various names exist in the literature, which are dependent on the context used (Corthay, 2009, Garon et al., 2015, Schnell et al., 2020, Wherry, Kurachi, 2015, Yi et al., 2010). As the expression of these receptors was missing in obese mice with an induced AAI, this mechanism might play an important role in the altered immune response seen in those mice.

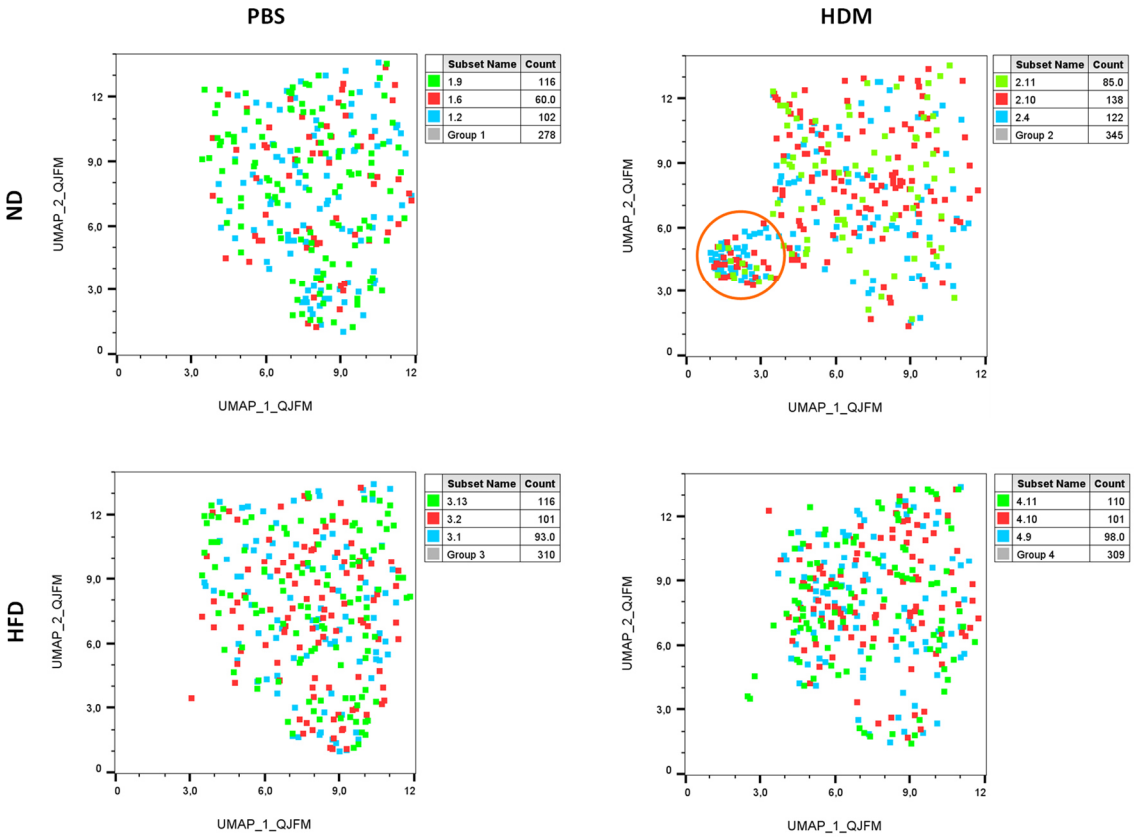

Figure 26: Subclustering of lung CD4⁺ T cells reveals an activated T cell population in the ND-fed C57BL/6 mice with an induced AAI, which is completely missing in HFD/HDM C57BL/6 mice.
Experimental groups separated for visualization of lung CD4⁺ T cells of C57BL/6 mice with Uniform Manifold Approximation and Projection (UMAP), colors indicate n=3 animals of each group, orange circle indicates phenograph cluster 7, ND: normal diet, PBS: phosphate-buffered saline, HDM: house dust mite, HFD: high fat diet.

3.4 Inflammatory mechanisms of the adipose tissue reduce co-inhibitory receptor expression by CD4$^+$ T cells

3.4.1 Flow cytometric analysis demonstrating the presence of lung CD4$^+$ T cells expressing co-inhibitory receptors in a HDM model

The presence of the distinct CD4$^+$ T cell population identified by the single cell analysis in lean mice with an induced AAI (i.e. phenograph cluster 7, see Figure 25 and Figure 26) was further demonstrated by flow cytometry in C57BL/6 mice exposed to the HDM model without HFD, i.e. just i.n. application of HDM was performed. To prove the successful induction of airway inflammation in the HDM group, the BAL was analyzed by morphological characterization of the BAL cells. The expected increase in eosinophil and neutrophil numbers was seen in the HDM group in comparison to the PBS control group, similarly to the previous results shown in Figure 18 (data not shown). Further, lung cells were isolated and analyzed via flow cytometry. Next to total CD4$^+$ T cells, also numbers of Th2 cells, here defined by expression of CCR4$^+$ and GATA3$^+$, as well as CD25$^+$ Foxp3$^+$ Treg cells were found to be increased in the lungs of the HDM-exposed C57BL/6 mice (Figure 27).

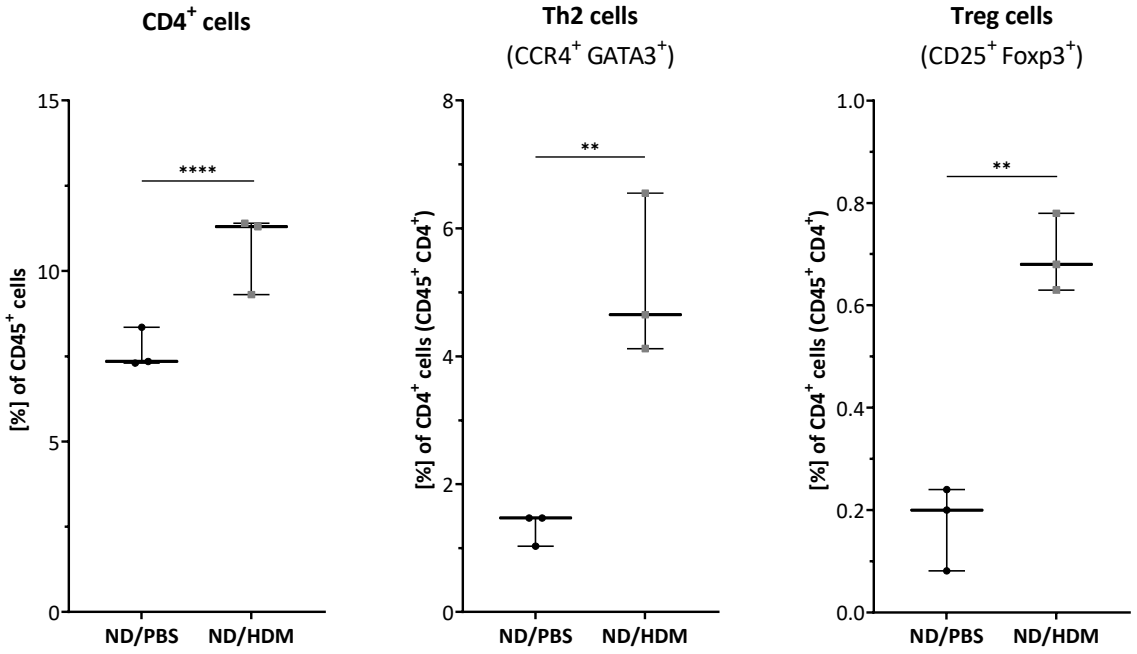

Figure 27: Relative presence of T cell populations in the lungs of HDM-exposed C57BL/6 mice.
Flow cytometric analysis of pulmonary CD4$^+$ T cells (left), CCR4$^+$ GATA3$^+$ Th2 cells (middle) and CD25$^+$ Foxp3$^+$ Treg cells (right) in C57BL/6 mice, n=3, ** $p \leq 0.01$, **** $p \leq 0.0001$, ND: normal diet, PBS: phosphate-buffered saline, HDM: house dust mite, Th: T helper cell, Treg: regulatory T cell.

Examining the distinct markers identified in the phenograph cluster 7 of $CD4^+$ T cells, the presence of PD-1, CTLA-4, and LAG-3 was measured on overall $CD4^+$ T cells, and Th2 and Treg subpopulations. Comparing HDM-exposed mice to the PBS controls, all three co-inhibitory receptors were significantly upregulated on $CD4^+$ T cells, individually as well as in combination (Figure 28A). Specifically, among Th2 cells the frequency of PD-1^+ as well as LAG-3^+ cells was found to be increased in HDM-exposed C57BL/6 mice (Figure 28B). The percentage of CTLA-4^+ cells did not differ between the HDM and PBS control groups. However, it needs to be considered that less $CD4^+$ T cells and accordingly also less Th2 and Treg cells were present, hence resulting in lower absolute cell numbers of activated T cells in the lungs of control mice. Evaluating the combined expression of all three co-inhibitory receptors on Th2 cells, an increase of triple positive Th2 cells was seen in HDM-exposed mice. One outlier was observed due to the lower percentage of LAG-3^+ cells in one of the mice. Similar results were seen when analyzing Treg cells, whereby significant increases in the relative numbers of PD-1^+ and LAG-3^+ Tregs cells were observed with no changes in the frequency of CTLA-4^+ cells (Figure 28C). Accordingly, numbers of Treg cells positive for all three co-inhibitory receptors were significantly higher in the HFD-exposed mice in comparison to the PBS control group. The presence of T cells expressing co-inhibitory receptors in the lungs of HDM-exposed mice detected via flow cytometric analysis confirmed the presence of the phenograph cluster 7 cell population identified in the single cell analysis of lung $CD4^+$ T cells.

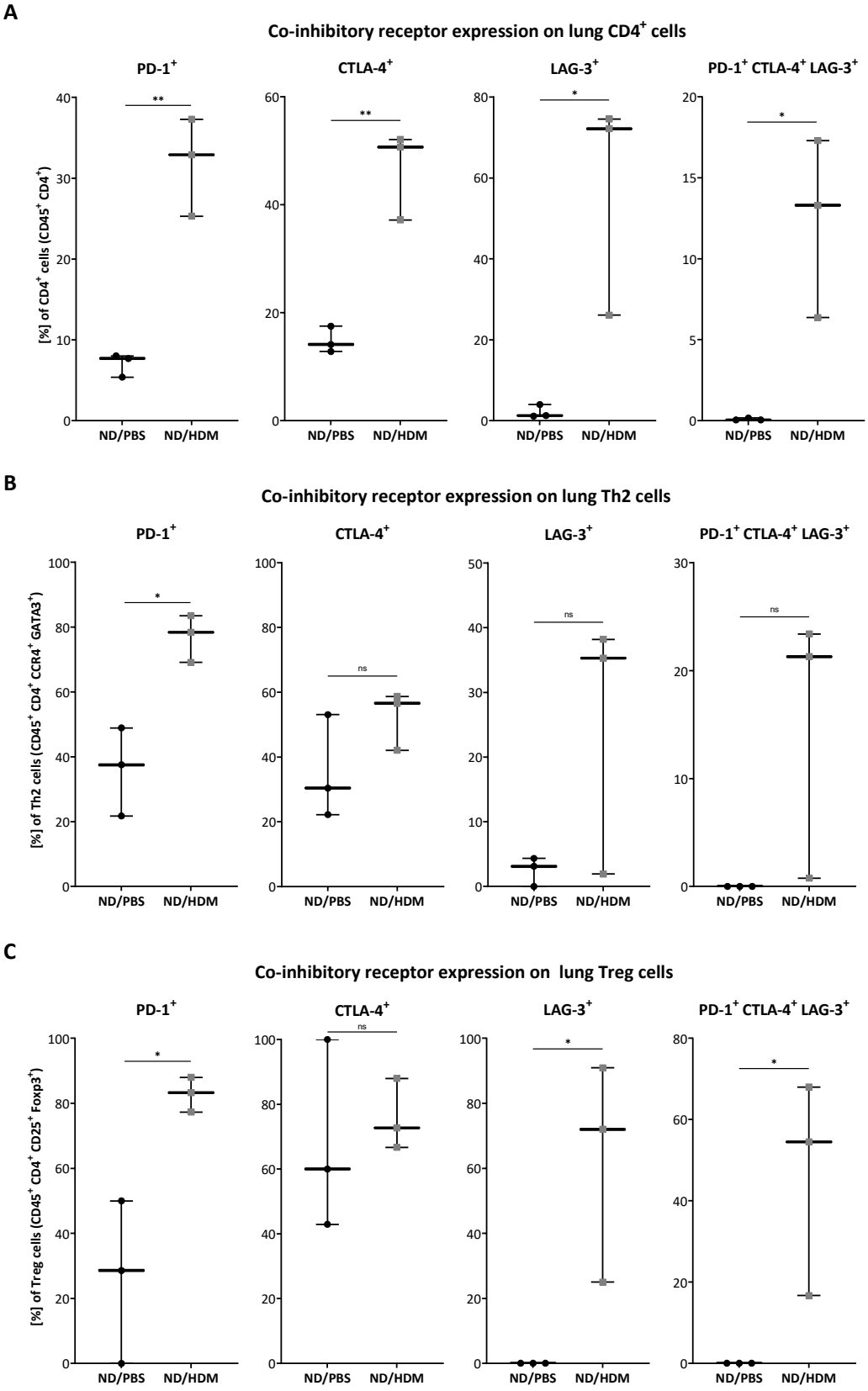

Figure 28: Flow cytometric demonstration of lung CD4⁺, Th2, and Treg cells expressing co-inhibitory receptors in lean HDM-exposed mice.

Flow cytometric analysis of PD-1, CTLA-4, and LAG-3 on CD4⁺ T cells (A), CCR4⁺ GATA3⁺ Th2 cells (B) and CD25⁺ Foxp3⁺ Treg cells (C) in the lungs of HDM-exposed versus PBS control C57BL/6 mice, n=3, * $p \leq 0.05$, ** $p \leq 0.01$, ns: not significant, ND: normal diet, PBS: phosphate-buffered saline, HDM: house dust mite, Th: T helper cell, Treg: regulatory T cell.

3.4.2 Signals released by adipocytes reduce co-inhibitory receptor expression on Th2 and Treg cells *in vitro*

In vitro activation via anti-CD3 of differentiated Th2 and Treg cells was used as model to investigate the idea that hypertrophic activated adipocytes may release factors involved in the regulation of co-inhibitory receptor expression of $CD4^+$ T cells. Therefore, a pool of supernatants from *in vitro* cultured adipocytes from HFD-fed mice was applied to differentiated Th2 and Treg cells during activation. Stimulation of Th2 and Treg cells for 48 h with anti-CD3 led to increased expression of co-inhibitory receptors, as they were positive for all three markers, either directly after the 48 h stimulation (Th2 cells) or another 48 h rest (Treg cells) (Figure 29). The expression of co-inhibitory receptors was reduced by addition of the adipocyte supernatant resulting in reduced numbers of Th2 and Treg cells triple positive for PD-1, CTLA-4, and LAG-3.

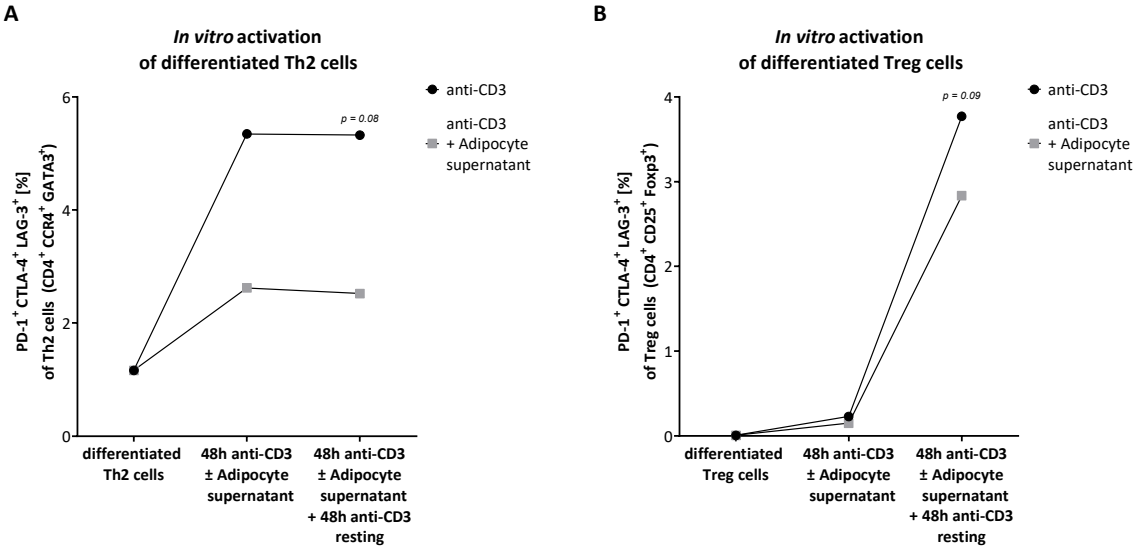

Figure 29: Adipocyte supernatant inhibits the activation of Th2 cells and to a small extent also in Treg cells.
Flow cytometric analysis of differentiated, anti-CD3 restimulated splenic $CCR4^+$ $GATA3^+$ Th2 cells (A) and $CD25^+$ $Foxp3^+$ Treg cells (B) incubated for 48 h with adipocyte supernatant and another 48 h resting, data shown as mean of n=3, Th: T helper cell, Treg: regulatory T cell.

To determine which of the three co-inhibitory receptors was or were mainly affected, every candidate marker was depicted individually. As seen in Figure 30, CTLA-4 and LAG-3 on the Th2 cells incubated with adipocyte supernatant were markedly reduced, whereas PD-1 was not uniformly affected by the stimulation with the adipocyte supernatant. In Treg cells, the inhibitory effect was not as strong, with a clear reduction

only in CTLA-4$^+$ Treg cells in response to adipocyte supernatant. In conclusion, inflammatory mechanisms taking place in the obese adipose tissue may be responsible for the reduced expression of co-inhibitory receptors on CD4$^+$ subpopulations, which subsequently might lead to a lack of control of the immune response. Altogether, this may ultimately result in the altered phenotype of the obesity-associated AAI phenotype in mice.

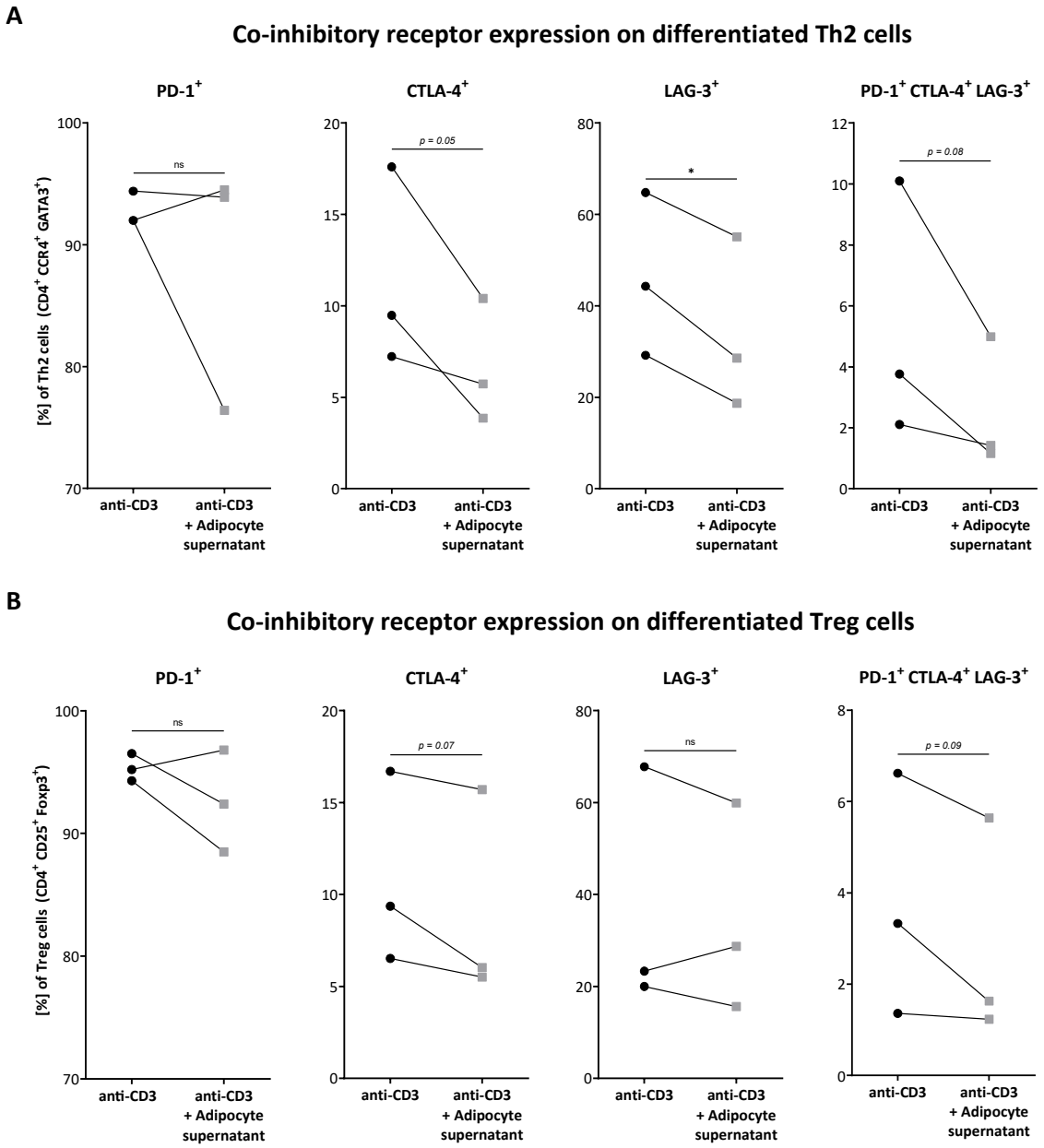

Figure 30: Frequencies of activated CTLA-4$^+$ and LAG-3$^+$ Th2 cells are reduced by adipocyte supernatant. Flow cytometric analysis of differentiated, anti-CD3 restimulated splenic CCR4$^+$ GATA3$^+$ Th2 cells (A) and CD25$^+$ Foxp3$^+$ Treg cells (B) incubated for 48 h with adipocyte supernatant and additional 48 h resting, n=3, ns: not significant, Th: T helper cell, Treg: regulatory T cell.

4. Discussion

Asthma and obesity are NCDs with high and still increasing prevalences. Both are characterized by the presence of local and systemic inflammatory processes, whereby the pathomechanistic relationships within obesity-associated asthma, a disease entity combining asthma and obesity, are not fully elucidated. Obesity-associated asthma is not defined as a single phenotype with one corresponding endotype, but a few different sub-phenotypes have been described underlain presumably by several various endotypes. Multiple factors such as genetics, environment, and diversity of immunological mechanisms play an important role in the development of allergic and other non-communicable systemic diseases. These complex interactions occur at the tissue, organ, and whole organism level. Therefore, they cannot be fully mimicked by *in vitro* experimental systems, which are always characterized by much lower levels of complexity. Hence, mouse models are still a necessary tool, also for the investigation of underlying mechanisms of the low-grade systemic inflammation of the adipose tissue and its interaction with the lung tissue.

Different mouse models are available for establishing experimental setups of obesity research. Genetically modified animals may be used as obesity-model, such as leptin (LEP)-, leptin-receptor (LEPR)- or proopiomelanocortin (POMC)-knock-out (KO) mice, which are prone to excess weight gain (Lutz, Woods, 2012). As an alternative to the KO models, a HFD may be applied to induce metabolic changes and obesity in mice. A HFD with 40-60% calories from fat is most commonly used in experimental setups, whereas the normal rodent diet is a 10% fat diet. In general, the duration of a HFD model is 10-12 weeks, whereby a 60% fat diet leads to faster development of obesity in mice (Speakman, 2019). With regard to weight gain, differences in the genetic background need to be considered. Useful readouts for the monitoring of obesity-like changes are body weight or body condition score and GTT/ITT (Kleinert et al., 2018).

In our studies, HFD was chosen in favor of a KO system to mimic obesity in a mouse model, providing a more translatable situation to the human condition, in which obesity

is commonly based on an unhealthy lifestyle including fat-rich nutrition and physical inactivity (WHO, 2021b). Both, BALB/c and C57BL/6 strains were involved to not only cover known differences in weight gain in response to a HFD but also to consider differently balanced immune responses, which will be discussed later (Fukushima et al., 2006, Jovicic et al., 2015). In line with the literature, the most prominent phenotypic difference observed between BALB/c and C57BL/6 mice receiving a HFD was the level of weight gain (Jovicic et al., 2015, Montgomery et al., 2013). C57BL/6 mice gained significantly more body weight compared to HFD-fed BALB/c mice, which did not differ in weight from control diet fed BALB/c mice. Although Tashiro et al. could show significant weight increase in BALB/c mice using a HFD model (Tashiro et al., 2017), this observation is in contrast to the remaining literature (Boi et al., 2016, Li et al., 2020, Nishikawa et al., 2007, Spielmann et al., 2021). However, BALB/c mice being resistant to a HFD could be an interesting research aspect for topics more specifically related to metabolic research (Boi et al., 2016).

Interestingly, despite the obvious weight gain differences, metabolic changes observed in this study were similar in both strains after receiving a HFD. Further, the results of increased plasma levels of both, HDL and LDL cholesterol were surprising as in human dyslipidemia commonly HDL cholesterol shows a low concentration, whereas LDL cholesterol is elevated (Alberti et al., 2006). Yet, also Brenachot et al. demonstrated increased plasma levels of both, HDL and LDL cholesterol in a mouse model with HFD (Brenachot et al., 2017), corroborating the results of the present study. Furthermore, metabolic features of T2D were seen as glucose intolerance and attenuated insulin sensitivity in HFD-fed BALB/c as well as C57BL/6 mice. Insulin resistance is not only an indicator of T2D (Heydemann, 2016), but it might also indicate chronic inflammation of the adipose tissue, which is considered to be an initiator of insulin resistance as demonstrated by Xu et al. (Xu et al., 2003).

In addition to metabolic changes, both strains developed hypertrophic adipocytes in response to the HFD, but the extent of hypertrophy was more pronounced in C57BL/6 mice. Yet, Jovicic et al. described that C57BL/6 mice on a HFD tend to have an increased adipocyte hyperplasia in comparison to BALB/c mice (Jovicic et al., 2015). Even though

adipocytes pathophysiology was not further investigated here, it is possible that these mice not only developed adipocyte hypertrophy but also hyperplasia. Hypertrophic adipocytes are known to release more inflammatory signals and their endocrine mechanisms are dysregulated (Greenberg, Obin, 2006, Makki et al., 2013). Therefore, it was not surprising that the analysis of adipocyte supernatants from obese C57BL/6 mice revealed increased levels of inflammatory mediators as well, e.g. inflammatory TNF-α and MCP-1, which was also seen in several other obesity models (Hotamisligil et al., 1993, Sartipy, Loskutoff, 2003).

Additionally, the transcriptome profile in the adipose tissue of obese mice was altered, demonstrating an increased expression of genes associated with several pathways of an activated innate immune system. This was also observed by Xu et al. in white adipose tissue of obese mice, additionally they related the upregulated genes in inflammatory pathways to inflammatory macrophage activities (Xu et al., 2003). Despite the restriction of having analyzed only three animals per group, substantial consistency of the transcriptome data was seen. Pathway analysis of the transcriptome data revealed increased expression of genes involved in B cell receptor signaling pathways in obese HDM-exposed C57BL/6 mice. This was in another way seen using flow cytometry in the same group by an increased number of B cells in the adipose tissue, highlighting the integrity of the transcriptome data. More inflammatory changes were seen by increased numbers of neutrophils in the obese adipose tissue of C57BL/6 mice, but not in BALB/c mice. However, numbers of anti-inflammatory M2 macrophages were reduced in the adipose tissue with HFD in both strains, yet higher numbers of anti-inflammatory M2 macrophages were still present in BALB/c mice. Altogether, this suggests that inflammatory processes were present to a higher extent in the obese adipose tissue of C57BL/6 mice than in BALB/c mice in response to the HFD. In turn, higher numbers of anti-inflammatory M2 macrophages in BALB/c mice might be associated with normal functionality of adipocytes and possibly indicating a link to the missing weight gain in response to the HFD. Accordingly, in HFD-fed BALB/c mice, with missing weight gain and less hypertrophic adipocytes, no increased inflammatory processes were found in the adipose tissue. On the other hand, the described results, which are linking adipocyte hypertrophy, increased inflammation in the adipose tissue and weight gain were in line

with previously discussed adipose tissue inflammation in the context of insulin resistance by Blüher (Blüher, 2016).

Apart from the obesity-associated asthma phenotype characterized by late onset, commonly found in women, and related to non-type 2 inflammatory processes, other more type 2 inflammation-related forms of asthma and obesity coexistence have been described (Lang, 2014, Wenzel, 2012). This suggests that several endotypes may underlie varying clinical forms of obesity-associated asthma. In order to understand the underlying pathomechanisms, mouse models are necessary, as the access to the human material is limited. Mouse models mimicking human asthma are much more complex to induce compared to obesity-models, as various types of asthma exist. Due to the heterogeneity of numerous phenotypes and endotypes, specific mouse models are needed to examine this disease. Using either HDM or OVA, several types of inflammatory phenotypes mimicking various human asthma forms can be established. Intranasal application of OVA in pre-sensitized mice is frequently used to induce a type 2-driven immune response with an increase in eosinophilic cells in the BAL (Nials, Uddin, 2008). With different application routes (intranasal and/or intraperitoneal) and their combinations as well as variation of dosage, HDM is able to provoke different types of AAI such as those mimicking Th2 (type 2), Th1/Th17 (non-type 2), and mixed (Th2/Th1/Th17) asthma endotypes (Hagner et al., 2020, Tan et al., 2019).

In this study, induction of a previously established mixed HDM-induced AAI was applied (Hagner et al., 2020), which is characterized by equal increases in eosinophil and neutrophil numbers corresponding to the concurrent activation of type 2 as well as non-type 2 immune mechanisms. This mixed phenotype was chosen to investigate a possible shift of the inflammatory phenotype in one or the other direction when combined with a HFD. Lung histology analysis is a widely used method to evaluate peribronchial inflammation as well as goblet cell hyperplasia in lung tissue of HDM-exposed mice (Woo et al., 2018). HDM-exposed BALB/c and C57BL/6 mice developed comparable lung tissue inflammation and mucus hypersecretion independently of the diet. The induction of a mixed inflammatory phenotype by the utilized HDM-model was successfully reproduced in BALB/c mice within this study. Investigating alterations by HFD on the induced AAI,

BALB/c mice did not show any impact of the HFD on the BAL cell composition in comparison to their ND-fed counterparts. Until this study, it was unknown how the model of the mixed HDM-induced AAI would develop in C57BL/6 mice. Genetic differences between BALB/c and C57BL/6 mice need to be considered also for the development of potentially different inflammatory responses such as the above-described differences in weight gain. The BALB/c strain is more prone to exhibit type 2-driven immune responses, whereas C57BL/6 mice rather develop Th1/Th17-driven immune reactions (Fukushima et al., 2006). Therefore, one would have rather expected a higher neutrophilic cell recruitment than an equal increase in the different granulocytes in the HDM-exposed C57BL/6 mice. Accordingly, the findings of even more eosinophils than neutrophils in HDM-exposed C57BL/6 were surprising. However, it was nevertheless possible to study the effect of a HFD and related weight gain associated with inflammation in the adipose tissue on the HDM-induced AAI in C57BL/6 mice. In particular, when focusing on BAL cell composition, a more eosinophilic inflammation was developed in HFD-fed HDM-exposed C57BL/6 mice. This effect was based on a further reduction of neutrophilic cell numbers in the BAL. Whether these changes point to a distinct shift to a more type 2-based endotype by the HFD remains questionable, as the HDM-induced AAI in lean C57BL/6 mice showed more eosinophils than neutrophils as well. Nevertheless, it could be hypothesized, that the HDM-induced inflammatory phenotype is aggravated by HFD induced weight gain in C57BL/6 mice.

Severity of the asthmatic outcome might be directly linked to the presence or absence of an alteration in neutrophil numbers in obese asthmatic patients. Telenga et al. demonstrated an increase of neutrophils numbers in the sputum of obese asthmatic patients with no difference in severity compared to non-obese asthmatics, whereas Desai et al. observed no difference of neutrophils but an increase in eosinophils within the airway walls of obese patients with severe asthma (Desai et al., 2013, Telenga et al., 2012). The increase of eosinophilic inflammation in a HFD/HDM mouse model was previously also seen in other studies. Everaere et al. found, next to the recruitment of eosinophils to BAL and lung tissue, further obesity related exacerbations of asthma, such as elevated serum IgE-concentrations and more pronounced AHR (Everaere et al., 2016). Combining the commonly used Th2 asthma model with OVA in combination with a HFD

yielded similar observations of increased eosinophil numbers in BAL of C57BL/6 mice (Calixto et al., 2010). However, other studies showed contrasting results, whereby a decrease of eosinophil numbers in BAL of HFD-fed OVA or HDM-exposed C57BL/6 mice was demonstrated (Diaz et al., 2015, Schröder et al., 2019, Vries et al., 2009). Yet, in contrast to the previously stated findings, in the studies by de Vries et al. and Schröder et al. mice did not show obvious weight gain in response to the HFD (Schröder et al., 2019, Vries et al., 2009). Although the aforementioned studies were conducted in C57BL/6 mice, this could be an explanation for the trending decrease of the ratio of eosinophil to neutrophil numbers in lungs of BALB/c mice with a HFD when compared to ND-fed mice. These results suggest that a HFD not associated with weight gain might lead to a decrease in eosinophil numbers of an induced AAI. Overall, in our experiments HFD without weight gain did not obviously change the inflammatory phenotype of a HDM-induced AAI, but alterations seemed rather to be linked to weight gain and inflammatory processes in the obese adipose tissue.

Besides changes in the ratio of eosinophil to neutrophil numbers in the BAL of HDM-exposed C57BL/6 mice, an increase in BAL lymphocyte numbers was seen. This change can be set into context by considering that cytokines released by T cells contribute to the recruitment of eosinophils and neutrophils (Potaczek et al., 2020). Lymphocyte subpopulations in lung tissue were further investigated by flow cytometric analysis. An altered ratio of $CD4^+$ to $CD8^+$ T cells and increased numbers of B cells in lungs of obese C57BL/6 mice with the induced AAI were demonstrated. Increased numbers of B cells could be correlated to the significant increase in HDM-specific IgG levels in the HFD/HDM group. This may suggest an enhanced sensitization in C57BL/6 mice exposed to HDM in combination with a continuing HFD. BALB/c mice in the HFD group, which were missing the increased inflammatory processes in the adipose tissue, did neither show differences in lung cell composition nor in HDM-specific IgG levels in HDM-exposed groups.

To further investigate the endotype of the induced AAI in obese C57BL/6 mice in more detail, $CD45^+$ lung leukocytes were examined in depth with a single cell analysis. Single cell sequencing is the up-to-date method to investigate cellular differences and

functions on an individual cellular basis. The BD Rhapsody single cell analysis system provides not only the advantage of being able to examine mRNA expression on a single cell level, but in addition it enables the examination and characterization of cells based on their surface molecules, detected by using surface marker-specific antibodies labeled with sequenceable DNA oligos, called AbSeqs. Use of AbSeqs allows distinct labeling, identification, and clustering of cells with a great number of cell-surface protein markers within one experiment (BD Biosciences, 2021).

Using UMAP and phenograph as methods for dimensionality reduction, visualization, and clustering for similarities of combined data on gene expression and expression of surface markers, a variety of different leukocyte subpopulations could be identified. In line with the flow cytometric results of the lung tissue, single cell sequencing data revealed differences between HDM groups with or without HFD in B cells, $CD4^+$ T cells and diverse myeloid cell populations. For initial evaluation of the extensive single cell data set, $CD4^+$ T cells were further analyzed, as they are considered to play a crucial role in the mechanistic dissection of asthma into type 2 and non-type 2 endotypes (Holgate et al., 2015, Schatz, Rosenwasser, 2014).

Subclustering of $CD4^+$ T cells enabled the identification of several cell clusters mainly consisting of cells fitting into the current concept of subdividing T cells such as Th1, Th17 or naïve T cells. However, the BD Rhapsody single cell analysis provides information of gene as well as surface marker expression of each cell. Therefore, a lot more cellular markers are acquired and considered for sub-phenotyping of cells, which makes it even more difficult to assign all cells to commonly defined T cell subpopulations. The central aim of this study was to identify underlying mechanisms responsible for the shift in the inflammatory phenotype of the HDM-induced AAI in obese mice. Therefore, analyses focused mainly on $CD4^+$ T cell subpopulations differently present in HDM-exposed ND and HFD mice. A highly interesting $CD4^+$ subcluster was found, described in the results as phenograph cluster 7, which showed distinct differences between the two HDM groups with or without HFD. This cluster was only present in lean HDM-exposed and not in obese HDM-exposed mice, and in addition also not observed in the non-HDM groups.

In-depth investigation of the cells within this cluster did not allow the distinct assignment to one or the other of the traditionally defined CD4 subpopulation such as Th2, Th1, Th17 or Treg. Investigation of transcription factor marker expression within this subcluster exhibited a considerable presence of cells with GATA3, Foxp3, and T-bet expression. Therefore, cells associated with typical characteristics of Th2, Treg, and Th1 cells were found in this cluster. Despite apparently different cell types present in this cluster, the clustering mechanism still mapped them into the same cluster. This indicates that those cells must have unique similarities that overruled their subpopulation characteristics in terms of clustering. Further investigation of specific gene expression patterns within this cluster revealed the high expression of genes for several receptors, such as PD-1, CTLA-4, LAG-3, and TIM-3. Not only the gene expression of these receptors (*Pdcd1*, *Ctla4*, *Lag3*, *Havcr2*), but also the corresponding surface proteins of PD-1 (CD297) and LAG-3 (CD223) indicated by the respective AbSeq signals were increased. Therefore, the presence of these receptors on $CD4^+$ T cells seemed to be the specific unifying features of cells in this cluster independently of their assignment to Th1, Th2, and Treg cells.

For further elaboration of the receptors found in this cell cluster, their known functions are briefly described. T cell activation requires not only the recognition of antigen via the T cell receptor but also the concomitant presence of co-stimulatory signals. For instance, the receptor CD28, expressed on T cells, binds to CD80 (B7.1) and CD86 (B7.2) on antigen presenting cells and thus the IL-2 production is triggered, which is a key cytokine required for T cell proliferation (Chen, Flies, 2013). In turn, the expression of receptors such as PD-1, CTLA-4, and LAG-3 is upregulated after the activation and expansion of T cells. Expression of such receptors can be found on several different T cell subsets, such as activated, regulatory, and exhausted T cells (Schnell et al., 2020). Many years ago, it has already been shown, that the CTLA-4 receptor has a high sequence similarity to CD28 but with a higher binding affinity to the same ligands CD80 and CD86 (Linsley et al., 1991). Expression of CTLA-4 acts as a negative regulator of T cell activation by sending inhibitory signals to T cells (Walunas et al., 1994). The receptor PD-1 is next to expression on T cells also expressed on B cells, monocytes, and some subtypes of DCs and mediates it's inhibitory signals via PD-L1 and PD-L2 ligands (Francisco et al., 2010).

Expression of LAG-3 is found on activated T cells and subsets for NK cells. LAG-3 resembles CD4 receptors, but it binds to major histocompatibility complex (MHC) class II with a higher affinity than the CD4 receptor. Interestingly, CTLA-4 and LAG-3 are associated with the activation of Treg cells, increasing their inhibitory functions during the course of ongoing immune reactions (Corthay, 2009). Expression of PD-1, LAG-3, and TIM-3 on activated effector T cells may indicate (down-)regulatory functions and as well may represent a sign of T cell exhaustion (Anderson et al., 2016, Wherry, Kurachi, 2015, Yi et al., 2010). Consequently, expression of receptors on Treg cells and effector T cells is associated with control and downregulation of immune responses. Depending on the perspective, these receptors may be referred to as exhaustion or activation markers, or immune co-signaling/inhibitory receptors. In tumor research, especially CTLA-4 and PD-1 are further known as immune checkpoint markers (Garon et al., 2015, Nakamura, 2019). In this study, PD-1, CTLA-4, and LAG-3 were termed co-inhibitory receptors. The presence of cells expressing such receptors in HDM-exposed lean mice suggests the presence of processes involved in the control of immune responses after an induced AAI in these mice. In turn, the absence of such cells in obese HDM-exposed mice might explain the elevated uncontrolled inflammatory processes in the obese HDM-exposed mice.

To understand the possible mechanisms that are involved in the expression of co-inhibitory receptors in the course of an ongoing immune response, the scientific literature was extensively reviewed. CTLA-4 was shown to be regulated by transcription factors such as nuclear factor of activated T-cells (NFAT) and FoxP3 (Chen et al., 2006, Gibson et al., 2007). In addition to the thymocyte selection-associated high mobility group box protein (TOX) and nuclear receptor subfamily 4A (NR4A), NFAT is one of the transcriptions factors the activation of which is essential for the initiation of exhaustion processes in $CD8^+$ T cells along with increased expression of PD-1, TIM-3, and LAG-3 (Seo et al., 2019). Another transcription factor regulating the expression of PD-1 is Foxo1, which antagonizes activities of the transcription factor T-bet and thus prevents the downregulation of PD-1 (Bally et al., 2016). Foxo1 is also known to be highly expressed in Treg cells, whereby it induces not only the expression of PD-1 but also CTLA-4 and CCR7, which enhances the formation and function of Treg cells (Cabrera-Ortega et al.,

2017). The particular single cell analysis performed in this study was limited by targeted examination of genes belonging to a pre-designed immune panel. Therefore, some of the transcription factors, which might be involved in the mechanistic processes behind the endotypes described here, were not included in the analyses. In the future, a whole transcriptome analysis or qPCR of the gene expression of transcription factors could be performed to further elaborate these findings.

To show that co-inhibitory receptor gene expression identified in the single cell analysis experiment also translates into protein expression on $CD4^+$ T cells, an additional animal experiment was conducted. Due to the relatively pronounced eosinophilic inflammation seen in the BAL, pointing to aggravated type 2 immune mechanisms, the initial focus was put on Th2 cells. Nevertheless, since for instance PD-1 and TIM-3 are crucial for maintaining Th1 cell numbers during malaria, the presence of co-inhibitory receptors on Th1 cells might also be expected (Dookie et al., 2020). Additionally, due to thesis-related time constraints this study was restricted to ND-fed with or without HDM exposure only. The results of these analyses could prove the presence of the co-inhibitory receptors PD-1, CTLA-4, and LAG-3 on lung $CD4^+$ T cells in general and more specifically on lung Th2 and Treg cells in a HDM-induced AAI in C57BL/6 mice, thus confirming the existence of the distinct cell population previously seen in the single cell analysis. This further supports the idea that inflammatory processes take place after an induced AAI in lean mice, which seem to be controlled and thus limited by the expression of co-inhibitory receptors on different T cell subtypes.

While mouse studies offer the great opportunity to study underlying mechanisms of the pathophysiology of the obesity-associated asthma, their findings still need to be translated to humans. Therefore, it was encouraging to find that investigations of $CD4^+$ T cells showed elevated expressions of PD-1, CTLA-4, and TIM-3 in asthmatic patients (Mosayebian et al., 2019, Wiest et al., 2018) . Additionally, it has been shown that the *in vitro* stimulation of human $CD4^+$ T cells with HDM also led to increased expression of PD-1, CTLA-4, and LAG-3 (Rosskopf et al., 2018). Furthermore, Rosskopf et al. demonstrated in their *in vitro* experiments using human PBMCs the role of PD-1 signaling in

dampening $CD4^+$ T cell responses against aeroallergens (Rosskopf et al., 2018), additionally supporting the above stated interpretations of the results.

The absence of a cell cluster with high expression of the mentioned co-inhibitory receptors in obese HDM-exposed mice initiated the idea that inflammatory processes of the obese adipose tissue might interfere with the regulation of these receptors on $CD4^+$ T cells. In line with this idea, an *in vitro* experiment was conducted in which supernatant of cultured adipocytes from HFD-fed mice was applied to differentiated T cells. Therefore, Th2 and Treg cells were differentiated and activated *in vitro* to induce the expression of co-inhibitory receptors. The simultaneous stimulation with adipocyte supernatant enabled the investigation of its impact on expression of the co-inhibitory receptors. In Th2 cells, especially the numbers of CTLA-4 and LAG-3 expressing cells were reduced, while in Treg cells a reduction of $CTLA\text{-}4^+$ cells could be observed in response to adipocyte supernatant. Similarly, in a study by Pizzolla et al. expression of CTLA-4 on Tregs was investigated by using an OVA/HFD model in C57BL/6 mice. Consistent with our results, their ND/OVA mice showed an increase in CTLA-4 expression on Treg cells, whereas no alteration was found in HFD-fed mice. Furthermore, the authors state that Treg activation but not Treg recruitment is reduced in mice on a HFD (Pizzolla et al., 2016). Altogether, these findings support the idea that inflammatory processes may proceed uncontrolled in the obesity condition. Further, considering increased levels of adipokines leptin and resistin but also TNF-α and IL-6 released by the adipocytes, they might be associated with the altered activation processes in lung $CD4^+$ T cells, as such adipokines and cytokines are known to induce naïve CD4 T cell proliferation and differentiation (Song, Deng, 2020).

In this study, expression of co-inhibitory receptors, so far more commonly associated with functions of $CD8^+$ T cells, was however deeply investigated on $CD4^+$ T cells. Therefore, data from the single cell analysis were also used for further subclustering of $CD8^+$ T cells. Similar results regarding the expression of co-inhibitory receptors were obtained, whereby one cell cluster was identified by high expression of the co-inhibitory receptors CTLA-4, LAG-3, PD-1, and TIM-3, which also demonstrated the highest presence of the cells from the ND-fed HDM-exposed mice (data not shown). Furthermore,

the *in vivo* experiment validating the single cell analysis data of co-inhibitory receptors on $CD4^+$ T cells also revealed an increase in the number of $CD8^+$ T cells expressing these receptors in lean HDM-exposed mice (data not shown). However, more in depth investigations of $CD8^+$ single cell data are needed. Co-inhibitory receptors are often examined on $CD8^+$ T cells in association with tumor development and thus are specifically known as immune checkpoint markers. For tumor therapy, so-called immune checkpoint inhibitors have been identified and tested for over a decade (Robert, 2020). Interestingly, obese patients have been found to show an increased expression of PD-1 on $CD8^+$ T cells in the liver. These patients tend to respond better to tumor therapy with checkpoint inhibitors assumingly because higher levels of surface markers are available for binding possibilities of the therapeutic agents (Wang et al., 2019). Co-inhibitory receptors are not only of interest in the context of obesity-associated asthma and in tumor research but gained further attention during the current COVID-19 pandemic. Association of the co-inhibitory receptors with higher expression of PD-1 and LAG-3 co-expression as well as PD-1 and TIM-3 co-expression was found on $CD4^+$ and $CD8^+$ T cells of COVID-19 patients (Herrmann et al., 2020). Risk factors for a severe progression of the disease in COVID-19 patients include also obesity next to elderly age, gender, COPD, and others (Gao et al., 2020, Gao et al., 2021). With regard to the knowledge gained within this study, it would be a conceivable idea to consider an association between the severe outcome in obese patients and missing expressions of co-inhibitory receptors on T cells due to the inflammatory mechanisms in the obese adipose tissue, thus potentially aggravating disease progression.

So far only the $CD4^+$ T cell compartment has been investigated in detail, while studies on the other aspects are still ongoing. Not only the $CD8^+$ T cells single cell data of this study but also the information about myeloid cell populations and B cells offer more possibilities for further in-depth investigations of underlying mechanisms. As the additional *in vivo* experiment, which was performed to demonstrate the expression of co-inhibitory receptors on T cells, only focused on HDM aspects, an experiment additionally involving HFD groups is already planned and will be conducted soon. Instead, the *in vitro* experiment with stimulation of differentiated T cells with supernatant of

cultured adipocytes was conducted to test whether adipocyte-derived soluble factors might be involved in the regulation of co-inhibitory receptor expression in T cells.

In the future, it would be interesting to investigate, whether inflammation is more persistent in the lungs of obese mice in comparison to lean mice in the HFD-model. Considering obese mice lacking the activation of co-inhibitory receptors, one would anticipate a more persistent inflammation in the lungs following HDM exposure. Recent data of human studies showed that obesity is not only a risk factor for asthma (Dixon, Nyenhuis, 2021), but also asthma might be a risk factor for obesity (Chen et al., 2017, Zhang et al., 2020). In the literature, the mechanistic impacts of AAI on adipose tissue have not been investigated in mouse models so far. However, the data of this study revealed this to be a highly interesting topic for further examination, as it was observed that AAI induction in the lungs lead to changes in the transcriptome profile of adipose tissue of lean mice. This suggests that inflammatory processes taking place in the lung directly or indirectly affect functions of the adipose tissue. Such effects in the adipose tissue were overlaid by inflammatory processes taking place in the obese adipose tissue itself and could thus not be detected in the two HFD groups in C57BL/6 mice. An essential task for the obesity research would be to further study the reasons behind the lack of weight gain of BALB/c mice on a HFD and association of AAI features. Using further *in vivo* models, this could additionally provide the basis for the investigation of potential stratified therapies for obese asthmatics.

ICSs are the most commonly applied medication for asthma patients. Their characteristics comprise nonspecific anti-inflammatory effects mediated by influencing the expression of several genes involved in the induction and maintenance of immune responses (Lin et al., 2013). However, not all patients respond adequately to the treatment with CS, especially when obesity-associated phenotypes are present (Peters-Golden et al., 2006). Although so far, the one-fits-all therapeutic approach is broadly used for the treatment of asthma patients with variations mostly considering only disease severity, this approach might in fact not be really successfully applicable in such a heterogenic disease. Until now, consideration of the inflammatory phenotype is only applied in the patients with the highest level of severity, when other medications are

not effective, e.g. anti-IL-5 treatment for eosinophilic asthma. However, this example and other personalized therapeutics have so far been developed only for the treatment of type-2-driven asthma. In patients, the clinical phenotype, the inflammatory/molecular phenotype and the endotype might show individual characteristics on all three levels. Therefore, the underlying endotype and its association to the phenotype needs be considered when developing a personalized therapeutic approach for a single patient. Even if the clinical phenotypes seem to be similar, underlying endotypes may differ between patients and thus medication might not be similarly appropriate for all patients showing the same disease phenotype. Therefore, applying a personalized medicine approach, not only the inflammatory phenotype, but also the underlying individual endotype should be considered for effective treatment of the respective asthma patient. Hence, more research on the non-type 2 endotypes is required, especially as obese patients with persistent asthma are also more likely to be hospitalized than lean asthma patients (Mosen et al., 2008). Lifestyle changes and bariatric surgery as procedures for losing weight have been associated with improvements of the asthmatic symptoms, life quality, and AHR of the obesity-associated asthma (Dixon et al., 2011, Hewitt et al., 2014). However, these methods only apply to patients exhibiting the non-type 2 endotype, whereas patients with an allergic type 2-driven asthma show no improvement of symptoms after weight loss (Chapman et al., 2014, Wenzel, 2012). Bridging possible treatments for the obesity-associated asthma with the results of this study, a therapeutic preventing inhibition of Treg cell activity and/or induction of co-inhibitory receptor expression on T cells would be a novel approach. Nowadays, drugs able to promote Treg function are already used to treat autoimmune diseases, including the mTOR-inhibitor rapamycin or various biologicals such as administration of IL-10 or low-dose IL-2 (Eggenhuizen et al., 2020). Another potentially applicable option would be the transplantation of *ex vivo* expanded Tregs, which nowadays are especially used for the treatment of graft-versus-host disease, a condition that arises after hematopoietic stem cell transplantation (Elias, Rudensky, 2019). An additional novel approach was suggested by Rosskopf et al., proposing that PD-1 agonists might be effective in dampening pathogenic $CD4^+$ T cell immune responses in autoimmune and allergic diseases (Rosskopf et al., 2018). More recently, treatment with PD-1 agonists have been shown to alleviate the outcomes of an induced airway inflammation in a mouse model

(Helou et al., 2020). Successful asthma treatment by use of Treg activating medications in obese patients would most likely not only offer an increased quality of life, but it would also provide them with an opportunity for gentle and healthy weight loss through exercise. This would offer alternatives to high-risk bariatric surgery for weight loss for such patients.

Summarizing the major findings of this study, the main hypotheses could be confirmed. It was proven that obesity affects the phenotype of an induced AAI. Furthermore, it was demonstrated that metabolic processes leading to weight gain in response to a HFD are associated with alterations of the HDM-induced inflammatory phenotype. The results additionally revealed that inflammatory signals in the obese adipose tissue are associated with changes in the cellular/molecular endotype of the induced AAI phenotype. More precisely, these inflammatory mechanisms in the obese adipose tissue inhibited the expression of co-inhibitory receptors on HDM-induced lung T cells, which may lead to uncontrolled immune responses, resulting in an altered and potentially aggravated and/or prolonged inflammatory phenotype (Figure 31).

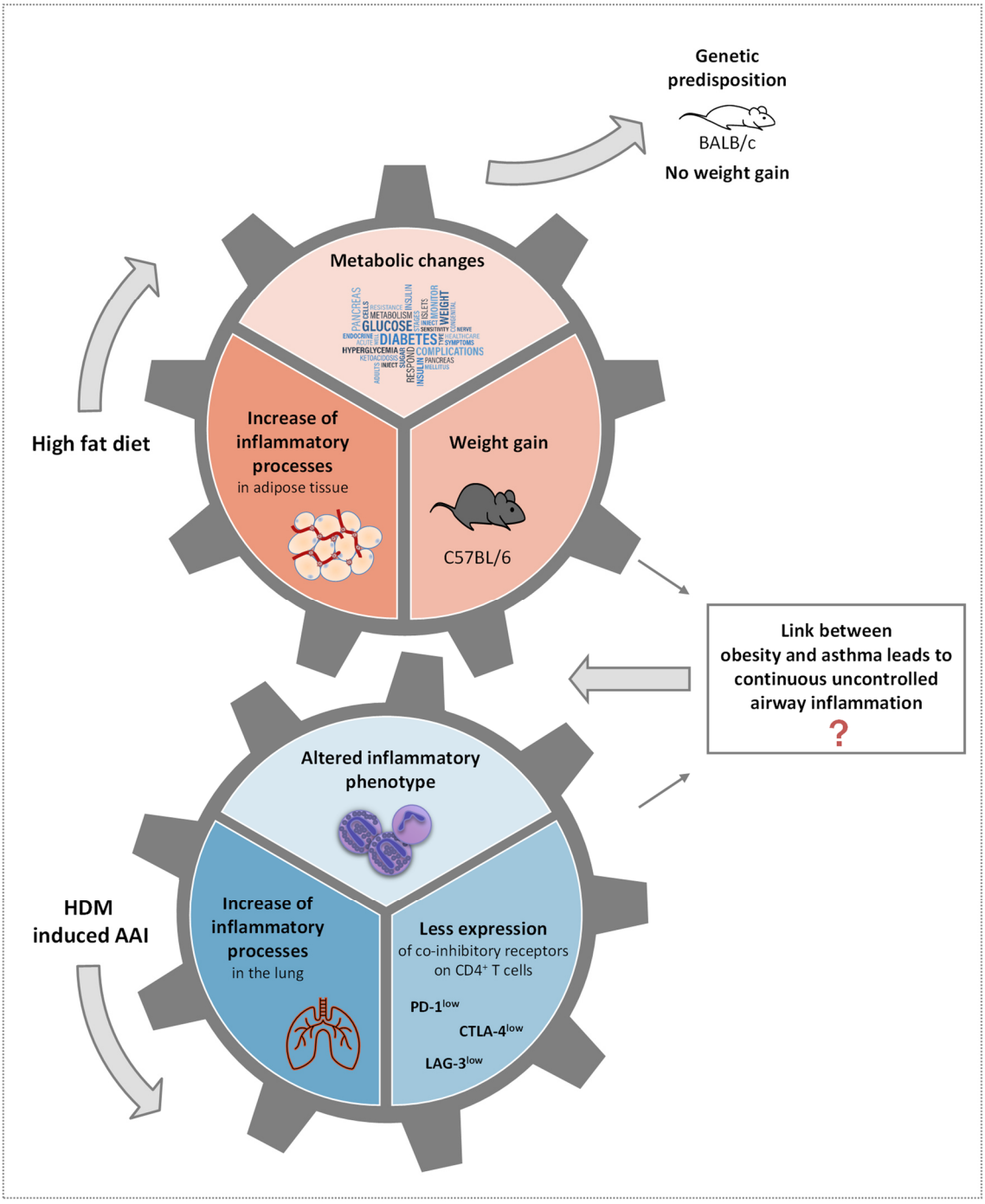

Figure 31: Schematic summary of the induced inflammatory phenotype altered by inflammatory mechanisms in the obese adipose tissue.

5. Summary

Asthma and obesity are non-communicable diseases with high and increasing prevalences. Both are characterized by the presence of local and systemic inflammatory processes, whereby their mutual pathomechanistic relationship within obesity-associated asthma are not fully elucidated. This research work hypothesized that inflammatory mechanisms in obese adipose tissue modify the inflammatory phenotype of an induced allergic airway inflammation (AAI) and that altered activation processes in $CD4^+$ T cells are crucially involved. To test this hypothesis, BALB/c and C57BL/6 mice were fed for several weeks with a high-fat diet (HFD) in order to induce obesity-like metabolic changes and a mixed inflammatory phenotype of AAI was induced in the animals by exposure to house dust mite (HDM) extracts. In both strains, HFD resulted in comparable metabolic changes, such as higher plasma levels of a variety of metabolic parameters and features of type 2 diabetes. However, strain-dependent differences were observed with regard to excessive weight gain, which occurred only in C57BL/6 mice, but not in BALB/c mice. Weight gain in HFD-fed C57BL/6 mice was associated with pronounced adipocyte hypertrophy and increased inflammatory processes in the obese adipose tissue. As intended, HDM-exposure of control diet (ND)-fed mice resulted in a mixed inflammatory phenotype characterized by an influx of eosinophils and neutrophils in the bronchoalveolar lavage (BAL) and in lung tissue in both mouse strains. While per se no differences in the induced AAI between the HFD/HDM group and the ND/HDM group were detected in BALB/c mice, a more eosinophilic inflammation was observed in HFD-fed HDM-exposed C57BL/6 mice in comparison to their lean counterparts. Further investigations revealed increased levels of inflammatory cytokines in the BAL and higher numbers of inflammatory immune cells in the lung tissue of HFD/HDM C57BL/6 mice. This suggested that weight gain and associated inflammatory processes in obese adipose tissue are crucial for modifying characteristic features of the induced AAI. Single cell analysis of $CD45^+$ lung cells was conducted to further analyze the cellular and molecular changes of the induced inflammatory phenotype in the airways of C57BL/6 mice. Interestingly, a $CD4^+$ T cell subcluster was identified to be exclusively present in the lungs of lean, but not in obese HDM-exposed mice. In this subcluster, expression of markers associated with typical characteristics of Th2, Th1, and Treg cells and in addition, co-

inhibitory receptors such as PD-1, CTLA-4, and LAG-3 was detected. Subsequent flow cytometric analyses confirmed the presence of Th2 and Treg cells expressing the co-inhibitory receptors identified in lungs of HDM-exposed mice. To further investigate whether hypertrophic activated adipocytes release factors that might be involved in the regulation of co-inhibitory receptor expression of $CD4^+$ T cells, supernatants from *in vitro* cultured adipocytes of HFD-fed mice were applied to differentiated Th2 and Treg cells. In line with the previous results, during the activation process lower numbers of Th2 cells were observed expressing CTLA-4 or LAG-3, while in Treg cells a reduction of CTLA-4^+ cells was seen in response to the adipocyte supernatant. Overall, HFD changes the inflammatory phenotype of a HDM-induced AAI only in association with weight gain and related inflammatory processes in the obese adipose tissue. Further, the expression of co-inhibitory receptors PD-1, CTLA-4, and LAG-3 on $CD4^+$ T cells, which may represent a putative disease-limiting mechanism, was observed in response to the induction of AAI only in lean mice. However, the absence of $CD4^+$ T cells expressing such receptors might in turn underlie altered and potentially aggravated and/or prolonged inflammatory processes in obese HDM-exposed mice. By demonstrating obesity-mediated alterations of the AAI phenotype and the identification of putative immune mechanisms behind this observation, these findings provide significant deeper insights into the specific pathophysiology of obesity-associated asthma with implications for the development of stratified therapy concepts for this disease condition.

6. Zusammenfassung

Asthma und Adipositas sind nicht übertragbare Krankheiten (engl. *non-communicable diseases; NCDs)* mit hohen und weiter steigenden Prävalenzen. Beide Erkrankungen sind durch das Vorhandensein lokaler und systemischer Entzündungsprozesse gekennzeichnet, wobei wechselseitige pathomechanistische Interaktionen bei Adipositas-assoziiertem Asthma nicht vollständig geklärt sind. In der vorliegenden Forschungsarbeit wurde die Hypothese verfolgt, dass Entzündungsmechanismen im adipösen Fettgewebe den inflammatorischen Phänotyp einer induzierten allergischen Atemwegsentzündung (AAI) beeinflussen und veränderte Aktivierungsprozesse in $CD4^+$ T-Zellen entscheidend daran beteiligt sind. Dazu wurden BALB/c- und C57BL/6-Mäuse über mehrere Wochen mit einer Hochfettdiät (HFD) gefüttert, um in ihnen Adipositas-ähnliche Stoffwechselveränderungen zu induzieren. Zusätzlich wurde in den Tieren ein gemischter inflammatorischer Phänotyp der AAI durch die Exposition mit Hausstaubmilbenextrakten (HDM) hervorgerufen. Bei beiden Stämmen führte die HFD zu vergleichbaren Stoffwechselveränderungen, wie z. B. höheren Plasmaspiegeln verschiedener Stoffwechselparameter und Merkmale von Typ-2-Diabetes. Stammabhängige Unterschiede wurden jedoch in Bezug auf die übermäßige Gewichtszunahme beobachtet, die selektiv nur bei C57BL/6-Mäusen, nicht aber bei BALB/c-Mäusen auftrat. Dabei war die Gewichtszunahme von HFD-gefütterten C57BL/6-Mäusen mit einer ausgeprägten Adipozytenhypertrophie und verstärkten Entzündungsprozessen im adipösen Fettgewebe assoziiert. Wie beabsichtigt, führte die HDM-Exposition in Kontrolldiät (ND)-gefütterten Mäusen zu einem gemischten inflammatorischen Phänotyp, der sich durch einen vergleichbaren Anstieg von Eosinophilen und Neutrophilen in der bronchoalveolären Lavage (BAL) und im Lungengewebe beider Mausstämme zeigte. Während in BALB/c-Mäusen keine Unterschiede in der induzierten AAI zwischen der HFD/HDM-Gruppe und der ND/HDM-Gruppe festgestellt wurden, zeigten HFD-gefütterte, HDM-exponierte C57BL/6-Mäuse im Vergleich zu normalgewichtigen HDM-exponierten Mäusen eine verstärkt eosinophile Entzündungsreaktion. Weitere Analysen ergaben erhöhte Konzentrationen von inflammatorischen Zytokinen in der BAL und eine höhere Anzahl von inflammatorischen Immunzellen im Lungengewebe von HFD/HDM-C57BL/6-Mäusen. Dies deutet darauf hin, dass die Gewichtszunahme und die damit verbundenen Entzündungsprozesse im adipösen Fettgewebe für die Veränderung der

charakteristischen Merkmale der induzierten AAI entscheidend sein können. Zur weiteren Analyse der zellulären und molekularen Veränderungen des induzierten inflammatorischen Phänotyps in den Atemwegen von C57BL/6-Mäusen wurde eine Einzelzellanalyse von $CD45^+$ Zellen aus den Lungen der Tiere durchgeführt. Interessanterweise wurde dabei ein $CD4^+$ T-Zell-Subcluster identifiziert, das ausschließlich in der Lunge von normalgewichtigen, aber nicht in adipösen HDM-exponierten Mäusen vorkommt. In diesem Subcluster wurde einerseits die Expression von Markern gefunden, die mit typischen Merkmalen von Th2-, Th1- und Treg-Zellen assoziiert sind, und darüber hinaus hohe Expressionsraten von ko-inhibitorischen Rezeptoren wie PD-1, CTLA-4 und LAG-3. Anschließende durchflusszytometrische Analysen bestätigten das Vorhandensein von Th2- und Treg-Zellen mit Oberflächenexpression der ko-inhibitorischen Rezeptoren PD-1, CTLA-4 und LAG-3 in Lungen von HDM-exponierten C57BL/6-Mäusen. Um weitergehend zu untersuchen, ob hypertrophe aktivierte Adipozyten Faktoren freisetzen, die an der Regulation der Expression ko-inhibitorischer Rezeptoren von $CD4^+$ T-Zellen beteiligt sein könnten, wurden differenzierte Th2- und Treg-Zellen mit Überständen von *in vitro* kultivierten Adipozyten aus HFD-gefütterten Mäusen inkubiert. In Übereinstimmung mit den vorherigen Ergebnissen führte dies zu einer verminderten Anzahl CTLA-4 oder LAG-3 exprimierender Th2-Zellen, während bei Treg-Zellen als Reaktion auf den Adipozytenüberstand eine Verringerung der Frequenz CTLA-4-positiver Zellen beobachtet wurde. Insgesamt verändert HFD den inflammatorischen Phänotyp einer HDM-induzierten AAI nur in Verbindung mit einer Gewichtszunahme und den damit verbundenen Entzündungsprozessen im adipösen Fettgewebe. Außerdem wurde die Expression der ko-inhibitorischen Rezeptoren PD-1, CTLA-4 und LAG-3 auf $CD4^+$ T-Zellen beobachtet, die möglicherweise einen krankheitsbegrenzenden Mechanismus als Reaktion auf die Induktion von AAI nur in normalgewichtigen Mäusen darstellt. Das Fehlen von $CD4^+$ T-Zellen, die diese Rezeptoren in adipösen, HDM-exponierten Mäusen exprimieren, könnte wiederum den veränderten und möglicherweise verstärkten und/oder verlängerten Entzündungsprozessen zugrunde liegen. Durch den Nachweis Adipositas-bedingter Veränderungen des AAI-Phänotyps und die Identifizierung daran beteiligter Immunmechanismen bieten die Ergebnisse dieser Arbeit wichtige neue Einblicke in die spezifische Pathophysiologie von Adipositas-assoziiertem Asthma, die wiederum Auswirkungen auf die Entwicklung stratifizierter Therapiekonzepte für diesen Erkrankungsphänotyp haben können.

7. References

Abel, A. M.; Yang, C.; Thakar, M. S.; Malarkannan, S. Natural Killer Cells: Development, Maturation, and Clinical Utilization. *Frontiers in immunology* **2018,** *9*, 1869. DOI: 10.3389/fimmu.2018.01869.

Agache, I.; Akdis, C. A. Endotypes of allergic diseases and asthma: An important step in building blocks for the future of precision medicine. *Allergology international: official journal of the Japanese Society of Allergology* **2016,** *65* (3), 243–252. DOI: 10.1016/j.alit.2016.04.011.

Ahima, R. S. Revisiting leptin's role in obesity and weight loss. *The Journal of clinical investigation* **2008,** *118* (7), 2380–2383. DOI: 10.1172/JCI36284.

Alberti, K. G. M. M.; Zimmet, P.; Shaw, J. Metabolic syndrome - a new world-wide definition. A Consensus Statement from the International Diabetes Federation. *Diabetic medicine: a journal of the British Diabetic Association* **2006,** *23* (5), 469–480. DOI: 10.1111/j.1464-5491.2006.01858.x.

Alhasson, F.; Seth, R. K.; Sarkar, S.; Kimono, D. A.; Albadrani, M. S.; Dattaroy, D.; Chandrashekaran, V.; Scott, G. I.; Raychoudhury, S.; Nagarkatti, M.; Nagarkatti, P.; Diehl, A. M.; Chatterjee, S. High circulatory leptin mediated NOX-2-peroxynitrite-miR21 axis activate mesangial cells and promotes renal inflammatory pathology in nonalcoholic fatty liver disease. *Redox biology* **2018,** *17*, 1–15. DOI: 10.1016/j.redox.2018.04.002.

Al-Sahrif, F. M. Impact of Obesity on Adipokines, Inflammatory Cytokines and Clinical Symptoms Control in Asthmatic Subjects. *JLPRR* **2017,** *4* (4). DOI: 10.15406/jlprr.2017.04.00136.

American Diabetes Association. 2. Classification and Diagnosis of Diabetes: Standards of Medical Care in Diabetes-2020. *Diabetes care* [Online] **2020,** Suppl 1, S14-S31.

Anderson, A. C.; Joller, N.; Kuchroo, V. K. Lag-3, Tim-3, and TIGIT: Co-inhibitory Receptors with Specialized Functions in Immune Regulation. *Immunity* **2016,** *44* (5), 989–1004. DOI: 10.1016/j.immuni.2016.05.001.

Bally, A. P. R.; Austin, J. W.; Boss, J. M. Genetic and Epigenetic Regulation of PD-1 Expression. *Journal of immunology (Baltimore, Md.: 1950)* **2016,** *196* (6), 2431–2437. DOI: 10.4049/jimmunol.1502643.

Bantulà, M.; Roca-Ferrer, J.; Arismendi, E.; Picado, C. Asthma and Obesity: Two Diseases on the Rise and Bridged by Inflammation. *Journal of clinical medicine* **2021,** *10* (2). DOI: 10.3390/jcm10020169.

BD Biosciences. BD AbSeq | Antibody Conjugates. https://www.bdbiosciences.com/en-us/products/reagents/single-cell-multiomics/abseq (accessed October 13, 2021).

Blüher, M. Adipose tissue inflammation: a cause or consequence of obesity-related insulin resistance? *Clinical science (London, England: 1979)* **2016,** *130* (18), 1603–1614. DOI: 10.1042/CS20160005.

Boi, S. K.; Buchta, C. M.; Pearson, N. A.; Francis, M. B.; Meyerholz, D. K.; Grobe, J. L.; Norian, L. A. Obesity alters immune and metabolic profiles: New insight from obese-resistant mice on high-fat diet. *Obesity (Silver Spring, Md.)* **2016,** *24* (10), 2140–2149. DOI: 10.1002/oby.21620.

Brenachot, X.; Gautier, T.; Nédélec, E.; Deckert, V.; Laderrière, A.; Nuzzaci, D.; Rigault, C.; Lemoine, A.; Pénicaud, L.; Lagrost, L.; Benani, A. Brain Control of Plasma Cholesterol Involves Polysialic Acid Molecules in the Hypothalamus. *Frontiers in neuroscience* **2017,** *11*, 245. DOI: 10.3389/fnins.2017.00245.

Buhl, R.; Bals, R.; Baur, X.; Berdel, D.; Criée, C.-P.; Gappa, M.; Gillissen, A.; Greulich, T.; Haidl, P.; Hamelmann, E.; Horak, F.; Kardos, P.; Kenn, K.; Klimek, L.; Korn, S.; Magnussen, H.; Nowak, D.; Pfaar, O.; Rabe, K. F.; Riedler, J.; Ritz, T.; Schultz, K.; Schuster, A.; Spindler, T.; Taube, C.; Vogelmeier, C.; Leupoldt, A. von; Wantke, F.; Wildhaber, J.; Worth, H.; Zacharasiewicz, A.; Lommatzsch, M. S2k-Leitlinie zur Diagnostik und Therapie von Patienten mit Asthma - Addendum 2020. *Pneumologie (Stuttgart, Germany)* **2021,** *75* (3), 191–200. DOI: 10.1055/a-1352-0296.

Cabrera-Ortega, A. A.; Feinberg, D.; Liang, Y.; Rossa, C.; Graves, D. T. The Role of Forkhead Box 1 (FOXO1) in the Immune System: Dendritic Cells, T Cells, B Cells, and Hematopoietic Stem Cells. *Critical reviews in immunology* **2017,** *37* (1), 1–13. DOI: 10.1615/CritRevImmunol.2017019636.

Calixto, M. C.; Lintomen, L.; Schenka, A.; Saad, M. J.; Zanesco, A.; Antunes, E. Obesity enhances eosinophilic inflammation in a murine model of allergic asthma. *British journal of pharmacology* **2010,** *159* (3), 617–625. DOI: 10.1111/j.1476-5381.2009.00560.x.

Camargo, C. A.; Weiss, S. T.; Zhang, S.; Willett, W. C.; Speizer, F. E. Prospective study of body mass index, weight change, and risk of adult-onset asthma in women. *Archives of internal medicine* **1999,** *159* (21), 2582–2588. DOI: 10.1001/archinte.159.21.2582.

Carding, S. R.; Egan, P. J. Gammadelta T cells: functional plasticity and heterogeneity. *Nature reviews. Immunology* **2002,** *2* (5), 336–345. DOI: 10.1038/nri797.

Carr, T. F.; Zeki, A. A.; Kraft, M. Eosinophilic and Noneosinophilic Asthma. *American journal of respiratory and critical care medicine* **2018,** *197* (1), 22–37. DOI: 10.1164/rccm.201611-2232PP.

Chan, S. S. Y.; Twigg, S. M.; Firth, S. M.; Baxter, R. C. Insulin-like growth factor binding protein-3 leads to insulin resistance in adipocytes. *The Journal of clinical endocrinology and metabolism* [Online] **2005**, 6588–6595.

Chapman, D. G.; Irvin, C. G.; Kaminsky, D. A.; Forgione, P. M.; Bates, J. H. T.; Dixon, A. E. Influence of distinct asthma phenotypes on lung function following weight loss in the obese. *Respirology (Carlton, Vic.)* **2014,** *19* (8), 1170–1177. DOI: 10.1111/resp.12368.

Chen, C.; Rowell, E. A.; Thomas, R. M.; Hancock, W. W.; Wells, A. D. Transcriptional regulation by Foxp3 is associated with direct promoter occupancy and modulation of histone acetylation. *The Journal of biological chemistry* **2006,** *281* (48), 36828–36834. DOI: 10.1074/jbc.M608848200.

Chen, L.; Flies, D. B. Molecular mechanisms of T cell co-stimulation and co-inhibition. *Nature reviews. Immunology* **2013,** *13* (4), 227–242. DOI: 10.1038/nri3405.

Chen, Z.; Salam, M. T.; Alderete, T. L.; Habre, R.; Bastain, T. M.; Berhane, K.; Gilliland, F. D. Effects of Childhood Asthma on the Development of Obesity among School-aged Children. *American journal of respiratory and critical care medicine* **2017,** *195* (9), 1181–1188. DOI: 10.1164/rccm.201608-1691OC.

Chong, L.; Zhang, W.; Yu, G.; Zhang, H.; Zhu, L.; Li, H.; Shao, Y.; Li, C. High-fat-diet induces airway hyperresponsiveness partly through activating CD38 signaling pathway. *International immunopharmacology* **2018,** *56*, 197–204. DOI: 10.1016/j.intimp.2018.01.033.

Chung, K. F. Targeting the interleukin pathway in the treatment of asthma. *The Lancet* **2015,** *386* (9998), 1086–1096. DOI: 10.1016/S0140-6736(15)00157-9.

Chylikova, J.; Dvorackova, J.; Tauber, Z.; Kamarad, V. M1/M2 macrophage polarization in human obese adipose tissue. *Biomedical papers of the Medical Faculty of the University Palacky, Olomouc, Czechoslovakia* **2018,** *162* (2), 79–82. DOI: 10.5507/bp.2018.015.

Corthay, A. How do regulatory T cells work? *Scandinavian journal of immunology* **2009,** *70* (4), 326–336. DOI: 10.1111/j.1365-3083.2009.02308.x.

de Lima Azambuja, R.; da Costa Santos Azambuja, L. S. E.; Costa, C.; Rufino, R. Adiponectin in Asthma and Obesity: Protective Agent or Risk Factor for More Severe Disease? *Lung* **2015,** *193* (5), 749–755. DOI: 10.1007/s00408-015-9793-8.

Desai, D.; Newby, C.; Symon, F. A.; Haldar, P.; Shah, S.; Gupta, S.; Bafadhel, M.; Singapuri, A.; Siddiqui, S.; Woods, J.; Herath, A.; Anderson, I. K.; Bradding, P.; Green, R.; Kulkarni, N.; Pavord, I.; Marshall, R. P.; Sousa, A. R.; May, R. D.; Wardlaw, A. J.; Brightling, C. E. Elevated sputum interleukin-5 and submucosal eosinophilia in obese individuals with severe asthma. *American journal of respiratory and critical care medicine* **2013,** *188* (6), 657–663. DOI: 10.1164/rccm.201208-1470OC.

Diaz, J.; Warren, L.; Helfner, L.; Xue, X.; Chatterjee, P. K.; Gupta, M.; Solanki, M. H.; Esposito, M.; Bonagura, V.; Metz, C. N. Obesity shifts house dust mite-induced airway cellular infiltration from eosinophils to macrophages: effects of glucocorticoid treatment. *Immunologic research* **2015,** *63* (1-3), 197–208. DOI: 10.1007/s12026-015-8717-2.

Dixit, V. D.; Schaffer, E. M.; Pyle, R. S.; Collins, G. D.; Sakthivel, S. K.; Palaniappan, R.; Lillard, J. W.; Taub, D. D. Ghrelin inhibits leptin- and activation-induced proinflammatory cytokine expression by human monocytes and T cells. *The Journal of clinical investigation* **2004,** *114* (1), 57–66. DOI: 10.1172/JCI200421134.

Dixon, A. E.; Poynter, M. E. Mechanisms of Asthma in Obesity. Pleiotropic Aspects of Obesity Produce Distinct Asthma Phenotypes. *American journal of respiratory cell and molecular biology* **2016,** *54* (5), 601–608. DOI: 10.1165/rcmb.2016-0017PS.

Dixon, A. E.; Pratley, R. E.; Forgione, P. M.; Kaminsky, D. A.; Whittaker-Leclair, L. A.; Griffes, L. A.; Garudathri, J.; Raymond, D.; Poynter, M. E.; Bunn, J. Y.; Irvin, C. G. Effects of obesity and bariatric surgery on airway hyperresponsiveness, asthma control, and inflammation. *The Journal of allergy and clinical immunology* **2011,** *128* (3), 508-15.e1-2. DOI: 10.1016/j.jaci.2011.06.009.

Dixon, Anne E., Nyenhuis, Sharmilee M. Obesity and asthma. https://www.uptodate.com/contents/obesity-and-asthma (accessed October 13, 2021).

Dookie, R. S.; Villegas-Mendez, A.; Kroeze, H.; Barrett, J. R.; Draper, S. J.; Franke-Fayard, B. M.; Janse, C. J.; MacDonald, A. S.; Couper, K. N. Combinatorial Tim-3 and PD-1 activity sustains antigen-specific Th1 cell numbers during blood-stage malaria. *Parasite immunology* **2020,** *42* (9), e12723. DOI: 10.1111/pim.12723.

Eggenhuizen, P. J.; Ng, B. H.; Ooi, J. D. Treg Enhancing Therapies to Treat Autoimmune Diseases. *International journal of molecular sciences* **2020,** *21* (19). DOI: 10.3390/ijms21197015.

Elias, S.; Rudensky, A. Y. Therapeutic use of regulatory T cells for graft-versus-host disease. *British journal of haematology* **2019,** *187* (1), 25–38. DOI: 10.1111/bjh.16157.

Everaere, L.; Ait-Yahia, S.; Molendi-Coste, O.; Vorng, H.; Quemener, S.; LeVu, P.; Fleury, S.; Bouchaert, E.; Fan, Y.; Duez, C.; Nadai, P. de; Staels, B.; Dombrowicz, D.; Tsicopoulos, A. Innate lymphoid cells contribute to allergic airway disease exacerbation by obesity. *The Journal of allergy and clinical immunology* **2016,** *138* (5), 1309-1318.e11. DOI: 10.1016/j.jaci.2016.03.019.

Fahy, J. V. Type 2 inflammation in asthma - present in most, absent in many. *Nature reviews. Immunology* **2015,** *15* (1), 57–65. DOI: 10.1038/nri3786.

Francisco, L. M.; Sage, P. T.; Sharpe, A. H. The PD-1 pathway in tolerance and autoimmunity. *Immunological reviews* **2010,** *236*, 219–242. DOI: 10.1111/j.1600-065X.2010.00923.x.

Francisco, V.; Pino, J.; Campos-Cabaleiro, V.; Ruiz-Fernández, C.; Mera, A.; Gonzalez-Gay, M. A.; Gómez, R.; Gualillo, O. Obesity, Fat Mass and Immune System: Role for Leptin. *Frontiers in physiology* **2018,** *9*, 640. DOI: 10.3389/fphys.2018.00640.

Fukushima, A.; Yamaguchi, T.; Ishida, W.; Fukata, K.; Taniguchi, T.; Liu, F.-T.; Ueno, H. Genetic background determines susceptibility to experimental immune-mediated blepharoconjunctivitis: comparison of Balb/c and C57BL/6 mice. *Experimental eye research* **2006,** *82* (2), 210–218. DOI: 10.1016/j.exer.2005.06.010.

Galic, S.; Oakhill, J. S.; Steinberg, G. R. Adipose tissue as an endocrine organ. *Molecular and cellular endocrinology* **2010,** *316* (2), 129–139. DOI: 10.1016/j.mce.2009.08.018.

Gandhi, N. A.; Bennett, B. L.; Graham, N. M. H.; Pirozzi, G.; Stahl, N.; Yancopoulos, G. D. Targeting key proximal drivers of type 2 inflammation in disease. *Nature reviews. Drug discovery* **2016,** *15* (1), 35–50. DOI: 10.1038/nrd4624.

Gao, F.; Zheng, K. I.; Wang, X.-B.; Sun, Q.-F.; Pan, K.-H.; Wang, T.-Y.; Chen, Y.-P.; Targher, G.; Byrne, C. D.; George, J.; Zheng, M.-H. Obesity Is a Risk Factor for Greater COVID-19 Severity. *Diabetes care* **2020,** *43* (7), e72-e74. DOI: 10.2337/dc20-0682.

Gao, Y.-D.; Ding, M.; Dong, X.; Zhang, J.-J.; Kursat Azkur, A.; Azkur, D.; Gan, H.; Sun, Y.-L.; Fu, W.; Li, W.; Liang, H.-L.; Cao, Y.-Y.; Yan, Q.; Cao, C.; Gao, H.-Y.; Brüggen, M.-C.; van de Veen, W.; Sokolowska, M.; Akdis, M.; Akdis, C. A. Risk factors for severe and critically ill COVID-19 patients: A review. *Allergy* **2021,** *76* (2), 428–455. DOI: 10.1111/all.14657.

Garon, E. B.; Rizvi, N. A.; Hui, R.; Leighl, N.; Balmanoukian, A. S.; Eder, J. P.; Patnaik, A.; Aggarwal, C.; Gubens, M.; Horn, L.; Carcereny, E.; Ahn, M.-J.; Felip, E.; Lee, J.-S.; Hellmann, M. D.; Hamid, O.; Goldman, J. W.; Soria, J.-C.; Dolled-Filhart, M.; Rutledge, R. Z.; Zhang, J.; Lunceford, J. K.; Rangwala, R.; Lubiniecki, G. M.; Roach, C.; Emancipator, K.; Gandhi, L. Pembrolizumab for the treatment of non-small-cell lung cancer. *The New England journal of medicine* **2015,** *372* (21), 2018–2028. DOI: 10.1056/NEJMoa1501824.

GBD. Global Burden of Disease: cause and risk summaries: Asthma. *The Lancet* **2020,** Vol. 396, 108–109.

Gelsinger, C.; Tschoner, A.; Kaser, S.; Ebenbichler, C. F. Adipokine update - neue Moleküle, neue Funktionen. *Wiener medizinische Wochenschrift (1946)* **2010,** *160* (15-16), 377–390. DOI: 10.1007/s10354-010-0781-6.

Gibson, H. M.; Hedgcock, C. J.; Aufiero, B. M.; Wilson, A. J.; Hafner, M. S.; Tsokos, G. C.; Wong, H. K. Induction of the CTLA-4 gene in human lymphocytes is dependent on NFAT binding the proximal promoter. *J Immunol* **2007,** *179* (6), 3831–3840. DOI: 10.4049/jimmunol.179.6.3831.

GINA. Pocket Guide for Asthma Management and Prevention. https://ginasthma.org/pocket-guide-for-asthma-management-and-prevention/ (accessed Oct. 20, 2021).

Green, R. H.; Brightling, C. E.; Woltmann, G.; Parker, D.; Wardlaw, A. J.; Pavord, I. D. Analysis of induced sputum in adults with asthma: identification of subgroup with isolated sputum neutrophilia and poor response to inhaled corticosteroids. *Thorax* **2002,** *57* (10), 875–879. DOI: 10.1136/thorax.57.10.875.

Greenberg, A. S.; Obin, M. S. Obesity and the role of adipose tissue in inflammation and metabolism. *The American journal of clinical nutrition* **2006,** *83* (2), 461S-465S. DOI: 10.1093/ajcn/83.2.461S.

Guedes, A. G. P.; Jude, J. A.; Paulin, J.; Kita, H.; Lund, F. E.; Kannan, M. S. Role of CD38 in TNF-alpha-induced airway hyperresponsiveness. *American journal of physiology. Lung cellular and molecular physiology* **2008,** *294* (2), L290-9. DOI: 10.1152/ajplung.00367.2007.

Hagner, S.; Keller, M.; Raifer, H.; Tan, H.-T. T.; Akdis, C. A.; Buch, T.; Sokolowska, M.; Garn, H. T cell requirement and phenotype stability of house dust mite-induced neutrophil airway inflammation in mice. *Allergy* **2020,** *75* (11), 2970–2973. DOI: 10.1111/all.14424.

Han, H.; Chung, S. I.; Park, H. J.; Oh, E. Y.; Kim, S. R.; Park, K. H.; Lee, J.-H.; Park, J.-W. Obesity-induced Vitamin D Deficiency Contributes to Lung Fibrosis and Airway Hyperresponsiveness. *American journal of respiratory cell and molecular biology* [Online] **2020**.

Hao, W.; Wang, J.; Zhang, Y.; Wang, Y.; Sun, L.; Han, W. Leptin positively regulates MUC5AC production and secretion induced by interleukin-13 in human bronchial epithelial cells. *Biochemical and biophysical research communications* [Online] **2017**, 979–984.

Hao, W.-M.; Sun, S.-F.; Tang, H.-P. The relationship between Muc5ac high secretion and Munc18b upregulation in obese asthma. *European review for medical and pharmacological sciences* **2018,** *22* (5), 1409–1414. DOI: 10.26355/eurrev_201803_14487.

Hegab, A. E.; Ozaki, M.; Meligy, F. Y.; Kagawa, S.; Ishii, M.; Betsuyaku, T. High fat diet activates adult mouse lung stem cells and accelerates several aging-induced effects. *Stem cell research* [Online] **2018**, 25–35.

Helou, D. G.; Shafiei-Jahani, P.; Lo, R.; Howard, E.; Hurrell, B. P.; Galle-Treger, L.; Painter, J. D.; Lewis, G.; Soroosh, P.; Sharpe, A. H.; Akbari, O. PD-1 pathway regulates ILC2 metabolism and PD-1 agonist treatment ameliorates airway hyperreactivity. *Nature communications* **2020,** *11* (1), 3998. DOI: 10.1038/s41467-020-17813-1.

Herrmann, M.; Schulte, S.; Wildner, N. H.; Wittner, M.; Brehm, T. T.; Ramharter, M.; Woost, R.; Lohse, A. W.; Jacobs, T.; zur Schulze Wiesch, J. Analysis of Co-inhibitory Receptor Expression in COVID-19 Infection Compared to Acute Plasmodium falciparum Malaria: LAG-3 and TIM-3 Correlate With T Cell Activation and Course of Disease. *Frontiers in immunology* **2020,** *11*, 1870. DOI: 10.3389/fimmu.2020.01870.

Hewitt, S.; Humerfelt, S.; Søvik, T. T.; Aasheim, E. T.; Risstad, H.; Kristinsson, J.; Mala, T. Long-term improvements in pulmonary function 5 years after bariatric surgery. *Obesity surgery* **2014,** *24* (5), 705–711. DOI: 10.1007/s11695-013-1159-9.

Heydemann, A. An Overview of Murine High Fat Diet as a Model for Type 2 Diabetes Mellitus. *Journal of diabetes research* **2016,** *2016*, 2902351. DOI: 10.1155/2016/2902351.

Holgate, S. T.; Wenzel, S.; Postma, D. S.; Weiss, S. T.; Renz, H.; Sly, P. D. Asthma. *Nature reviews. Disease primers* **2015,** *1*, 15025. DOI: 10.1038/nrdp.2015.25.

Hotamisligil, G. S.; Shargill, N. S.; Spiegelman, B. M. Adipose expression of tumor necrosis factor-alpha: direct role in obesity-linked insulin resistance. *Science (New York, N.Y.)* **1993,** *259* (5091), 87–91. DOI: 10.1126/science.7678183.

Jartti, T.; Saarikoski, L.; Jartti, L.; Lisinen, I.; Jula, A.; Huupponen, R.; Viikari, J.; Raitakari, O. T. Obesity, adipokines and asthma. *Allergy* **2009,** *64* (5), 770–777. DOI: 10.1111/j.1398-9995.2008.01872.x.

Jovicic, N.; Jeftic, I.; Jovanovic, I.; Radosavljevic, G.; Arsenijevic, N.; Lukic, M. L.; Pejnovic, N. Differential Immunometabolic Phenotype in Th1 and Th2 Dominant Mouse Strains in Response to High-Fat Feeding. *PloS one* **2015,** *10* (7), e0134089. DOI: 10.1371/journal.pone.0134089.

Kanda, H.; Tateya, S.; Tamori, Y.; Kotani, K.; Hiasa, K.; Kitazawa, R.; Kitazawa, S.; Miyachi, H.; Maeda, S.; Egashira, K.; Kasuga, M. MCP-1 contributes to macrophage infiltration into adipose tissue, insulin resistance, and hepatic steatosis in obesity. *The Journal of clinical investigation* **2006,** *116* (6), 1494–1505. DOI: 10.1172/JCI26498.

Kato, A. Group 2 Innate Lymphoid Cells in Airway Diseases. *Chest* **2019,** *156* (1), 141–149. DOI: 10.1016/j.chest.2019.04.101.

Kim, H. Y.; Lee, H. J.; Chang, Y.-J.; Pichavant, M.; Shore, S. A.; Fitzgerald, K. A.; Iwakura, Y.; Israel, E.; Bolger, K.; Faul, J.; DeKruyff, R. H.; Umetsu, D. T. Interleukin-17-producing innate lymphoid cells and the NLRP3 inflammasome facilitate obesity-associated airway hyperreactivity. *Nature medicine* **2014,** *20* (1), 54–61. DOI: 10.1038/nm.3423.

Kim, S.-H. Clinical and Pathophysiological Characteristics of Severe Asthma. *Korean J Med* **2012,** *83* (4), 424. DOI: 10.3904/kjm.2012.83.4.424.

Kleinert, M.; Clemmensen, C.; Hofmann, S. M.; Moore, M. C.; Renner, S.; Woods, S. C.; Huypens, P.; Beckers, J.; Angelis, M. H. de; Schürmann, A.; Bakhti, M.; Klingenspor, M.; Heiman, M.; Cherrington, A. D.; Ristow, M.; Lickert, H.; Wolf, E.; Havel, P. J.; Müller, T. D.; Tschöp, M. H. Animal models of obesity and diabetes mellitus. *Nature reviews. Endocrinology* **2018,** *14* (3), 140–162. DOI: 10.1038/nrendo.2017.161.

Koczulla, A. R.; Vogelmeier, C. F.; Garn, H.; Renz, H. New concepts in asthma: Clinical phenotypes and pathophysiological mechanisms. *Drug discovery today* **2017,** *22* (2), 388–396. DOI: 10.1016/j.drudis.2016.11.008.

Komakula, S.; Khatri, S.; Mermis, J.; Savill, S.; Haque, S.; Rojas, M.; Brown, L.; Teague, G. W.; Holguin, F. Body mass index is associated with reduced exhaled nitric oxide and higher exhaled 8-isoprostanes in asthmatics. *Respiratory research* [Online] **2007**, 32.

Kuruvilla, M. E.; Lee, F. E.-H.; Lee, G. B. Understanding Asthma Phenotypes, Endotypes, and Mechanisms of Disease. *Clinical reviews in allergy & immunology* **2019,** *56* (2), 219–233. DOI: 10.1007/s12016-018-8712-1.

Kwak, S.; Kim, Y.-D.; Na, H. G.; Bae, C. H.; Song, S.-Y.; Choi, Y. S. Resistin upregulates MUC5AC/B mucin gene expression in human airway epithelial cells. *Biochemical and biophysical research communications* [Online] **2018**, 655–661.

Lambrecht, B. N.; Hammad, H. The immunology of asthma. *Nature immunology* **2015,** *16* (1), 45–56. DOI: 10.1038/ni.3049.

Lang, J. E. Obesity and asthma in children: Current and future therapeutic options. *Paediatric drugs* **2014,** *16* (3), 179–188. DOI: 10.1007/s40272-014-0069-1.

Langen, U.; Schmitz, R.; Steppuhn, H. Häufigkeit allergischer Erkrankungen in Deutschland: Ergebnisse der Studie zur Gesundheit Erwachsener in Deutschland (DEGS1). *Bundesgesundheitsblatt, Gesundheitsforschung, Gesundheitsschutz* **2013,** *56* (5-6), 698–706. DOI: 10.1007/s00103-012-1652-7.

Li, J.; Wu, H.; Liu, Y.; Yang, L. High fat diet induced obesity model using four strainsof mice: Kunming, C57BL/6, BALB/c and ICR. *Experimental animals* **2020,** *69* (3), 326-335. DOI: 10.1538/expanim.19-0148.

Lin, T.-Y.; Poon, A. H.; Hamid, Q. Asthma phenotypes and endotypes. *Current opinion in pulmonary medicine* **2013,** *19* (1), 18–23. DOI: 10.1097/MCP.0b013e32835b10ec.

Linsley, P. S.; Brady, W.; Urnes, M.; Grosmaire, L. S.; Damle, N. K.; Ledbetter, J. A. CTLA-4 is a second receptor for the B cell activation antigen B7. *The Journal of experimental medicine* **1991,** *174* (3), 561–569. DOI: 10.1084/jem.174.3.561.

Lötvall, J.; Akdis, C. A.; Bacharier, L. B.; Bjermer, L.; Casale, T. B.; Custovic, A.; Lemanske, R. F.; Wardlaw, A. J.; Wenzel, S. E.; Greenberger, P. A. Asthma endotypes: A new approach to classification of disease entities within the asthma syndrome. *The Journal of allergy and clinical immunology* **2011,** *127* (2), 355–360. DOI: 10.1016/ j.jaci.2010.11.037.

Lutz, T. A.; Woods, S. C. Overview of animal models of obesity. *Current protocols in pharmacology* **2012,** *Chapter 5*, Unit5.61. DOI: 10.1002/0471141755.ph0561s58.

Makki, K.; Froguel, P.; Wolowczuk, I. Adipose tissue in obesity-related inflammation and insulin resistance: Cells, cytokines, and chemokines. *ISRN inflammation* **2013,** 139239. DOI: 10.1155/2013/139239.

Mehta, P.; Nuotio-Antar, A. M.; Smith, C. W. γδ T cells promote inflammation and insulin resistance during high fat diet-induced obesity in mice. *Journal of leukocyte biology* [Online] **2015**, 121–134.

Miethe, S.; Guarino, M.; Alhamdan, F.; Simon, H.-U.; Renz, H.; Dufour, J.-F.; Potaczek, D. P.; Garn, H. Effects of obesity on asthma: Immunometabolic links. *Polish archives of internal medicine* **2018,** *128* (7-8), 469–477. DOI: 10.20452/pamw.4304.

Montgomery, M. K.; Hallahan, N. L.; Brown, S. H.; Liu, M.; Mitchell, T. W.; Cooney, G. J.; Turner, N. Mouse strain-dependent variation in obesity and glucose homeostasis in response to high-fat feeding. *Diabetologia* **2013,** *56* (5), 1129–1139. DOI: 10.1007/ s00125-013-2846-8.

Moore, W. C.; Hastie, A. T.; Li, X.; Li, H.; Busse, W. W.; Jarjour, N. N.; Wenzel, S. E.; Peters, S. P.; Meyers, D. A.; Bleecker, E. R. Sputum neutrophil counts are associated with more severe asthma phenotypes using cluster analysis. *The Journal of allergy and clinical immunology* **2014,** *133* (6), 1557-63.e5. DOI: 10.1016/j.jaci.2013.10.011.

Mosayebian, A.; Koohini, Z.; Hossein-Nataj, H.; Abediankenari, S.; Abedi, S.; Asgarian-Omran, H. Elevated Expression of Tim-3 and PD-1 Immune Checkpoint Receptors on T-CD4+ Lymphocytes of Patients with Asthma. *IJAAI* [Online] **2019**.

Mosen, D. M.; Schatz, M.; Magid, D. J.; Camargo, C. A. The relationship between obesity and asthma severity and control in adults. *The Journal of allergy and clinical immunology* **2008,** *122* (3), 507-11.e6. DOI: 10.1016/j.jaci.2008.06.024.

Muc, M.; Todo-Bom, A.; Mota-Pinto, A.; Vale-Pereira, S.; Loureiro, C. Leptin and resistin in overweight patients with and without asthma. *Allergologia et immunopathologia* **2014,** *42* (5), 415–421. DOI: 10.1016/j.aller.2013.03.004.

Nakamura, Y. Biomarkers for Immune Checkpoint Inhibitor-Mediated Tumor Response and Adverse Events. *Frontiers in medicine* **2019,** *6*, 119. DOI: 10.3389/fmed.2019.00119.

National Asthma Education and Prevention Program. Expert Panel Report 3: Guidelines for the Diagnosis and Management of Asthma. *National Heart, Lung, and Blood Institute (US)* [Online] **2007,** Report No.: 07-4051.

Nials, A. T.; Uddin, S. Mouse models of allergic asthma: acute and chronic allergen challenge. *Disease models & mechanisms* **2008,** *1* (4-5), 213–220. DOI: 10.1242/dmm.000323.

Nishikawa, S.; Yasoshima, A.; Doi, K.; Nakayama, H.; Uetsuka, K. Involvement of sex, strain and age factors in high fat diet-induced obesity in C57BL/6J and BALB/cA mice. *Experimental animals* **2007,** *56* (4), 263–272. DOI: 10.1538/expanim.56.263.

Nishimura, S.; Manabe, I.; Nagasaki, M.; Eto, K.; Yamashita, H.; Ohsugi, M.; Otsu, M.; Hara, K.; Ueki, K.; Sugiura, S.; Yoshimura, K.; Kadowaki, T.; Nagai, R. CD8+ effector T cells contribute to macrophage recruitment and adipose tissue inflammation in obesity. *Nature medicine* **2009,** *15* (8), 914–920. DOI: 10.1038/nm.1964.

Okita, K.; Iwahashi, H.; Kozawa, J.; Okauchi, Y.; Funahashi, T.; Imagawa, A.; Shimomura, I. Usefulness of the insulin tolerance test in patients with type 2 diabetes receiving insulin therapy. *Journal of diabetes investigation* **2014,** *5* (3), 305–312. DOI: 10.1111/jdi.12143.

Ordoñez, C. L.; Shaughnessy, T. E.; Matthay, M. A.; Fahy, J. V. Increased neutrophil numbers and IL-8 levels in airway secretions in acute severe asthma: Clinical and biologic significance. *American journal of respiratory and critical care medicine* **2000,** *161* (4 Pt 1), 1185–1190. DOI: 10.1164/ajrccm.161.4.9812061.

Oțelea, M. R.; Rașcu, A. The Asthma Obese Phenotype. In *Asthma Diagnosis and Management - Approach Based on Phenotype and Endotype*; Huang, K.-H. G., Tsai, C. H. S., Eds.; InTech, 2018. DOI: 10.5772/intechopen.74327.

Pan, W. W.; Myers, M. G. Leptin and the maintenance of elevated body weight. *Nature reviews. Neuroscience* **2018,** *19* (2), 95–105. DOI: 10.1038/nrn.2017.168.

Parikh, S. J.; Edelman, M.; Uwaifo, G. I.; Freedman, R. J.; Semega-Janneh, M.; Reynolds, J.; Yanovski, J. A. The relationship between obesity and serum 1,25-dihydroxy vitamin D concentrations in healthy adults. *The Journal of clinical endocrinology and metabolism* **2004,** *89* (3), 1196–1199. DOI: 10.1210/jc.2003-031398.

Parlee, S. D.; Lentz, S. I.; Mori, H.; MacDougald, O. A. Quantifying size and number of adipocytes in adipose tissue. *Methods in enzymology* **2014,** *537*, 93–122. DOI: 10.1016/B978-0-12-411619-1.00006-9.

Peters-Golden, M.; Swern, A.; Bird, S. S.; Hustad, C. M.; Grant, E.; Edelman, J. M. Influence of body mass index on the response to asthma controller agents. *The European respiratory journal* **2006,** *27* (3), 495–503. DOI: 10.1183/09031936.06.00077205.

Pham, D. L.; Ban, G.-Y.; Kim, S.-H.; Shin, Y. S.; Ye, Y.-M.; Chwae, Y.-J.; Park, H.-S. Neutrophil autophagy and extracellular DNA traps contribute to airway inflammation in severe asthma. *Clinical and experimental allergy: journal of the British Society for Allergy and Clinical Immunology* **2017,** *47* (1), 57–70. DOI: 10.1111/cea.12859.

Pizzolla, A.; Oh, D. Y.; Luong, S.; Prickett, S. R.; Henstridge, D. C.; Febbraio, M. A.; O'Hehir, R. E.; Rolland, J. M.; Hardy, C. L. High Fat Diet Inhibits Dendritic Cell and T Cell Response to Allergens but Does Not Impair Inhalational Respiratory Tolerance. *PloS one* **2016,** *11* (8), e0160407. DOI: 10.1371/journal.pone.0160407.

Potaczek, D. P.; Harb, H.; Michel, S.; Alhamwe, B. A.; Renz, H.; Tost, J. Epigenetics and allergy: From basic mechanisms to clinical applications. *Epigenomics* **2017,** *9* (4), 539–571. DOI: 10.2217/epi-2016-0162.

Potaczek, D. P.; Kabesch, M. Current concepts of IgE regulation and impact of genetic determinants. *Clinical and experimental allergy: journal of the British Society for Allergy and Clinical Immunology* **2012,** *42* (6), 852–871. DOI: 10.1111/j.1365-2222.2011.03953.x.

Potaczek, D. P.; Miethe, S.; Schindler, V.; Alhamdan, F.; Garn, H. Role of airway epithelial cells in the development of different asthma phenotypes. *Cellular signalling* **2020,** *69*, 109523. DOI: 10.1016/j.cellsig.2019.109523.

Ralston, J. C.; Lyons, C. L.; Kennedy, E. B.; Kirwan, A. M.; Roche, H. M. Fatty Acids and NLRP3 Inflammasome-Mediated Inflammation in Metabolic Tissues. *Annual review of nutrition* **2017,** *37*, 77–102. DOI: 10.1146/annurev-nutr-071816-064836.

Ray, A.; Oriss, T. B.; Wenzel, S. E. Emerging molecular phenotypes of asthma. *American journal of physiology. Lung cellular and molecular physiology* **2015,** *308* (2), L130-40. DOI: 10.1152/ajplung.00070.2014.

Robert, C. A decade of immune-checkpoint inhibitors in cancer therapy. *Nature communications* **2020,** *11* (1), 3801. DOI: 10.1038/s41467-020-17670-y.

Rosskopf, S.; Jahn-Schmid, B.; Schmetterer, K. G.; Zlabinger, G. J.; Steinberger, P. PD-1 has a unique capacity to inhibit allergen-specific human CD4+ T cell responses. *Scientific reports* **2018,** *8* (1), 13543. DOI: 10.1038/s41598-018-31757-z.

Sartipy, P.; Loskutoff, D. J. Monocyte chemoattractant protein 1 in obesity and insulin resistance. *Proceedings of the National Academy of Sciences of the United States of America* **2003,** *100* (12), 7265–7270. DOI: 10.1073/pnas.1133870100.

Schatz, M.; Rosenwasser, L. The allergic asthma phenotype. *The journal of allergy and clinical immunology. In practice* **2014,** *2* (6), 645-8; quiz 649. DOI: 10.1016/j.jaip.2014.09.004.

Schnell, A.; Bod, L.; Madi, A.; Kuchroo, V. K. The yin and yang of co-inhibitory receptors: toward anti-tumor immunity without autoimmunity. *Cell research* **2020,** *30* (4), 285-299. DOI: 10.1038/s41422-020-0277-x.

Schröder, T.; Wiese, A. V.; Ender, F.; Quell, K. M.; Vollbrandt, T.; Duhn, J.; Sünderhauf, A.; Künstner, A.; Moreno-Fernandez, M. E.; Derer, S.; Aherrahrou, Z.; Lewkowich, I.; Divanovic, S.; Sina, C.; Köhl, J.; Laumonnier, Y. Short-term high-fat diet feeding protects from the development of experimental allergic asthma in mice. *Clinical and experimental allergy: journal of the British Society for Allergy and Clinical Immunology* **2019,** *49* (9), 1245–1257. DOI: 10.1111/cea.13454.

Seo, H.; Chen, J.; González-Avalos, E.; Samaniego-Castruita, D.; Das, A.; Wang, Y. H.; López-Moyado, I. F.; Georges, R. O.; Zhang, W.; Onodera, A.; Wu, C.-J.; Lu, L.-F.; Hogan, P. G.; Bhandoola, A.; Rao, A. TOX and TOX2 transcription factors cooperate with NR4A transcription factors to impose CD8+ T cell exhaustion. *Proceedings of the National Academy of Sciences of the United States of America* **2019,** *116* (25), 12410-12415. DOI: 10.1073/pnas.1905675116.

Shahana, S.; Björnsson, E.; Lúdvíksdóttir, D.; Janson, C.; Nettelbladt, O.; Venge, P.; Roomans, G. M. Ultrastructure of bronchial biopsies from patients with allergic and non-allergic asthma. *Respiratory medicine* **2005,** *99* (4), 429–443. DOI: 10.1016/j.rmed.2004.08.013.

Shore, S. A.; Terry, R. D.; Flynt, L.; Xu, A.; Hug, C. Adiponectin attenuates allergen-induced airway inflammation and hyperresponsiveness in mice. *The Journal of allergy and clinical immunology* **2006,** *118* (2), 389–395. DOI: 10.1016/j.jaci.2006.04.021.

Silha, J. V.; Gui, Y.; Murphy, L. J. Impaired glucose homeostasis in insulin-like growth factor-binding protein-3-transgenic mice. *American journal of physiology. Endocrinology and metabolism* **2002,** *283* (5), E937-45. DOI: 10.1152/ajpendo.00014.2002.

Simpson, J. L.; Phipps, S.; Baines, K. J.; Oreo, K. M.; Gunawardhana, L.; Gibson, P. G. Elevated expression of the NLRP3 inflammasome in neutrophilic asthma. *The European respiratory journal* **2014,** *43* (4), 1067–1076. DOI: 10.1183/09031936.00105013.

Sivapalan, P.; Diamant, Z.; Ulrik, C. S. Obesity and asthma: current knowledge and future needs. *Current opinion in pulmonary medicine* **2015,** *21* (1), 80–85. DOI: 10.1097/MCP.0000000000000119.

Song, J.; Deng, T. The Adipocyte and Adaptive Immunity. *Frontiers in immunology* **2020,** *11*, 593058. DOI: 10.3389/fimmu.2020.593058.

Sood, A.; Shore, S. A. Adiponectin, Leptin, and Resistin in Asthma: Basic Mechanisms through Population Studies. *Journal of allergy* **2013,** 785835. DOI: 10.1155/2013/785835.

Speakman, J. R. Use of high-fat diets to study rodent obesity as a model of human obesity. *International journal of obesity (2005)* **2019,** *43* (8), 1491–1492. DOI: 10.1038/s41366-019-0363-7.

Spielmann, J.; Naujoks, W.; Emde, M.; Allweyer, M.; Fänder, J.; Kielstein, H.; Quandt, D.; Bähr, I. The Impact of High-Fat Diet and Restrictive Feeding on Natural Killer Cells in Obese-Resistant BALB/c Mice. *Frontiers in nutrition* **2021,** *8*, 711824. DOI: 10.3389/fnut.2021.711824.

Steppan, C. M.; Bailey, S. T.; Bhat, S.; Brown, E. J.; Banerjee, R. R.; Wright, C. M.; Patel, H. R.; Ahima, R. S.; Lazar, M. A. The hormone resistin links obesity to diabetes. *Nature* **2001,** *409* (6818), 307–312. DOI: 10.1038/35053000.

Tan, H.-T. T.; Hagner, S.; Ruchti, F.; Radzikowska, U.; Tan, G.; Altunbulakli, C.; Eljaszewicz, A.; Moniuszko, M.; Akdis, M.; Akdis, C. A.; Garn, H.; Sokolowska, M. Tight junction, mucin, and inflammasome-related molecules are differentially expressed in eosinophilic, mixed, and neutrophilic experimental asthma in mice. *Allergy* **2019,** *74* (2), 294–307. DOI: 10.1111/all.13619.

Tashiro, H.; Takahashi, K.; Sadamatsu, H.; Kato, G.; Kurata, K.; Kimura, S.; Sueoka-Aragane, N. Saturated Fatty Acid Increases Lung Macrophages and Augments House Dust Mite-Induced Airway Inflammation in Mice Fed with High-Fat Diet. *Inflammation* **2017,** *40* (3), 1072–1086. DOI: 10.1007/s10753-017-0550-4.

Telenga, E. D.; Tideman, S. W.; Kerstjens, H. A. M.; Hacken, N. H. T. ten; Timens, W.; Postma, D. S.; van den Berge, M. Obesity in asthma: more neutrophilic inflammation as a possible explanation for a reduced treatment response. *Allergy* **2012,** *67* (8), 1060–1068. DOI: 10.1111/j.1398-9995.2012.02855.x.

Todd, D. C.; Armstrong, S.; D'Silva, L.; Allen, C. J.; Hargreave, F. E.; Parameswaran, K. Effect of obesity on airway inflammation: a cross-sectional analysis of body mass index and sputum cell counts. *Clinical and experimental allergy: journal of the British Society for Allergy and Clinical Immunology* **2007,** *37* (7), 1049–1054. DOI: 10.1111/j.1365-2222.2007.02748.x.

Tschöp, M.; Weyer, C.; Tataranni, P. A.; Devanarayan, V.; Ravussin, E.; Heiman, M. L. Circulating Ghrelin Levels Are Decreased in Human Obesity. *Diabetes* **2001,** *50* (4), 707–709. DOI: 10.2337/diabetes.50.4.707.

Vries, A. de; Hazlewood, L.; Fitch, P. M.; Seckl, J. R.; Foster, P.; Howie, S. E. M. High-fat feeding redirects cytokine responses and decreases allergic airway eosinophilia. *Clinical and experimental allergy: journal of the British Society for Allergy and Clinical Immunology* **2009,** *39* (5), 731–739. DOI: 10.1111/j.1365-2222.2008.03179.x.

Wabitsch, M.; Heinze, E.; Debatin, K. M.; Blum, W. F. IGF-I- and IGFBP-3-expression in cultured human preadipocytes and adipocytes. *Hormone and metabolic research = Hormon- und Stoffwechselforschung = Hormones et metabolisme* **2000,** *32* (11-12), 555–559. DOI: 10.1055/s-2007-978685.

Walunas, T. L.; Lenschow, D. J.; Bakker, C. Y.; Linsley, P. S.; Freeman, G. J.; Green, J. M.; Thompson, C. B.; Bluestone, J. A. CTLA-4 can function as a negative regulator of T cell activation. *Immunity* **1994,** *1* (5), 405–413. DOI: 10.1016/1074-7613(94)90071-X.

Wang, Z.; Aguilar, E. G.; Luna, J. I.; Dunai, C.; Khuat, L. T.; Le, C. T.; Mirsoian, A.; Minnar, C. M.; Stoffel, K. M.; Sturgill, I. R.; Grossenbacher, S. K.; Withers, S. S.; Rebhun, R. B.; Hartigan-O'Connor, D. J.; Méndez-Lagares, G.; Tarantal, A. F.; Isseroff, R. R.; Griffith, T. S.; Schalper, K. A.; Merleev, A.; Saha, A.; Maverakis, E.; Kelly, K.; Aljumaily, R.; Ibrahimi, S.; Mukherjee, S.; Machiorlatti, M.; Vesely, S. K.; Longo, D. L.; Blazar, B. R.; Canter, R. J.; Murphy, W. J.; Monjazeb, A. M. Paradoxical effects of obesity on T cell function during tumor progression and PD-1 checkpoint blockade. *Nature medicine* **2019,** *25* (1), 141–151. DOI: 10.1038/s41591-018-0221-5.

Watanabe, K.; Suzukawa, M.; Arakawa, S.; Kobayashi, K.; Igarashi, S.; Tashimo, H.; Nagai, H.; Tohma, S.; Nagase, T.; Ohta, K. Leptin enhances cytokine/chemokine production by normal lung fibroblasts by binding to leptin receptor. *Allergology international: official journal of the Japanese Society of Allergology* [Online] **2019**, S3-S8.

Wenzel, S. E. Asthma phenotypes: the evolution from clinical to molecular approaches. *Nature medicine* **2012,** *18* (5), 716–725. DOI: 10.1038/nm.2678.

Wherry, E. J.; Kurachi, M. Molecular and cellular insights into T cell exhaustion. *Nature reviews. Immunology* **2015,** *15* (8), 486–499. DOI: 10.1038/nri3862.

WHO. Welt-Adipositas-Tag: Adipositas und ihre Folgen für die Gesellschaft. http://www.euro.who.int/de/health-topics/noncommunicable-diseases/obesity/news/news/2017/10/world-obesity-day-understanding-the-social-consequences-of-obesity (accessed October 14, 2020).

WHO. Chronic respiratory diseases: Asthma. https://www.who.int/news-room/q-a-detail/asthma (accessed October 20, 2020).

WHO. Non communicable diseases. https://www.who.int/news-room/fact-sheets/detail/noncommunicable-diseases (accessed January 5, 2021).

WHO. Obesity and overweight. https://www.who.int/news-room/fact-sheets/detail/obesity-and-overweight (accessed October 13, 2021).

Wiedmer, P.; Nogueiras, R.; Broglio, F.; D'Alessio, D.; Tschöp, M. H. Ghrelin, obesity and diabetes. *Nature clinical practice. Endocrinology & metabolism* **2007,** *3* (10), 705–712. DOI: 10.1038/ncpendmet0625.

Wiest, M.; Upchurch, K.; Yin, W.; Ellis, J.; Xue, Y.; Lanier, B.; Millard, M.; Joo, H.; Oh, S. Clinical implications of CD4+ T cell subsets in adult atopic asthma patients. *Allergy, asthma, and clinical immunology: official journal of the Canadian Society of Allergy and Clinical Immunology* **2018,** *14*, 7. DOI: 10.1186/s13223-018-0231-3.

Winnica, D.; Corey, C.; Mullett, S.; Reynolds, M.; Hill, G.; Wendell, S.; Que, L.; Holguin, F.; Shiva, S. Bioenergetic Differences in the Airway Epithelium of Lean Versus Obese Asthmatics Are Driven by Nitric Oxide and Reflected in Circulating Platelets. *Antioxidants & redox signaling* [Online] **2019**, 673–686.

Woo, L. N.; Guo, W. Y.; Wang, X.; Young, A.; Salehi, S.; Hin, A.; Zhang, Y.; Scott, J. A.; Chow, C. W. A 4-Week Model of House Dust Mite (HDM) Induced Allergic Airways Inflammation with Airway Remodeling. *Scientific reports* **2018,** *8* (1), 6925. DOI: 10.1038/s41598-018-24574-x.

Woodruff, P. G.; Modrek, B.; Choy, D. F.; Jia, G.; Abbas, A. R.; Ellwanger, A.; Koth, L. L.; Arron, J. R.; Fahy, J. V. T-helper type 2-driven inflammation defines major subphenotypes of asthma. *American journal of respiratory and critical care medicine* **2009,** *180* (5), 388-395. DOI: 10.1164/rccm.200903-0392OC.

Wortsman, J.; Matsuoka, L. Y.; Chen, T. C.; Lu, Z.; Holick, M. F. Decreased bioavailability of vitamin D in obesity. *The American journal of clinical nutrition* **2000,** *72* (3), 690-693. DOI: 10.1093/ajcn/72.3.690.

Wright, T. K.; Gibson, P. G.; Simpson, J. L.; McDonald, V. M.; Wood, L. G.; Baines, K. J. Neutrophil extracellular traps are associated with inflammation in chronic airway disease. *Respirology (Carlton, Vic.)* [Online] **2016**, 467–475.

Xu, H.; Barnes, G. T.; Yang, Q.; Tan, G.; Yang, D.; Chou, C. J.; Sole, J.; Nichols, A.; Ross, J. S.; Tartaglia, L. A.; Chen, H. Chronic inflammation in fat plays a crucial role in the development of obesity-related insulin resistance. *The Journal of clinical investigation* **2003,** *112* (12), 1821–1830. DOI: 10.1172/JCI19451.

Yi, J. S.; Cox, M. A.; Zajac, A. J. T-cell exhaustion: characteristics, causes and conversion. *Immunology* **2010,** *129* (4), 474–481. DOI: 10.1111/j.1365-2567.2010.03255.x.

Yuksel, H.; Sogut, A.; Yilmaz, O.; Onur, E.; Dinc, G. Role of adipokines and hormones of obesity in childhood asthma. *Allergy, asthma & immunology research* **2012,** *4* (2), 98-103. DOI: 10.4168/aair.2012.4.2.98.

Zhang, J.-H.; Chen, Y.-P.; Yang, X.; Li, C.-Q. Vitamin D3 levels and NLRP3 expression in murine models of obese asthma: Association with asthma outcomes. *Brazilian journal of medical and biological research = Revista brasileira de pesquisas medicas e biologicas* **2017,** *51* (1), e6841. DOI: 10.1590/1414-431X20176841.

Zhang, Y.; Chen, Z.; Berhane, K.; Urman, R.; Chatzi, V. L.; Breton, C.; Gilliland, F. D. The Dynamic Relationship Between Asthma and Obesity in Schoolchildren. *American journal of epidemiology* **2020,** *189* (6), 583–591. DOI: 10.1093/aje/kwz257.

Zheng, H.; Wu, D.; Wu, X.; Zhang, X.; Zhou, Q.; Luo, Y.; Yang, X.; Chock, C. J.; Liu, M.; Yang, X. O. Leptin Promotes Allergic Airway Inflammation through Targeting the Unfolded Protein Response Pathway. *Scientific reports* **2018,** *8* (1), 8905. DOI: 10.1038/s41598-018-27278-4.

Zhu, L.; Chen, X.; Chong, L.; Kong, L.; Wen, S.; Zhang, H.; Zhang, W.; Li, C. Adiponectin alleviates exacerbation of airway inflammation and oxidative stress in obesity-related asthma mice partly through AMPK signaling pathway. *International immunopharmacology* **2019,** *67*, 396–407. DOI: 10.1016/j.intimp.2018.12.030.

Zhu, X. L.; Qin, X. Q.; Xiang, Y.; Tan, Y. R.; Qu, X. P.; Liu, H. J. Adipokine adiponectin is a potential protector to human bronchial epithelial cell for regulating proliferation, wound repair and apoptosis: comparison with leptin and resistin. *Peptides* [Online] **2013**, 34–41.

8. Appendix

a. *Curriculum vitae*

b. Verzeichnis der akademischen Lehrerinnen und Lehrer

c. Danksagung

d. Ehrenwörtliche Erklärung

Curriculum vitae

Die Seiten 110-111 enthalten persönliche Daten. Sie sind deshalb nicht Bestandteil der Online-Veröffentlichung.

Die Seiten 110-111 enthalten persönliche Daten. Sie sind deshalb nicht Bestandteil der Online-Veröffentlichung.

Verzeichnis der akademischen Lehrerinnen und Lehrer

Meine akademischen Lehrerinnen und Lehrer waren die Damen und Herren aus Gießen:

Alter, Breckow, Cemic, Czermak, Dannhofer, Elter, Fiebich, Gokorsch, Gundlach, Heck, Hemberger, Kleinöder, Koch, Kügler, Lange, Maas, Platen, Röhm, Röhricht, Runkel, Schneider, Schummer, Seipp, Steffens, Subke, von Hagen, Weigand, Windisch, Zink, Zirn

Danksagung

Abschließend möchte ich mich an dieser Stelle bei allen bedanken, die mir diese Promotion ermöglicht und mich während dieser Zeit unterstützt haben.

Mein Dank gilt Prof. Dr. Holger Garn, der mir diese hochinteressante Dissertation im Forschungsbereich für Translationale Entzündungsforschung der Universität Marburg ermöglicht hat. Lieber Holger, ich danke dir für die intensive Betreuung meiner Arbeit, das Vorantreiben mit stetig neuen Ideen und die Hilfestellung bei jeglichen Fragen. An dieser Stelle bedanke ich mich besonders bei PD Dr. Daniel P. Potaczek, der mir stets mit seinem umfangreichen Fachwissen zur Seite stand und für seine zahlreichen Tipps zum Schreiben der Thesis.

Ein ganz herzlicher Dank gilt Kim Pauck und Kathrin Balz, die mir immer mit ihrem Wissen zur Seite standen und mich auch in holprigen Phasen sehr unterstützt haben. Ich danke euch, liebe Kim und Kathrin, für die gemeinsamen Erfahrungen und die vielen freundschaftlichen Gespräche, aber auch für die wissenschaftlichen Diskussionen, die mich stets auf neue Ideen gebracht haben.

Des Weiteren möchte ich mich bei denjenigen bedanken, die mich in jeder Hinsicht tatkräftigt unterstützt haben. Andrea Berlin, für ihre Mitarbeit an diesem Projekt im Rahmen ihrer medizinischen Doktorarbeit. Nicole Löwer, die mit ihrem langjährigen Erfahrungswissen im Labor die praktische Durchführung der Tierversuche ermöglicht hat. Fahd Alhamdan, für seine Unterstützung bei der Auswertung der Transkriptomdaten. Den Mitarbeiterinnen und Mitarbeitern der Core Facilities, Dr. Hartmann Raifer, Dr. Andrea Nist und Kim Pauck, für ihre Expertisen und die Durchführung von hochspezifischen Messungen. Dr. Bilal Alashkar Alhamwe, Dr. Verena von Bülow, Dr. Stefanie Hanger-Benes, Thomas Ruppersberg, Lukas Hintz, Felix Picard, Laura Kühl und der gesamten Arbeitsgruppe für die Unterstützung bei der experimentellen Durchführung meiner Arbeit. Vielen Dank für die angenehme Arbeitsatmosphäre.

Ein besonderer Dank gilt meinen Eltern. Sie geben mir Rückhalt und Stärke auf meinem Weg durch alle Lebenslagen.

Herzlich bedanke ich mich bei Fabian Feuerbach, für die emotionale Unterstützung und die Motivation während der gesamten Zeit.

Ehrenwörtliche Erklärung

Die Seite 114 enthält persönliche Daten. Sie ist deshalb nicht Bestandteil der Online-Veröffentlichung.